

**Design of Protective Covers Against Natural Hazards**

by

Vladimir Quinones Silva

A thesis submitted to the Graduate Faculty of  
Auburn University  
in partial fulfillment of the  
requirements for the Degree of  
Master of Science

Auburn, Alabama  
May 9, 2011

Copyright 2011 by Vladimir Quinones Silva

Approved by

Gwynedd A. Thomas, Chair, Associate Professor of Polymer and Fiber Engineering  
Peter Schwartz, Professor of Polymer and Fiber Engineering  
Sabit Adanur, Professor of Polymer and Fiber Engineering

## Abstract

The purpose of this project is to design a protective cover against natural hazards for aircraft, vehicles, and ground structures. Protection against natural hazards is necessary for maintaining the integrity of a vehicle or aircraft. Some of the most commonly encountered natural hazards include exposure to sun (UV light), heat, and hailstones. The design of a protective cover against such natural hazards for aircraft, land vehicles, and structures was studied in this thesis. The objective of this research was the creation of a polymer-fabric based flexible structure designed to protect aircraft, ground vehicles, and housing and storage structures in a wide range of naturally challenging or hostile environments from impact damage, thermal damage, and ice loading damage. The protective cover was designed and evaluated using different methods for their physical characteristics. For this purpose, individual tests were performed to evaluate the best material for each layer; the mentioned tests were: area density, abrasion, friction, folding, UV resistance, impact resistance, tear resistance, bursting strength, static charge resistance, flame resistance, air permeability and hail impact simulation. The consolidated composite was assessed in a test chamber simulating real hail stones. The ice projectiles that were used had different constructions and diameters. Information, such as velocity, peak force and displacement was collected using a high speed camera, dynamic force transducer, and a laser displacement transducer. Results of this experiment revealed that the material is suitable against hailstone impact for hailstones up to 1.6 inches in diameter, which are more common than 2 inch diameters.

Resistance to impact is most critical for protection during hail storms, and therefore, we set out to develop an impact resistant covering against hail stones up to 2 inches in diameter. Future work

should be performed using additional layers utilizing high strength ballistic grade yarns such as Kevlar® or ballistic nylon.

## Acknowledgments

The author would like to express his utmost thanks to his advisor and mentor, Dr. Thomas, for her guidance, encouragement, support, and valuable advice for every step in the completion of this research work. The author is also grateful to his committee members, Dr. Peter Schwartz, and Dr. Sabit Adanur for serving on my graduate committee and for offering their suggestions and help. In addition, he is thankful for Dr. Ramsis Farag's continuous support and help during the project's laboratory studies. Special thanks to Mr. Jeremy Duffey for his excellent help and technical support. The author would like to give thanks to the Department of Polymer and Fiber Engineering for providing support and an exciting research environment, especially to the technicians for their discussion and brilliant recommendations. Thanks also go to his research colleagues, Katie, Idris, and David. Finally, the author would like to express his deepest thanks to his parents who supported him from a distance.

## Table of Contents

|  |      |
|--|------|
| Abstract .....                                       | ii   |
| Acknowledgments .....                                | iv   |
| List of Tables .....                                 | viii |
| List of Figures.....                                 | x    |
| 1. Introduction .....                                | 1    |
| 2. Literature Review.....                            | 3    |
| 2.1 Summary.....                                     | 3    |
| 2.2 Objective .....                                  | 4    |
| 2.3 Effects of natural hazards in expected use ..... | 4    |
| 2.3.1 Sun and heat .....                             | 5    |
| 2.3.2 Bird and animal nests .....                    | 6    |
| 2.3.3 Blowing sand .....                             | 6    |
| 2.3.4 Freezing rain, frost, ice and snow .....       | 6    |
| 2.3.5 Thunderstorms and rain .....                   | 6    |
| 2.3.6 Thunderstorms and hail.....                    | 7    |
| 2.4 Deterioration of polymers.....                   | 8    |
| 2.4.1 Sun (UV and IR radiation).....                 | 8    |
| 2.4.2 Blowing sand .....                             | 11   |
| 2.4.3 Thunderstorms and rain .....                   | 12   |
| 2.4.4 Freezing rain, frost, ice and snow.....        | 13   |

|        |   |    |
|--------|---|----|
| 2.4.5  | Thunderstorms and hail.....             | 14 |
| 3.     | Experimental Design.....                | 31 |
| 3.1    | Materials.....                          | 31 |
| 3.2    | Methodology to test the materials ..... | 33 |
| 3.2.1  | Areal density .....                     | 36 |
| 3.2.2  | Abrasion test.....                      | 36 |
| 3.2.3  | Friction test.....                      | 37 |
| 3.2.4  | Folding test .....                      | 38 |
| 3.2.5  | UV resistance test .....                | 38 |
| 3.2.6  | Impact resistance (impact test) .....   | 39 |
| 3.2.7  | Tear resistance .....                   | 40 |
| 3.2.8  | Bursting strength test .....            | 40 |
| 3.2.9  | Static charge resistance.....           | 41 |
| 3.2.10 | Flame resistance .....                  | 42 |
| 3.2.11 | Air permeability.....                   | 43 |
| 3.2.12 | Hail impact simulation .....            | 43 |
| 4.     | Experimental Results.....               | 56 |
| 4.1    | Areal density.....                      | 56 |
| 4.2    | Abrasion test .....                     | 57 |
| 4.3    | Friction test .....                     | 59 |
| 4.4    | Folding test.....                       | 59 |
| 4.5    | UV resistance test.....                 | 59 |
| 4.6    | Impact resistance (impact test).....    | 61 |
| 4.7    | Tear resistance .....                   | 62 |

|      |                                      |    |
|------|--------------------------------------|----|
| 4.8  | Bursting strength resistance .....   | 63 |
| 4.9  | Static charge resistance .....       | 63 |
| 4.10 | Flame resistance.....                | 64 |
| 4.11 | Air permeability .....               | 65 |
| 4.12 | Hail impact simulations .....        | 67 |
| 5.   | Conclusions .....                    | 79 |
| 6.   | Recommendations for Future Work..... | 81 |
|      | References .....                     | 82 |
|      | Appendices.....                      | 86 |

## List of Tables

|  |    |
|--|----|
| Table 1 Mass calculations of hailstones .....  | 15 |
| Table 2 Analytical comparison of terminal speed models .....                                 | 19 |
| Table 3 Resultant velocity and kinetic energy of hailstones at 45° angle and free-fall ..... | 22 |
| Table 4 Terminal velocities and energies of hailstones .....                                 | 23 |
| Table 5 Kinetic energies produced by ASTM, FM, and UL standards test methods .....           | 23 |
| Table 6 Kinetic energy of hailstones using Ross' equation.....                               | 24 |
| Table 7 Filler weight for each diameter .....  | 51 |
| Table 8 Areal density results.....   | 56 |
| Table 9 Comparison of weight loss on samples after abrasion.....                             | 57 |
| Table 10 Visual comparison of wear abrasion on samples .....                                 | 58 |
| Table 11 Friction test results .....   | 59 |
| Table 12 Impact test results.....  | 62 |
| Table 13 Tear resistance test results.....   | 62 |
| Table 14 Burst resistance test results .....   | 63 |
| Table 15 Electrostatic charge of materials tested.....                                       | 63 |
| Table 16 Air permeability test .....   | 65 |
| Table 17 Material selection matrix base layer .....  | 66 |
| Table 18 Material selection matrix inner layer .....   | 66 |
| Table 19 Material selection matrix outside layer .....                                       | 67 |



|   |     |
|---|-----|
| Table 20 Test summary of ice constructions .....  | 73  |
| Table 21 Displacement in material.....  | 75  |
| Table 22 Results after abrasion of the heat reflecting fabric .....   | 88  |
| Table 23 Results after abrasion of the single bubble/white foil .....   | 89  |
| Table 24 Results after abrasion of the two-sided film with polyester scrim reinforcement .....                  | 90  |
| Table 25 Results after abrasion of the single bubble/double foil (circular embossing) .....                     | 91  |
| Table 26 Results after abrasion of the single bubble/double foil (triaxial embossing) .....                     | 92  |
| Table 27 Results after impact resistance test of the two-sided film with polyester scrim<br>reinforcement ..... | 93  |
| Table 28 Results after impact resistance test of the single bubble/double foil .....                            | 94  |
| Table 29 Results after impact resistance test of heat reflecting fabric .....                                   | 95  |
| Table 30 Results after impact resistance test of single bubble/double foil.....                                 | 96  |
| Table 31 Results after impact resistance test of bubble wrap .....  | 97  |
| Table 32 Results after impact resistance test of polyethylene film.....   | 98  |
| Table 33 Results after tear resistance test.....  | 99  |
| Table 34 Results after bursting strength test of outside layers.....  | 101 |
| Table 35 Results after bursting strength test of inner layers .....   | 102 |

## List of Figures

|   |    |
|---|----|
| Figure 1 General lay-up of multilayer protective cover design .....   | 3  |
| Figure 2 Cause – Effect tree.....   | 5  |
| Figure 3 Vehicle damage caused by hail .....  | 7  |
| Figure 4 Electromagnetic spectrum .....   | 8  |
| Figure 5 Principal reactions and interactions of solar radiation in polymeric materials.....                              | 9  |
| Figure 6 Degradation of PE caused by UV radiation.....  | 10 |
| Figure 7 Modes of failure in ice as a function of strain rate.....  | 16 |
| Figure 8 Analytical comparison of terminal speed models.....  | 20 |
| Figure 9 Resultant impact speed at $\theta$ .....   | 21 |
| Figure 10 Quasi–static hail impact characterization spring-mass model.....  | 25 |
| Figure 11 Structural model during small mass impact on plates.....  | 26 |
| Figure 12 Schematic of contact between two elastic solids (rigid, spherical indenter, and flat, non-rigid specimen) ..... | 27 |
| Figure 13 Response during small mass impact on plates.....  | 29 |
| Figure 14 Physical appearance of materials used in designs.....   | 32 |
| Figure 15 Depictions of multilayer protective cover design (units in inches).....   | 34 |
| Figure 16 Abraser.....  | 37 |
| Figure 17 Friction test fixture .....   | 37 |
| Figure 18 Folding endurance tester.....   | 38 |

|   |    |
|---|----|
| Figure 19 QUV Weathering tester.....                                | 39 |
| Figure 20 Instron Dynatup.....                                      | 39 |
| Figure 21 Tear test.....  | 40 |
| Figure 22 Burst test.....   | 41 |
| Figure 23 Static test .....   | 42 |
| Figure 24 Chamber flame resistant test .....                        | 42 |
| Figure 25 Frazier low differential pressure.....                    | 43 |
| Figure 26 Experimental scheme set-up .....                          | 44 |
| Figure 27 Experimental set-up.....                                  | 45 |
| Figure 28 Compressed air cannon.....                                | 46 |
| Figure 29 Air cannon fixture .....                                  | 46 |
| Figure 30 Test chamber .....  | 47 |
| Figure 31 Experimental set-up frame .....                           | 48 |
| Figure 32 Targets at 45° and 90° .....                              | 48 |
| Figure 33 Ice constructions .....                                   | 50 |
| Figure 34 Foam sabot for varying diameter projectiles.....          | 51 |
| Figure 35 Pressure vs. Velocity .....                               | 52 |
| Figure 36 Force transducer set-up.....                              | 53 |
| Figure 37 Laser displacement transducer set-up .....                | 54 |
| Figure 38 Composite target model detailing its composition.....     | 54 |
| Figure 39 Expected ice projectile path .....                        | 55 |
| Figure 40 Comparison of weight loss on samples after abrasion ..... | 57 |
| Figure 41 FTIR spectra of the outside layers.....                   | 60 |
| Figure 42 FTIR spectra of the outside layers.....                   | 61 |

|   |    |
|---|----|
| Figure 43 Test of flame resistance.....   | 64 |
| Figure 44 Sample after test of flame resistance .....   | 65 |
| Figure 45 Volts vs. time (output signal).....   | 68 |
| Figure 46 Peak force of layered ice (57 mm diameter) at 90° impact .....  | 68 |
| Figure 47 Peak force of layered ice (40.5 mm diameter) at 90° impact .....  | 69 |
| Figure 48 Peak force of layered ice (28.5 mm diameter) at 90° impact .....  | 69 |
| Figure 49 Peak force vs. Kinetic energy .....   | 70 |
| Figure 50 Summary of ice with cotton fillers (57 mm diameter) at 90° impact.....  | 70 |
| Figure 51 Summary of layered ice (57 mm diameter) at 90° impact .....   | 71 |
| Figure 52 Peak force of ice with cotton fillers (57 mm diameter) at 45° impact.....   | 72 |
| Figure 53 Peak force of ice with cotton fillers (40.5 mm diameter) at 45° impact.....   | 72 |
| Figure 54 Peak force of ice with cotton fillers (28.5 mm diameter) at 45° impact.....   | 73 |
| Figure 55 Peak force vs. Kinetic energy for all ice construction projectiles .....  | 74 |
| Figure 56 Comparison of force history all ice construction projectiles.....   | 74 |
| Figure 57 Composite material with polyethylene film impacted by an ice projectile with cotton fillers<br>(40.5 mm) .....            | 76 |
| Figure 58 Composite material with bubble wrap inner impacted by an ice projectile with cotton<br>fillers (40.5 mm) coefficient..... | 76 |
| Figure 59 Summary of deformation of composite specimen.....   | 77 |
| Figure 60 Sequence of the ice impact (57 mm diameter) on specimen .....   | 78 |
| Figure 61 Average of weight loss vs. number cycles of the heat reflecting fabric .....  | 88 |
| Figure 62 Average of weight loss vs. number cycles of the single bubble/white foil .....  | 89 |
| Figure 63 Average of weight loss vs. number cycles of the two-sided film with polyester scrim<br>reinforcement .....                | 90 |

|   |     |
|---|-----|
| Figure 64 Average of weight loss vs. number cycles of the single bubble/double foil (circular embossing)..... | 91  |
| Figure 65 Average of weight loss vs. number cycles of the single bubble/double foil (triaxial embossing)..... | 92  |
| Figure 66 Load vs. Time of two-sided film with polyester scrim reinforcement.....                             | 93  |
| Figure 67 Load vs. Time of single bubble/white foil.....  | 94  |
| Figure 68 Load vs. Time of heat reflecting fabric.....  | 95  |
| Figure 69 Load vs. Time of single bubble/double foil .....  | 96  |
| Figure 70 Load vs. Time of bubble wrap .....  | 97  |
| Figure 71 Load vs. Time of polyethylene film.....   | 98  |
| Figure 72 Load vs. Extension of outside layers.....   | 100 |
| Figure 73 Load vs. Extension of outside layers.....   | 101 |
| Figure 74 Load vs. Extension of inner layers .....  | 102 |

## 1. INTRODUCTION

Damage of personal property due to natural hazard is both a nuisance and an expensive problem that plagues vehicle and aircraft owners. Protection against natural hazards is necessary for maintaining the integrity of a vehicle or aircraft. Some of the most commonly encountered natural hazards include exposure to the sun, heat, hail, rain, bird and animal nesting and droppings, freezing rain, frost, ice, snow and extreme cold, and others. These environmental hazards are responsible for protective covering failures and ultimately for damage of vehicles and aircraft due to abrasion, surface deterioration (paints, coating), and structural damage from hailstones. These hazards are generally very expensive and potentially dangerous. In order to prevent damage, and unnecessary repairs, the development of a suitable protective material is critical.

The design of a protective cover against natural hazards for aircraft, land vehicles, and structures is studied in this thesis. Development of a proposed design is based on the material properties and testing needed to prevent damage from natural hazards. The protective cover configuration proposed consists of an internal layer, inflatable bladder, and external protective layer. Experiments are performed to evaluate the material properties. These results are used to determine an appropriate configuration of various proposed material layers.

In order to evaluate the proposed material layers, an experimental enclosure for impact analysis of polymeric materials has been developed. The capabilities of the experimental enclosure include data acquisition, high speed camera, compressed air cannon suitable for large diameter, and low speed impact.

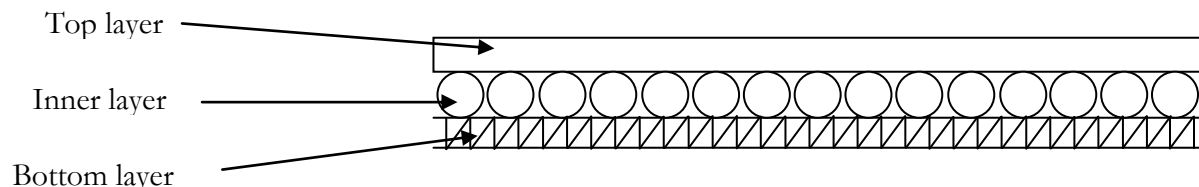
In addition to the expected functionality of conventional protective coverings, a covering with significant impact resistance is needed. Although conventional protective coverings are available from several commercial suppliers, none of these materials offer significant impact resistance against hailstones.

## 2. LITERATURE REVIEW

### 2.1 Summary

A reasonable and logical device for protection of exterior aircraft or other vulnerable surfaces from ice formation, wind, blowing sand or falling hailstones is a cover, designed from a combination of appropriate polymer materials. A new approach for such a cover could consist of an individual inflatable/deflatable blanket system of a design, configuration and size to completely cover exposed surfaces of flight vehicles, land vehicles and ground structures.

The proposed solution design consists of three different layers (Figure 1). The bottom layer of the protective cover may be inflatable/deflatable with a layer of soft material suitable to protect an aircraft or other damage prone surfaces. The inner layer or layers of the cover could be designed so they have numerous individual air or fiber filled pockets within the structure as shock absorbing and/or temperature insulating layers. The number of rows and layers within is determined to protect an aircraft, vehicle or structure from damage from hail and other foreign objects striking it. The top layer of the cover includes a lightweight layer of highly reflective material to allow for greater protection in extreme heat environments such as the desert.



**Figure 1** General lay-up of multilayer protective cover design



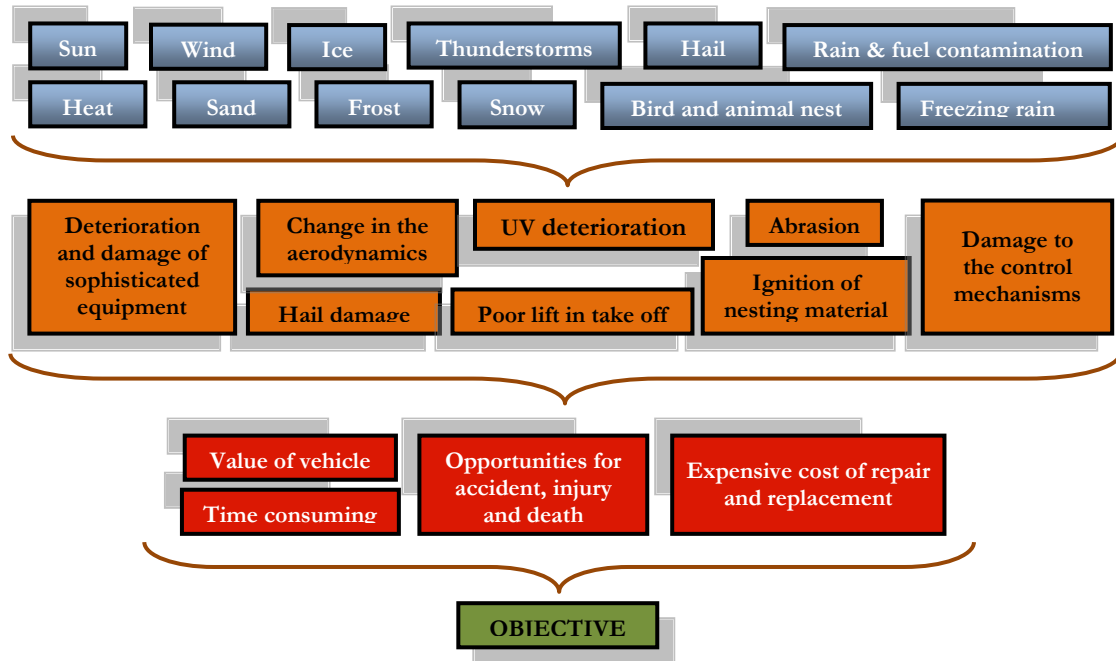
## **2.2 Objective**

This project is directed toward the creation of a polymer-fabric based flexible structure designed to protect aircraft, ground vehicles, and housing and storage structures in a wide range of naturally challenging or hostile environments from impact damage, thermal damage, and ice loading damage. The protective cover is designed and evaluated using different methods for their physical characteristics.

This work also includes determining and testing a basic design to most effectively perform these and other requirements such as lightweight and low storage volume to stow the material in an aircraft or ground vehicle. It is also proposed to design the optimized device for easy deployment and adjustment when placing it over the aircraft, vehicle or ground unit.

## **2.3 Effects of natural hazards in expected use**

Aircrafts, land vehicles and ground structures are exposed during short and long periods of time to different natural hazards. Figure 2, depicts the effects that natural hazards pose on such structures.



**Figure 2** Cause – Effect tree

### 2.3.1 Sun and heat

Long term exposure of flight and land vehicles to ultraviolet rays from the sun deteriorates various vehicle parts. For example, the various parts capable of being degraded are painted surfaces, glass, Plexiglass, and exterior appendages such as antennas, lights and lenses.

The thermal expansion of metals, composite materials, and other materials changes a surface's dimensions during elevated temperature exposure during long or short periods of time. The surface also changes from the cycles of elevated and lowered temperatures, such as the changes that occur in the materials between daytime and nighttime exposure. By this, thermal damage introduces stress to the exterior material, fades the paint, and reduces its integrity; therefore, the long term value of the vehicles decreases.

### **2.3.2 Bird and animal nests**

Deterioration and corrosion of painted surfaces and external materials can be caused by bird droppings and nests. Since an airplane's turbine is a weather protected unit, birds sometimes build nests inside this part. As a result, it is possible to ignite the bird's nest when the engine is started, thus causing a fire.

### **2.3.3 Blowing sand**

Wear and scratches on the painted surfaces may be present by the effect of sand particles that are transported under blowing air conditions. It is similar to the process of sandblasting but at low velocities in which this abrasion can create oxidation on the surface. This incurs increased cost of maintenance caused by the accelerated aging and the devaluation of the vehicle.

### **2.3.4 Freezing rain, frost, ice and snow**

These critical environmental hazards for aircrafts can cause serious accidents even if the aircraft has no mechanical problems or airframe damage. Parked aircrafts are exposed to weather conditions such as extreme cold and freezing rain leading to the formation of frost, snow, and ice on the lifting surface of the airplane. Accident history shows that takeoff accidents have been related to ice contamination as the probable origin or causal factor. A reduction of the lift and an increase of the drag are caused by these large accretions [1]. It is extremely costly and time consuming to remove, and public deicing facilities are not available in all airports.

### **2.3.5 Thunderstorms and rain**

Heavy rainfall may introduce the possibility of water leaking past the fuel filler caps and then the fuel tank. In consequence of this, the engine and other components such as the fuel filter and the

carburetor bowl might not work properly. Catastrophic results can occur from rain water contamination.

### 2.3.6 Thunderstorms and hail

Thunderstorms accompanied by torrential amounts of hail could cause damage to the windscreen and the exterior of a vehicle, such as the formation of hail dimples. Damage from hailstones may affect the aerodynamics of aircrafts creating opportunities for accident, injury and death. Also, other navigational components for safe flights may be impacted. Body panels of truck trailers and automobiles which were parked outdoors are also exposed to hail damage (Figure 3). The cost of replacement or repair combined with the cost of the airplane out of commission is expensive. Impact of a large mass falling at low velocity on composites' surfaces may cause non-visible manifestations of impact damage, such as internal delamination, which carry a significant loss of strength or stiffness of the components [2].



**Figure 3** Vehicle damage caused by hail

The following sections present a study of the specific weathering effects caused by natural hazards on the outdoor protective covers.

## 2.4 Deterioration of polymers

Deterioration of polymers could occur as a result of exposure to heat, mechanical action, ultrasonic and sonic energy, radiation, electrical action in the form of dielectric effects, and chemical effects [3]. Polymer deterioration in the cover yields lower the mechanical properties; therefore, the outdoor cover must be designed to withstand each of these effects.

### 2.4.1 Sun (UV and IR radiation)

There are different gaseous constituents of the earth's atmosphere which modify and attenuate light irregularly. Solar energy is released in the form of ultraviolet waves, visible light waves, and infrared waves (Figure 4). Within the solar spectrum range, the ultraviolet (UV) and infrared (IR) light regions yield more damage on structures than light from the visible range. Despite the fact that UV radiation is so destructive to structures, it only accounts for 6% of the solar radiation in the wavelength range below 400 nm. Non-visible radiation is around 42% in the wavelength range above 800 nm, while visible radiation accounts for 52% of total radiation and ranges from 400-800 nm [4].

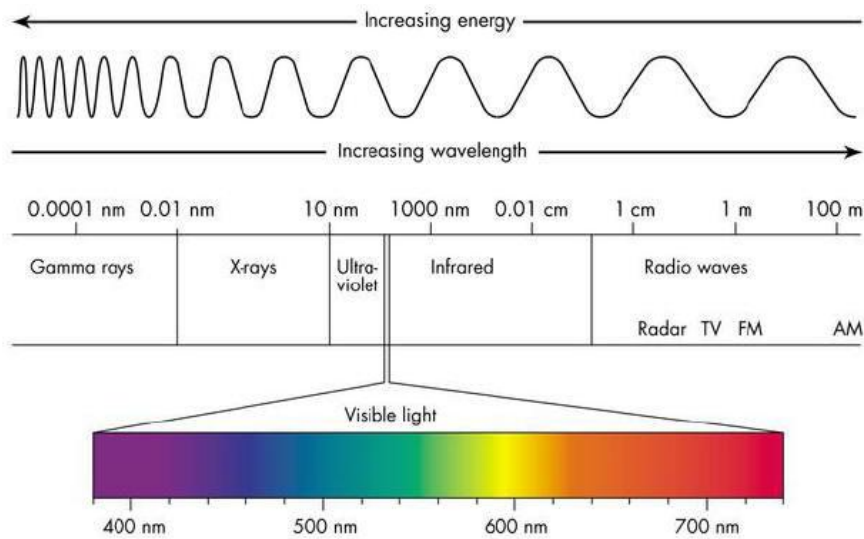
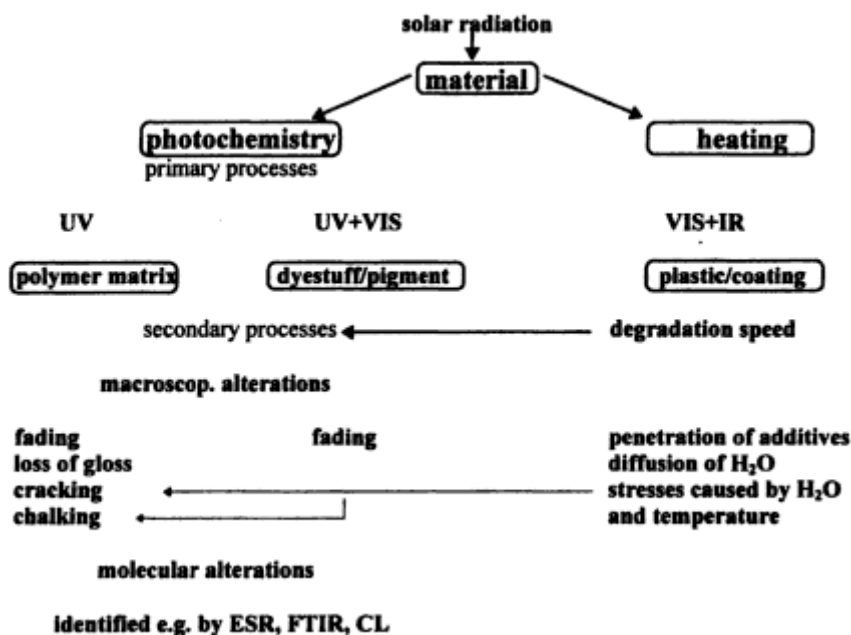


Figure 4 Electromagnetic spectrum [5]

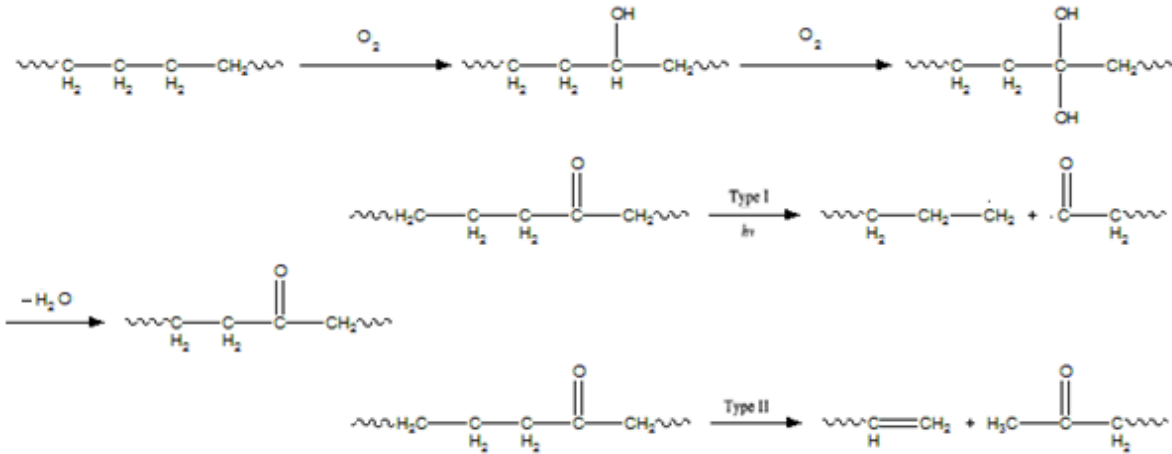
The principal reactions and interactions of solar radiation in polymeric materials are described in Figure 5. The major degradation process occurs from exposure of the polymer matrix to ultraviolet radiation due to the greater quantum energy. Secondary processes of degradation result from thermal energy heating the sample when visible and IR radiation are absorbed by the material. This thermal energy accelerates the aging process for the material [6].



**Figure 5** Principal reactions and interactions of solar radiation in polymeric materials [6]

A wide variety of chemical reactions and physical processes occur when macromolecules are exposed for extended time periods to outdoors conditions, involving UV radiation, temperature variations and frequent changes in humidity. The stabilization of polymers against weathering damage entails the retardation or elimination of primary photochemical processes. The degradation of the polymer's molecular weight may result from scission of the ketone carbonyl group located in the main chain or on the adjacent carbon in a sidechain [7].

Figure 6 illustrate the UV degradation of polyethylene. There is a direct correlation between the decrease in the physical properties of the polyethylene and the increase in the oxygen content caused by photodegradation.



**Figure 6** Degradation of PE caused by UV radiation [7]

This degradation makes the materials more vulnerable to stress fatigue causing fractures such as microcracks; therefore, the material loses its mechanical performance. Discoloration, erosion, embrittlement, and reduction in light transmission are other consequences of UV radiation [8]. In order to identify and measure the changes in the properties of polymeric materials, several standard test methods are available. These changes represent a valid situation of normal service life conditions.

UV fluorescent lamps, open-flame carbon arc lamps, or Xenon arc lamps with different energy outputs and humidity conditions are common artificial weathering test equipment used for simulating polymeric materials exposed to solar radiation. The obtained values of these standard tests are spectral irradiance, which is the quantity of radiant flux striking a surface ( $\text{W}/\text{m}^2\cdot\text{nm}$ ), and the radian exposure, which is the amount of irradiance acting upon the surface for a period of time ( $\text{J}/\text{m}^2$ ) [6].

Some specific properties of the material such as the absorption ratio or the thermal conductivity would influence the temperature increase on the irradiated surface. Ovens are used to compare the change in a defined property or properties of a polymeric material produced by the exposure of this material to different temperatures for a number of exposure times. Original test results such as tensile strength, elongation, and hardness can be compared with the measured results obtained after the exposure of the material to a variation of temperature [6].

A thermal insulation covering is required on the external surface of aircrafts and vehicles to maintain a stable inside temperature. The market offers canvas covers that lie over the windows and are attached to the outside of vehicles or smaller aircraft in an attempt to restrict the sun from entering the cockpit. This application appears to be marginally effective at best. Also, there are custom fit reflective materials that are installed in the inside window openings of an aircraft or vehicle. Since the reflective material is on the inside of the Plexiglass window, a great deal of heat builds up between the actual reflective material and the inside of the window or Plexiglass. As a result, this causes great stress to the window or Plexiglass and reduces its life-span.

#### **2.4.2 Blowing sand**

Blowing air with sand particles may affect the friction and wear behavior of polymeric materials [9]. A layer of sand or dust may separate material from the cover material surface while it is exposed to air-sand condition; therefore resistance to abrasion is an important requirement for this application. Resistance to abrasion is the ability of a material to resist the removal of material pieces from its surface when it is in contact with or rubbing against another surface [10].

There are standard test methods for the determination of abrasion resistance in materials such as textile fabrics and plastics using different apparatus. For example, the equipment utilized for this



testing method are a flexing and abrasion tester, rotary platform double head abrader, and loose abrasive abrading machine.

These standard test methods are not directly applicable to this research due to the different failure criteria of the utilized materials for the end-use. As well, the type of material being tested for this application does not conform to the testing standards; the material is not a transparent plastic. These standards determine the abrasion resistance as a function of the breaking load, volume loss, and weight loss. Textiles fabrics, flat plastics, and transparent plastics are tested. Some procedures will be combined in order to find the abrasion failure criteria of this experiment that not only involves weight loss but detachments of the coating which can cause a change of the reflectance.

### **2.4.3 Thunderstorms and rain**

Water may cause material failure by contributing to a loss in stiffness, an increase in creep, and stress relaxation. Mechanical stressing, swelling, and contraction of the polymeric material caused by water occur when the material is exposed to water or absorbs moisture from humid outdoor conditions. When the polymer absorbs water, it causes swelling of the material or washes away coatings and additives. During the absorption of water, compressive stresses are imposed superficially, and inside the material, tensile stresses are predominant. A volume contraction appears when the surface is exposed to a dry period which dries off the surface layers while the core layers are still swollen. Therefore, it creates compressive stresses in the interior and tensile stresses on the exterior surfaces. As a result of the tensile forces on the exterior surface, cracking of the material surface may occur. Also, as a consequence of this, the material's dielectric properties, dimensions and appearance would be change [4].

Solar radiation and rain water or dew are a combination of weathering processes which may accelerate failure due to the photochemical ageing process that induces embrittlement of the

polymeric material [4]. Therefore in order to evaluate the effect of water in the material, the same test methods are used as outlined previously for the simulation of sunlight exposure with the use of UV fluorescent lamps, carbon or Xenon arc lamps.

#### **2.4.4 Freezing rain, frost, ice and snow**

The protective cover is important for elimination of ice on the outside surface of an aircraft or vehicle while it is parked. However, snow, frost, and ice are capable of accumulating on the surfaces of polymeric material. The performance of the material at low temperatures may decrease due to a reduction in the flexibility and mobility of polymer chains. At low temperatures, the polymeric material can become brittle and rigid; the modulus of the material increases, therefore the elongation and the impact strength, which depends on the degree of crystallinity of the polymer, may decrease. As soon as the brittle failure starts, the crack will propagate with a small amount of load without noticeable deformation of the polymeric material [10].

A standard test method, ASTM D746, for calculating the brittleness temperature of plastic and elastomers by means of impact is used for research and development purposes on applications in which the conditions of deformation are similar to those specified in the test. Brittleness temperature can also be defined as the temperature at which 50% of tested samples have brittle failure under specified impact conditions. However, brittleness temperature is often a useless parameter since the data obtained by testing under these specified conditions rarely matches the actual material's conditions during application. [10].

## 2.4.5 Thunderstorms and hail

### *Falling hailstones*

A hailstone is a single collection of ice that is formed during cycles of updrafts and downdrafts within a thunderstorm that contains water droplets and ice crystal frozen particles. The cycles of updrafts and downdrafts within a cloud cause the growing of the hail while it accumulates ice particles creating a layered structure. Larger hail is formed during severe thunderstorms when stronger updrafts are necessary [11].

### *Hailstone mass and geometry*

Hailstones may grow from 0.2 inch (pea size) to 7 inch (volleyball size). Typically, hail is around 0.4-1.2 inches (nickel size) in diameter. There are reports of hailstones with 6 inch diameters and weighing 1.5 pounds which occurred in July of 1928 near Potter, Nebraska. As well, in Coffeyville, Kansas on September 3, 1970 hailstones with a diameter of 6.5 inches and 1.3 pounds were recorded [12].

Previous research concluded that the hailstone geometry is spherical or nearly spherical in large size hail [13], and reported hail densities are between 0.7 and 0.91 gm/cm<sup>3</sup>. Matson and Huggins classified spherical hailstones when they photographed more than 600 of them. [14].

The mass of hail can be calculated using the following equations:

$$V_{sphere} = \frac{4}{3}\pi r^3$$

$$m = \rho V$$

Where:

r = radius of the hail

V= volume of a sphere

$\rho$ = density of hail

m = mass

Table 1 summarizes the approximate mass of hail with a density of 0.91gr/cm<sup>3</sup> based on the diameter size of hail stones formed.

**Table 1** Mass calculations of hailstones

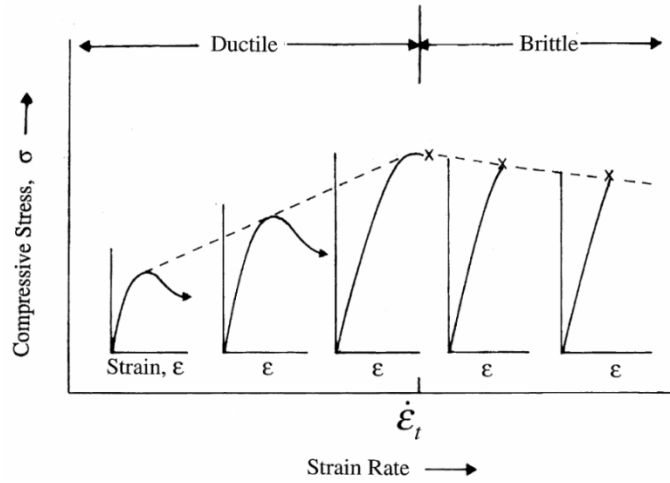
| Diameter  |           | Radius    | Volume                | Mass      |
|-----------|-----------|-----------|-----------------------|-----------|
| <i>in</i> | <i>cm</i> | <i>cm</i> | <i>cm<sup>3</sup></i> | <i>gr</i> |
| 1/4       | 0.64      | 0.318     | 0.13                  | 0.12      |
| 1/2       | 1.27      | 0.635     | 1.07                  | 1.00      |
| 3/4       | 1.91      | 0.953     | 3.62                  | 3.29      |
| 1         | 2.54      | 1.270     | 8.58                  | 8.20      |
| 1 1/4     | 3.18      | 1.588     | 16.76                 | 15.25     |
| 1 1/2     | 3.81      | 1.905     | 28.96                 | 26.35     |
| 1 3/4     | 4.45      | 2.223     | 45.98                 | 41.85     |
| 2         | 5.08      | 2.540     | 68.64                 | 66.40     |
| 2 1/4     | 5.72      | 2.858     | 97.73                 | 88.94     |

### ***Hail impact***

The resulting damage for hail impact has been categorized at different levels according to the diameter, and it depends on the hail ice properties as well as the falling speed and wind speed. Hail with diameters from 5 to 20 mm may yield minor damage in vegetation and plants. Hail from 21 to 40 mm diameter causes severe damage in glass and plastic structures, and vehicle bodywork. Significant risk of injuries, severe roof damage, and bodywork damage in grounded aircraft are caused by hailstone with diameters higher than 41 mm [15].

Ice properties change depending on the temperature of ice formation. At a low velocity, the internal crystallinity of the ice has an effect on the relationship of force-time history and resulting

stress-strain curves [16] . The modulus and the modes of failure in ice can vary from ductile to brittle fractures.



**Figure 7** Modes of failure in ice as a function of strain rate [17]

Schulson [17] explained the ice behavior and its dependency on deformation rate. Ice is ductile at low deformation rates and brittle at high rates. Schulson characterized ice for NASA with different compressive strengths from 6.1MPa in columnar structures to 14.8 MPa for single crystals. The transition takes place around the order of  $10^{-3} \text{ s}^{-1}$ . Haynes [18] concluded that over  $-10^{\circ}\text{C}$  the compressive strength of ices is between 5-25 MPa. In the temperature range  $-10$  to  $-20^{\circ}\text{C}$  the mean is 1.43 MPa. The effect of temperature on the tensile and compressive strength is inversely proportional, being higher in compression than in tension. Petrovic [19] summarized information collected from other researchers with reference to the effect of grain size and volume in the properties of ice. When the grain size increases, the tensile strength decreases. Additionally, the tensile strength of ice decreases with increasing the volume of the ice.

The elastic modulus and Poisson's ratio of ice were measured by Gold [20] at temperatures of -10°C and were reported in the range of 9.7 - 11.2 GPa and 0.29 - 0.32 respectively. Schroeder and McMaster [21] described the phase change of ice at -10°C from solid to liquid. Pressures around 23.5 GPa are needed in order to generate a phase change. For ice impact applications, 23.5GPa is an extremely large pressure. Thus, ice impact can be connected with solid-body impact phenomena.

### ***Impact velocity***

During his tests, Gokhale found that the hailstones with diameters of 100 mm fall at a terminal velocity of nearly 30 m/s [22]. Ross and Carte [23] established that terminal speeds and the impact speeds of hailstones falling in air with the same mass can be found by the following equation:

$$v_o = 124\sqrt{D_{ice}}$$

Where

$v_o$  = terminal speed

$D_{ice}$  = diameter of ice

The density of the air used in that research was of  $10^{-3}$  g/cm<sup>3</sup> and the ice density of  $0.89 \pm 0.05$  g/cm<sup>3</sup>. This equation presents a direct relationship between the terminal velocity and the diameter of the ice.

Matson and Huggins [14] also studied the connection between the diameter of hailstones and their kinematics. They concluded in their research that the vertical velocities of hailstones close to the surface (air density is equal to  $9.93 \times 10^{-4}$  g/cm<sup>3</sup>) can be predicted by:

$$v_o = 11.45\sqrt{D_{ice}}$$

for a drag coefficient of 0.87 and Reynolds numbers from  $10^3$  to  $2 \times 10^4$ , where diameter of the ice is in centimeters.

Theoretically, the force of drag, in fluid dynamics, is:

$$F_D = \frac{1}{2} \rho C_D v^2 A$$

Where:

$C_D$  = drag coefficient

$A$  = cross sectional area of the hailstone

$\rho$  = air density

$v$  = velocity

An initial condition is that the force is equal to the mass of the hailstone times the acceleration of gravity. Therefore, the terminal velocity can be calculated theoretically with the following expression:

$$v = \left( \frac{2mg}{\rho AC_D} \right)^{1/2}$$

For spherical hail, the equation can be resumed in:

$$v = \left( \frac{4\rho_{hail}g}{3\rho_{air}C_D} \right)^{1/2} D_{hail}^{1/2}$$

Drag coefficient can be inferred, although it is not an exact figure due to velocity variation. By assuming that the fall speed is the terminal velocity and that it has a circular cross sectional area, the following expression is valid:

$$C_D = \frac{2\rho_{hail}gVol}{\rho_{air}v^2A}$$

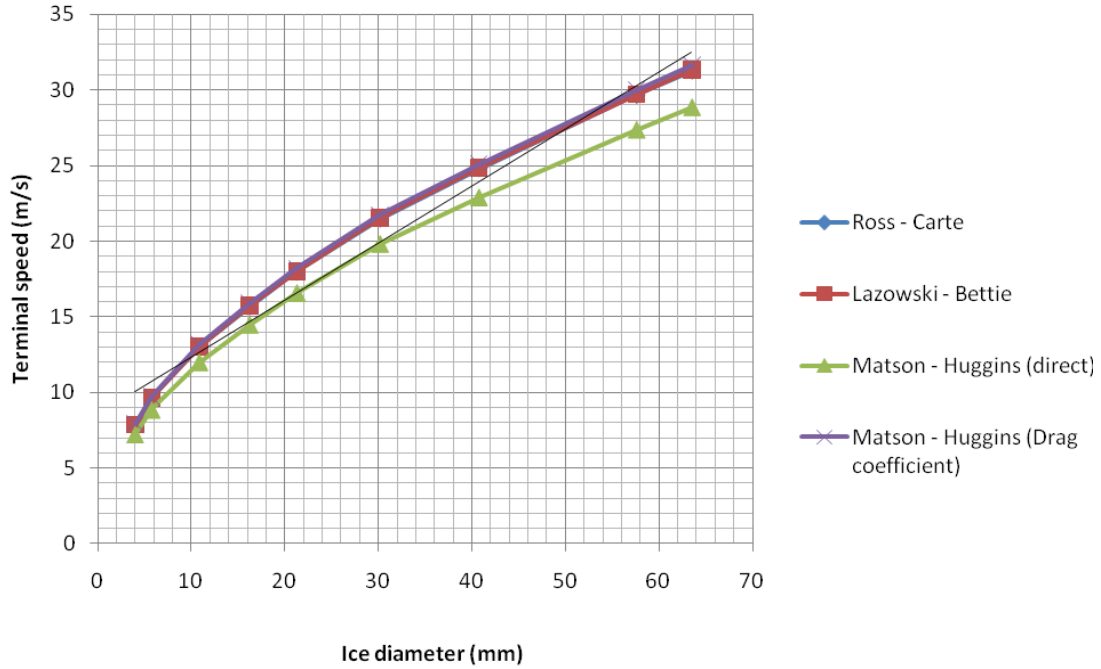
Lazowski [24] and Bettie [25] determined the relationship  $v = 12.43D_{max}^{1/2}$ . The drag coefficient was inferred to be 0.61 at sea level.

Table 2 and Figure 8 show a comparison of the terminal speed of those models for hailstone with ice density of  $0.89 \text{ g/cm}^3$ , air density  $1.23 \times 10^{-3} \text{ g/cm}^3$ , and drag coefficient of 0.6.

**Table 2** Analytical comparison of terminal speed models

| Ice Diameter (mm) | Terminal speed (m/s)      |                          |                             |  |
|-------------------|---------------------------|--------------------------|-----------------------------|--|
|                   | Ross - Carte              | Lazowski - Bettie        | Matson - Huggins            |  |
|                   | $v_o = 124\sqrt{D_{ice}}$ | $v = 12.43D_{max}^{1/2}$ | $v_o = 11.45\sqrt{D_{ice}}$ | $v = \left(\frac{4\rho_{hail}g}{3\rho_{air}C_D}\right)^{1/2} D_{hail}^{1/2}$ |
| 4                 | 7.842                     | 7.861                    | 7.242                       | 7.939  |
| 6                 | 9.605                     | 9.628                    | 8.869                       | 9.724  |
| 11                | 13.005                    | 13.037                   | 12.009                      | 13.166   |
| 16                | 15.685                    | 15.723                   | 14.483                      | 15.878   |
| 21                | 17.969                    | 18.013                   | 16.593                      | 18.191   |
| 30                | 21.477                    | 21.529                   | 19.832                      | 21.743   |
| 40                | 24.800                    | 24.860                   | 22.900                      | 25.106   |
| 57.15             | 29.644                    | 29.715                   | 27.372                      | 30.009   |
| 63.50             | 31.247                    | 31.323                   | 28.853                      | 31.986   |





**Figure 8** Analytical comparison of terminal speed models

### ***Kinetic energy***

Kinetic energy is a significant factor used to validate design criteria. The law of conservation of energy states that potential energy (PE) before an event must equal the kinetic energy (KE) after an event [26].

$$PE = KE$$

$$mgh = \frac{1}{2}mv^2$$

Where:

m = mass

h = drop height

g = acceleration of gravity

v = velocity at impact

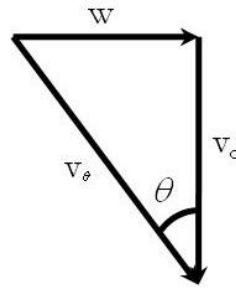
The net work ( $W_{net}$ ) required to stop an object in movement is equal to its kinetic energy. During an impact, the change in kinetic energy is equal to the average force of impact times the distance traveled for the object. This leads to the work-energy equation:

$$W_{net} = \frac{1}{2} m(v_{final}^2 - v_{initial}^2)$$

In a drop test, the initial velocity ( $v_{initial}$ ) is equal to zero, therefore  $W_{net} = 1/2 m v_{final}^2$ .

### ***Impact angle***

Impact angle has a significant influence on the kinetic energy, as the resultant velocity increases with respect to the angle of the surface. Wind changes the falling direction of a hailstone from a vertical falling path to form a new trajectory impact angle  $\theta$  as shown in Figure 9, that is equal to the arctan  $w/v_o$ , where  $w$  is the wind speed. The impact speed is  $v_{\theta} = (v_o^2 + w^2)^{1/2}$ .



**Figure 9** Resultant impact speed at  $\theta$

Table 3 shows the results of hail of an impact resistant test method for roof coverings in targets at 45° and 90° angles [27].

**Table 3** Resultant velocity and kinetic energy of hailstones at 45° angle and free-fall [26]

| Diameter<br>nom. | Weight   |           | Terminal<br>Free-Fall<br>Velocity | Resultant<br>Velocity<br>45° Angle | Kinetic Energy                  |                            |
|------------------|----------|-----------|-----------------------------------|------------------------------------|---------------------------------|----------------------------|
|                  | <i>g</i> | <i>lb</i> |                                   |                                    | <i>ft-lb<br/>Free-<br/>Fall</i> | <i>ft-lb<br/>45° Angle</i> |
| 1                | 7.85     | 0.0174    | 73                                | 103                                | 1.43                            | 2.57                       |
| 1.5              | 26.5     | 0.0588    | 90                                | 127                                | 7.35                            | 14.72                      |
| 2                | 62.81    | 0.1394    | 105                               | 148                                | 23.71                           | 47.49                      |
| 2.5              | 122.67   | 0.2723    | 117                               | 165                                | 57.48                           | 115.17                     |
| 3                | 211.98   | 0.4705    | 130                               | 183                                | 122.55                          | 245.70                     |

### ***Impact energy***

Impact testing is performed to determine the energy absorbed and corroborate designs to guarantee the product’s durability and safety requirements. The total energy is conserved while no other external factors are present during the impact event; hence, the kinetic energy absorbed by the surface during a hail impact event can be calculated by

$$E_{absorbed} = \frac{1}{2}mv_{final}^2$$

Laurie [28] analyzed the data collected by Bilham and Relf [29] in prior research in Table 4 related to hail sizes, terminal velocity, and impact energy.

**Table 4** Terminal velocities and energies of hailstones [28]

| Diameter      |           | Terminal Velocity |              |              | Approximate Impact Energy |               |
|---------------|-----------|-------------------|--------------|--------------|---------------------------|---------------|
| <i>inches</i> | <i>cm</i> | <i>ft/s</i>       | <i>mi/hr</i> | <i>m/sec</i> | <i>ft-lb</i>              | <i>Joules</i> |
| 1             | 2.5       | 73                | 50           | 22.3         | < 1                       | <1.36         |
| 1-1/4         | 3.2       | 82                | 56           | 25.0         | 4                         | 5.4           |
| 1-1/2         | 3.8       | 90                | 61           | 27.4         | 8                         | 10.9          |
| 1-3/4         | 4.5       | 97                | 66           | 29.6         | 14                        | 19.0          |
| 2             | 5.1       | 105               | 72           | 32.0         | 22                        | 29.8          |
| 2-1/2         | 6.4       | 117               | 80           | 35.7         | 53                        | 71.9          |
| 2-3/4         | 7.0       | 124               | 85           | 37.8         | 81                        | 109.8         |
| 3             | 7.6       | 130               | 88           | 39.6         | 120                       | 162.7         |

Different impact standard test methods were performed for roof covering and membranes concluding that there are significant variations in the procedure, and also in the results [27]. The following table, Table 5, presents the kinetic energies of the ASTM, FMRC and UL methods.

**Table 5** Kinetic energies produced by ASTM, FM, and UL standards test methods [27]

| Standard      | Missile Parameters         |                        |                            |                            |
|---------------|----------------------------|------------------------|----------------------------|----------------------------|
|               | Diameter<br><i>in (mm)</i> | Mass<br><i>lb (kg)</i> | Distance<br><i>ft (mm)</i> | Energy<br><i>ft-lb (J)</i> |
| ASTM D3746    | 2 (50)                     | (2.27)                 | 4'5" (1355)                | 22 (30)                    |
| FM Class I-SH | 1.75 (45)                  | (0.360)                | 17' 9.5" (5400)            | 14 (19)                    |
| FM Class I-SH | 2 (51)                     | (0.737)                | 5 (1500)                   | 8 (10.8)                   |
| UL Class 1    | 1.25 (32)                  | 0.28 (0.127)           | 12 (3700)                  | 3.36 (4.6)                 |
| UL Class 2    | 1.5 (38)                   | 0.48 (0.218)           | 15 (4600)                  | 7.2 (9.8)                  |
| UL Class 3    | 1.75 (46)                  | 0.79 (0.358)           | 17 (5200)                  | 13.43 (18.3)               |
| UL Class 4    | 2 (51)                     | 1.15 (0.521)           | 20 (6100)                  | 23 (31.2)                  |

Under windy conditions the kinetic energy can be determined by

$$E_{absorbed \theta} = \frac{mv_{final}^2}{2 \cos^2 \theta}$$

Ross [23] deduced that the kinetic energy of hailstones can be determined with the following expression:

$$E_{absorbed \theta} = \frac{3.62 \times 10^6 D_{ice}^4}{\cos^2 \theta}$$

The resulting kinetic energies from this equation are presented below in Table 6.

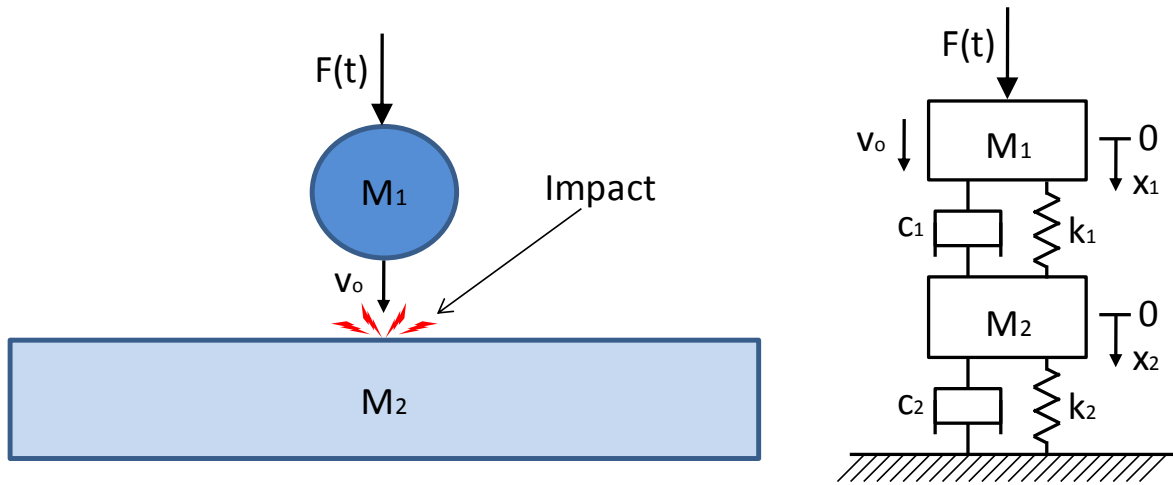
**Table 6** Kinetic energy of hailstones using Ross' equation

| Ice diameter (mm) | Kinetic energy (J) | Kinetic energy (J)    |
|-------------------|--------------------|-----------------------|
|                   | wind speed = 0 m/s | wind speed = 17.5 m/s |
| 25.4              | 1.51               | 2.01                  |
| 31.8              | 3.68               | 4.90                  |
| 38.1              | 7.63               | 10.17                 |
| 44.5              | 14.13              | 18.84                 |
| 50.8              | 24.11              | 32.14                 |
| 63.5              | 58.86              | 78.48                 |
| 69.9              | 86.17              | 114.90                |
| 76.2              | 122.05             | 162.73                |

### ***Impact behavior in material***

Metallic impactors such as steel balls or steel darts in impact test methods can be used to equate the impact energy to the kinetic energy of the ice in the form of hail. Nevertheless, when ice spheres hit a surface such as concrete tile, the ice compresses and crushes upon impact because the surface is much harder. Under the same conditions but using steel balls the concrete tile will fail. Ice spheres and steel balls will have the same impact energy, but the impact failure will be different. These test methods do not always replicate the hail resistance of the material [27]. Experimental, analytical solutions, and simulations conducted in explicit codes via FEA are founded for sphere impact against composited panels or metal surfaces.

The following figure, Figure 10, shows a representation of the sphere impact simulation based on the equation of motion of a single degree of freedom system due to the indentation and geometrical nonlinearities are neglected [30].



**Figure 10** Quasi-static hail impact characterization spring-mass model

$M_1$  = mass of ice

$M_2$  = mass of material

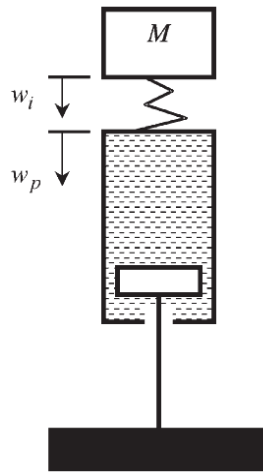
$k_1$  and  $c_1$  correspond to the interaction ice-panel, where  $k_1$  could be nonlinear

$k_2$  and  $c_2$  correspond to the stiffness of the supporting panel

$F(t)$  = Impact force

Some of the parameters for the above model are known or can be determined by physical measurement or numerical simulation. Because the function that describes the contact force which produces an indentation is nonlinear, this model does not provide a rigorous description of the impact event and outcome.

Olsson [31, 32] concluded in his research that the impact response type is related with the impactor and the plate mass rather than impact velocity. He also stated that impact velocity only influences the deflection amplitude. Figure 11 represents the structural model of a composite panel under small mass impact.



**Figure 11** Structural model during small mass impact on plates [32]

Fischer-Cripps [33] analyzed the relationship between elastic contact surfaces during an impact. Figure 12 represents a sphere impacting on a flat specimen. Following the law of the conservation of momentum and the Hertz contact equations, Fischer-Cripps deduced the equation for the impact load that can be used to determine the stress field and displacement:

$$P = \left[ \left( \frac{5}{4} \right)^3 \frac{16}{3} E^{*2} m^3 v_0^6 \right]^{1/5}$$

Where:

P = maximum load

m = mass of sphere

v<sub>0</sub> = sphere velocity

E\* = the combined modulus of the sphere and the specimen given by Johnson [34]

$$\frac{1}{E^*} = \frac{(1 - \nu^2)}{E} + \frac{(1 - \nu'^2)}{E'}$$

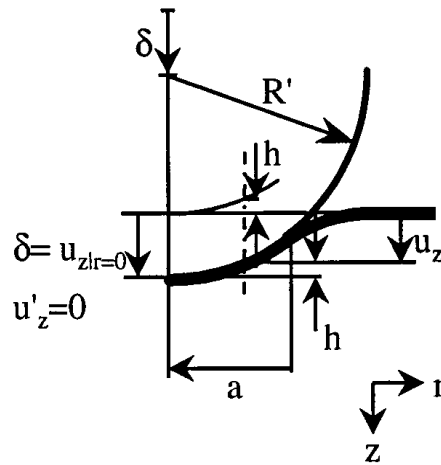
Where:

$E$  = elastic modulus of the sphere

$\nu$  = Poisson's ratio of the sphere

$E'$  = elastic modulus of the specimen

$\nu'$  = Poisson's ratio of specimen



**Figure 12** Schematic of contact between two elastic solids (rigid, spherical indenter, and flat, non-rigid specimen) [35]

The notations for Figure 12 are:

$u'_z$  and  $u_z$  are deformations.

$h$  is the distance between a point on the periphery of the sphere to the specimen surface.

$R'$  is the radius of the sphere.

$a$  is the radius of a circle of contact.

$\delta$  is the load-point displacement.



Kim and Welch [36] determined kinetic energy of a projectile using force transducers and strain gages for measuring the elastic response of the composite panels. Also they performed the test with increased velocities of the ice spheres; therefore, impact energies have slightly higher values for representing aerospace structures in flight. The goal of their research was to study the resulting damage on carbon/epoxy composites panels caused by impacts of ice projectiles. Jackson [2] remarked that the impact force that is developed for large-masses can be use as a key parameter in order to predict delamination damage formation on structures.

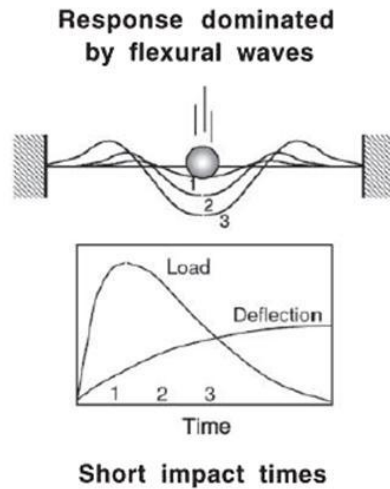
Asp [37] compared the empirical methods of Kim [36] and the analytical models Olsson [32, 38] using Ultrasonic C-scan pictures and a laser displacement transducer. The result of Asp's work determined that the empirical methods offer a close approximation of the damage resistance of composites for high velocity impacts (100 to 150 m/s). Asp also determined that the analytical models are not satisfactory when ice impact is used against the non-crimp fabric composite plates.

Other experiments [2] and standard test methods are used to analyze the impact of metallic indenters or spheres at low velocity on thick composite plates. Since all the proceeding work [2, 32, 36-38] involves ice impacts at velocities much greater than 30 m/s on thick and hard composite surfaces, those experimental analyses cannot be applied for the designs assembled for the work in this research.

### ***Wave propagation***

The stress waves caused by the impact of a spherical object on a composite induce plastic deformation near the point of impact and elastic deformation in the surrounding area of the composite [39]. The stress waves travel from the front surface to rear surface and then return from the rear surface. Also, there is a reflected stress wave which goes through the spherical object

producing a fluctuation phenomenon [40]. Olsson [31, 32] related the response on composites plates impacted by hail with flexural waves and shear waves.



**Figure 13** Response during small mass impact on plates [32]

Researchers have studied impacts on composite fabrics using simulations with finite element methods. Nasr-Isfahani [41] compared his results with previous reported experiments observing that when a spherical object initially contacts a fabric or panel, the deformation wave is equal at the origin point of contact from the impact, and then the longitudinal waves propagate much faster than the transverse waves.

Replication of experiments from relevant references is needed in order to extend the capabilities to specifically study the effects of hail damage in personal aircraft, vehicles, and ground structures. This investigation is intended to utilize the aforementioned information to evaluate and design more effective protective fabrics of various textile fabric configurations and plastic materials.

At the present time, there is no work which represents any concept, product, application or process that completely or effectively addresses the safety and environmental hazards that expose the aircraft, vehicle, and ground unit to costly damage and serious injury and possible death as a

result of the damage imposed. For example, the exterior and interior of an aircraft are constructed with materials that are very susceptible to deterioration and damage from various environmental elements such as sun, heat, thunderstorms, hail, rain & fuel contamination, bird and animal nesting and droppings, freezing rain, frost, ice, snow, and extreme cold.

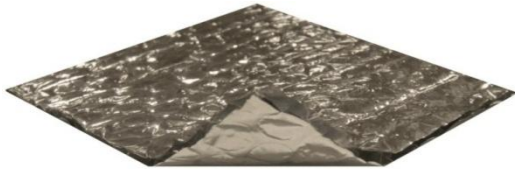
### 3. EXPERIMENTAL DESIGN

#### 3.1 Materials

Commercial polymer films and fabrics were used for this research. These materials were chosen as the best candidates for evaluating the physical properties that need to be studied in this project based on laboratory sampling of critical characteristics. The materials used for the experiments were:

- (a) TempShield™ Single Bubble/Double Foil - one layer of 5/32" barrier bubble film laminated between two layers of metalized film [42]. One of its reflecting sides has a circular embossing while the other side has triaxial embossing on the surface.
- (b) TempShield™ Single Bubble/White Foil - one layer of 5/32" barrier bubble film laminated between one layer of metalized film and one layer of polyethylene [42].
- (c) Super R Plus™ - two-sided reflecting metalized film with polyester scrim reinforcement [42].
- (d) Temptrol™ Heat Reflecting Fabric - polypropylene based non-woven perforated and metallized one side [42].
- (e) 100% stitchbonded carbon fiber fabric.
- (f) 50% carbon fiber / 50% aramid (Kevlar® 49 brand) stitchbonded fabric.
- (g) Bubble wrap produced by IPS Packaging.
- (h) Polyethylene film

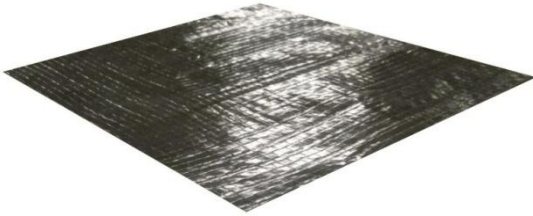
The materials are shown in Figure 14.



(a)



(b)



(c)



(d)



(e)



(f)



(g)



(h)

**Figure 14** Physical appearance of materials used in designs

The complete specifications and the applied methods of the material of Innovative Insulation Inc. are presented in Appendix A.

### **3.2 Methodology to test the materials**

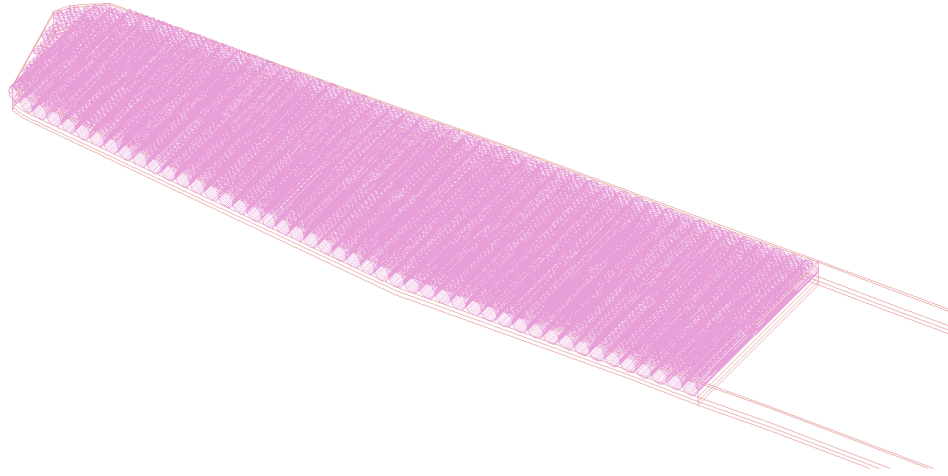
In order to find a methodology for a solution design, a cover for an aircraft such as Cessna 172 with a wingspan of 11 m (36 ft 1 in), illustrated in Figure 15, is used to describe the layer requirements. The total plan of development and testing the cover design consists of two steps.

#### ***Step 1: Characterization of layers***

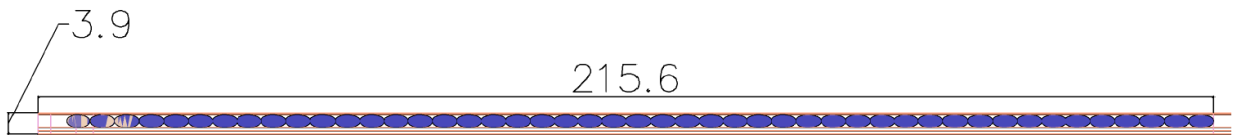
In this step the individual layers were tested in order to identify their physical characteristics using different testing methodology standards according to the layer requirement.

Outside layer requirements:

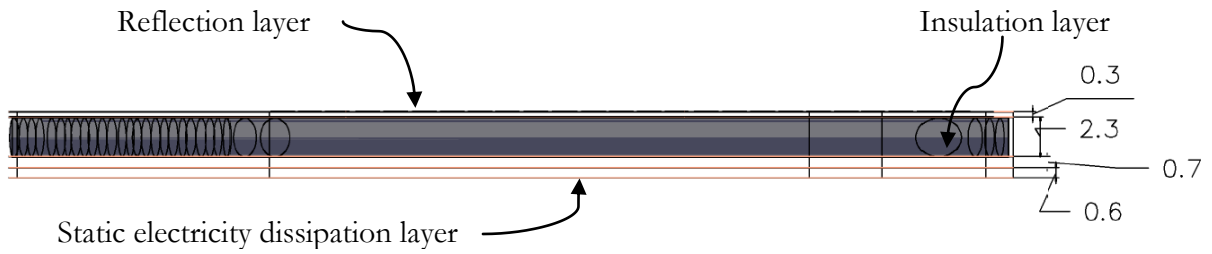
1. Lightweight.
2. Abrasion resistant.
3. Low friction coefficient.
4. Folding capability.
5. Infrared/heat reflection.
6. UV resistant.
7. Impact resistant.
8. Tear and puncture resistant.
9. Burst resistant.



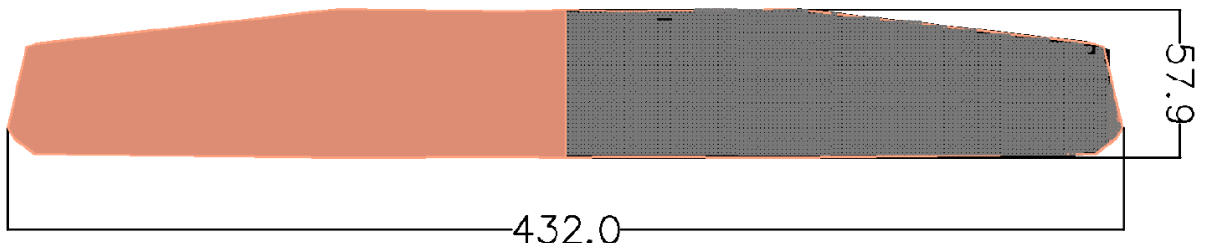
(a) Perspective view



(b) Front view



(c) Side view



(d) Top view

**Figure 15** Depictions of multilayer protective cover design (units in inches)

Inner layer requirements:

1. Lightweight.
2. Impact resistant.
3. Burst/rupture resistant, also strength and elongation.

Base layer requirement

1. Lightweight.
2. Static charge resistant.
3. Flame resistant.
4. Air permeability.

The test results for each layer were organized and ranked in a matrix that permits a direct comparison between the expected use properties and the actual properties of the candidate materials. The selection of the materials is made based on the material with the highest sum.

### ***Step 2: Composite characteristics***

With the outcome information of Step 1, Step 2 consisted of creating two reasonable sample composites of vehicle and structure coverings which can serve to simulate the actual final form and construction of the composite. Afterward, the conglomerate composite structures were tested in order to determine if it still passed the impact absorption test.

This step also determined feasible methods of forming and consolidating any or all of the proposed final structures and testing the fastening and consolidating points for possible tensile, reflectance and or pneumatic seal failure.



### **3.2.1 Areal density**

The protective cover has to be lightweight because it needs to be carried and stored easily either in the airplane or vehicle. By measuring each sample's weight, dimension, and the knowing the area of the airplane, the total mass or areal density of the protective cover can be predicted depending on the material combinations being used.

### **3.2.2 Abrasion test**

This test was conducted in order to evaluate the resistance of the outside layers to abrasion by measuring the weight loss. The abrasion testing was performed by using the "Abraser" standard abrasion tester, Figure 16. The abrading wheels used in this test were CS-10 which have mild-medium abrasive action for coatings, plastics, and textiles products. The load applied against the specimen was 500 g per wheel.

The specimen of 4 in (102 mm) diameter was weighted using a digital balance. Then, the specimen was placed on the specimen holder and subjected it to the wear action of the two abrading wheels. The measurements of weight loss were made after 10, 25, 50 and 100 cycles of abrasion. A stereoscope was used for observing the removal of the metalized coating of the materials from its surface after the defined cycles of abrasion.



**Figure 16** Abraser

### 3.2.3 Friction test

The friction test was used to measure the frictional properties of the outside layers when these layers undergo sliding contact with other surfaces. The specimen was clamped to the rectangular metal table that was mounted on the Instron testing machine as is shown in Figure 17. The 100 N load cell is connected to the sled weight (210 g) by a thin nylon rope. The aluminum sled was pulled at 150 mm/min across the material's surface by the cross head.



**Figure 17** Friction test fixture

### 3.2.4 Folding test

The folding endurance tester was used to determine the number of folds that the material would resist after rupture failure. The outside layer materials were tested in the folding endurance tester under a constant tension load of 1.5 kg. The specimens were held in jaws and then folded until cracks or ruptures occurred at the crease. Due to the dimensional capacities of the available holding jaws, the inner and the base layers were not tested.



**Figure 18** Folding endurance tester

### 3.2.5 UV resistance test

The QUV accelerated weathering tester was used to evaluate UVA light of the outside layer materials. This test chamber apparatus reproduces damage caused by sunlight UV. The reflective side of each material faced the UVA 340 lamp for two weeks. After the requisite 14 days of irradiation, the samples were removed from the chamber. No measurements of irradiance or radiant exposure were made during the exposure. FTIR was used to identify changes in structure of the polymeric material during the exposure. A specimen of Single Bubble/Double foil was tested to observe impact properties changes.



**Figure 19** QUV Weathering tester

### **3.2.6 Impact resistance (impact test)**

The impact testing was performed by using the Instron Dynatup. This machine has a tup with a semi circular shaped end that is dropped onto the sample to be impacted. The tup is connected to the load cell by a weight of 2.3814 kg.



**Figure 20** Instron Dynatup

The total weight falling down to impact the samples was 2.7258 kg including the tup and tup bolt. It is evident that this weight was much higher than a typical hailstone. The samples used in this impact resistant test were the outside and inner layers. As shown in Figure 20 the sample was placed in a frame that prevents rotation of the specimen.

### **3.2.7 Tear resistance**

The tear resistance test was used to measure the tear propagation resistance of the outside layers when these experience a tear load. The specimen was secured to the grips where one grip was fixed and the other moved by the cross head at 250 mm/min. The tear propagation test has been done on the Instron testing machine as shown in Figure 21.



**Figure 21** Tear test

### **3.2.8 Bursting strength test**

The bursting strength test was used to measure the bursting strength of the outside and inner layers to simulate what happens in the end use. The specimen was placed on the ring of the ball

burst attachment that was mounted on the Instron testing machine as is shown in Figure 22. A steel ball bursts the material when the specimen is pushed by the action of the cross head at 12 in/min



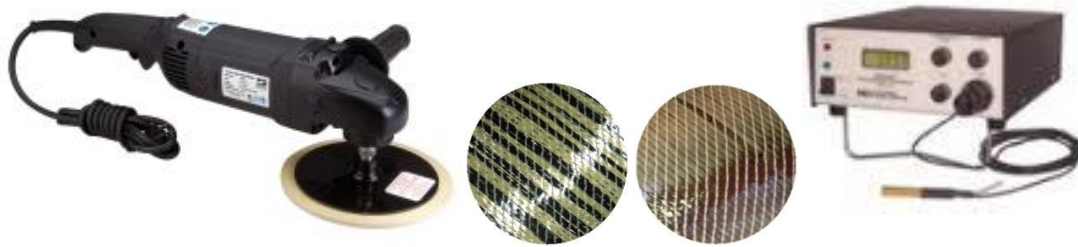
**Figure 22** Burst test

### **3.2.9 Static charge resistance**

This innermost (or bottom layer) has to dissipate the static charge and inhibit electrical spark. Cold weather can exacerbate the occurrence of static discharge spark generation where certain polymeric materials are in contact with polymer film paints and where a high dielectric constant exists between the two surfaces. Removal of the vehicle or aircraft covers in those or similar conditions can cause a dangerous spark near fuel tanks that could result in an explosion.

ASTM standards for measuring static dissipation and dielectric constants do not have relevant methodologies applied to this end use. A static measuring device (Voltmeter Isoprobe Model 244 Monroe-electronics) provided by the department of Electrical Engineering (Auburn University) was used for testing of the inner (base) layer of the composite structure.

The prepared sample was attached to a buffer, and the buffer rubbed at high rpm against the painted and unpainted aircraft's surface. Then, using an electrostatic voltmeter, the aircraft's surfaces electrostatic charges were measured.



**Figure 23** Static test

### 3.2.10 Flame resistance

Samples were cut to 3 by 12 inches, and the exposed sample ends were covered with aluminum tape. The specimen was positioned vertically as shown in Figure 24. The flame was applied to the specimen for 12 seconds and then removed. The outside layers were tested to determine their response to an ignition source. The afterflame time was recorded as a characteristic of this test.



**Figure 24** Chamber flame resistant test

### 3.2.11 Air permeability

Using the Frazier low differential pressure air permeability tester, the air permeability of the samples were obtained. The specimens of the base layer were placed on the specimen holder to create vacuum. Air is forced to pass through a nozzle with an orifice of 4 mm due to an applied suction from a motor.



**Figure 25** Frazier low differential pressure

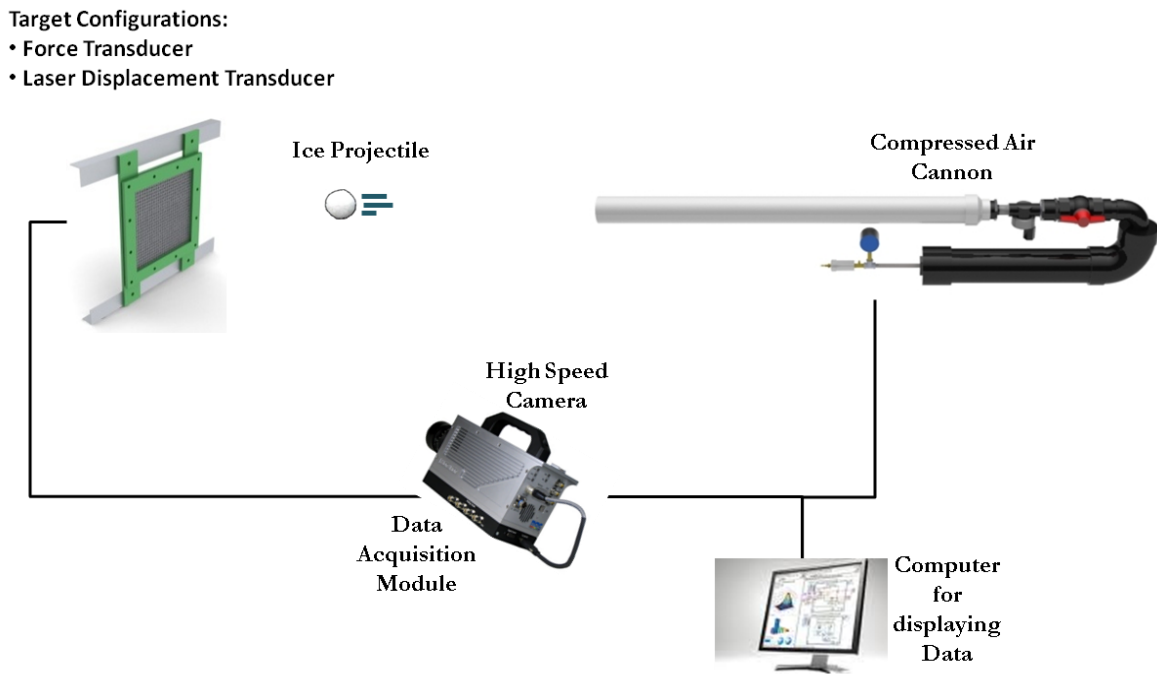
### 3.2.12 Hail impact simulation

To test different designs and determine the impact resistance requirements from a combination of appropriate polymeric materials, an experimental test chamber was designed and constructed. The experimental set-up allows running test samples using ice projectiles instead of running test samples in drop weight testing machines where a steel penetrator is utilized. This equipment helped to simulate impact absorbing tests on materials with a closer approximation to the real events.

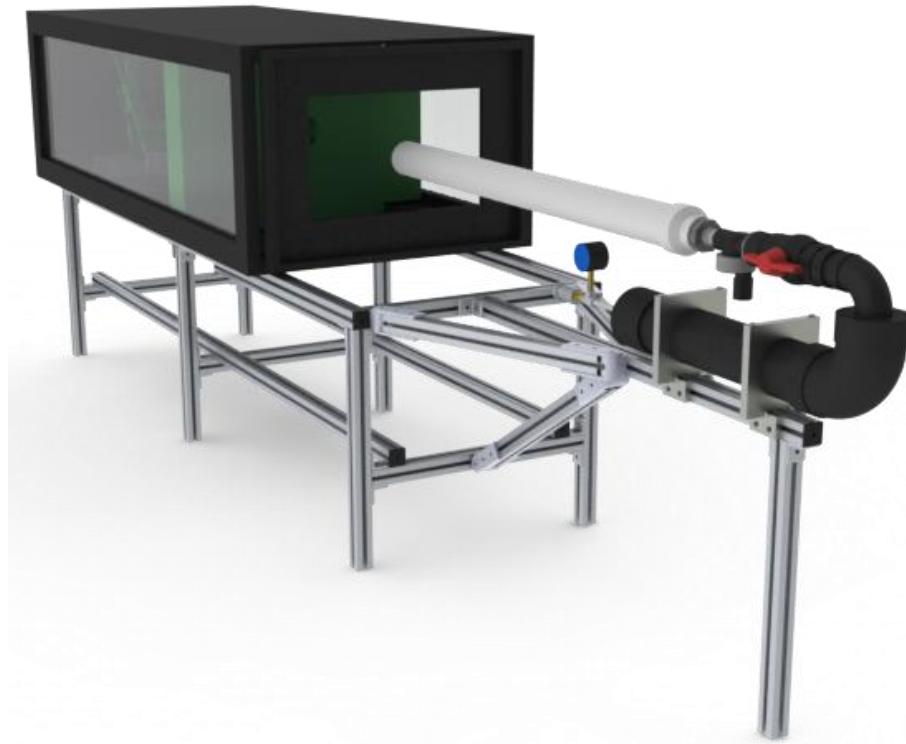


In order to test the sample composite covers, an experimental set-up was built and assembled. The following information is a description of the experimental set-up including specific technical details of the test equipment, instrumentations, and apparatuses.

The test cabinet houses the illumination source and the frame where the target is fixed. A high speed camera is located outside the cabinet with a data acquisition system. A compressed air cannon launches an ice projectile to the target configurations. A schematic representation of the experimental set-up is shown in Figures 26 and 27.



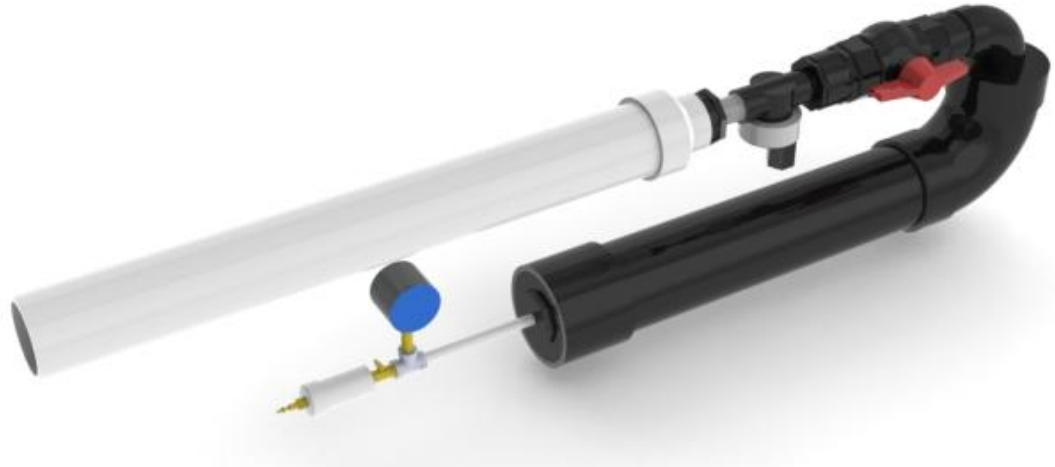
**Figure 26** Experimental scheme set-up



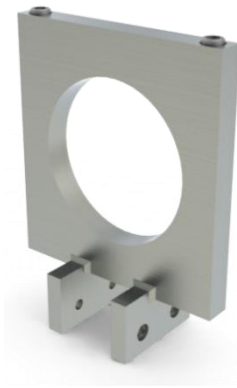
**Figure 27** Experimental set-up

### **Compress air cannon**

The high velocity cannon (Figure 28) was made with schedule 40 PVC pipe and braid reinforced using a braiding machine. Multiples layers of fiber glass were applied over the reservoir. Polyester resin was applied along with resin transfer molding to infuse fiber to the resin matrix, and with this process a higher level of safety is achieved. An electro-valve is in line with the reservoir and barrel for the trigger mechanism; this system uses a solenoid to release pressure through the barrel. The system for aiming incorporates a fixed reservoir (Figure 29), and the barrel is minutely adjustable with a screw-type system in order to fine tune its accuracy. With this compressed air cannon it is only possible to fire single ice projectiles.



**Figure 28** Compressed air cannon

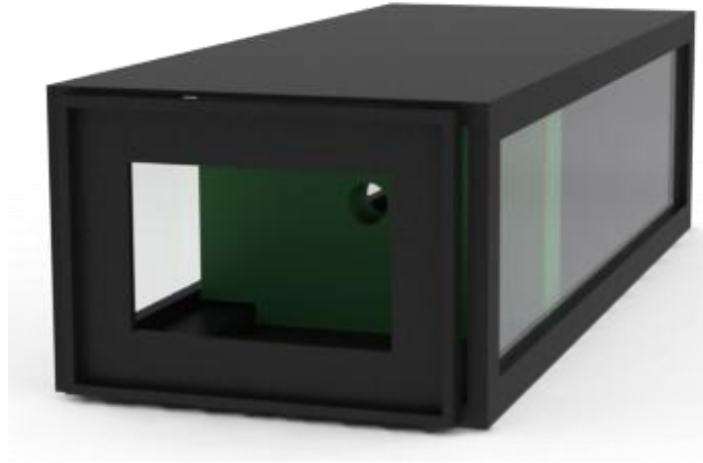


**Figure 29** Air cannon fixture

### **Test chamber**

A cabinet measuring 2 x 0.84 x 0.58 meters (Figure 30) was redesigned with two sections divided by a safety wall composite assembled of contact film, balsa wood and polystyrene foam. The first sectional area is where the discarding sabot used to secure the ice is trapped by the wall to prevent a possible second impact from the sabot, and the second sectional area is where the final velocity is determined using a high speed camera. Impact and deformation measurements are logged upon

registration. The test chamber shown in Figure 30 is mounted onto an aluminum frame shown in Figure 31.



**Figure 30** Test chamber

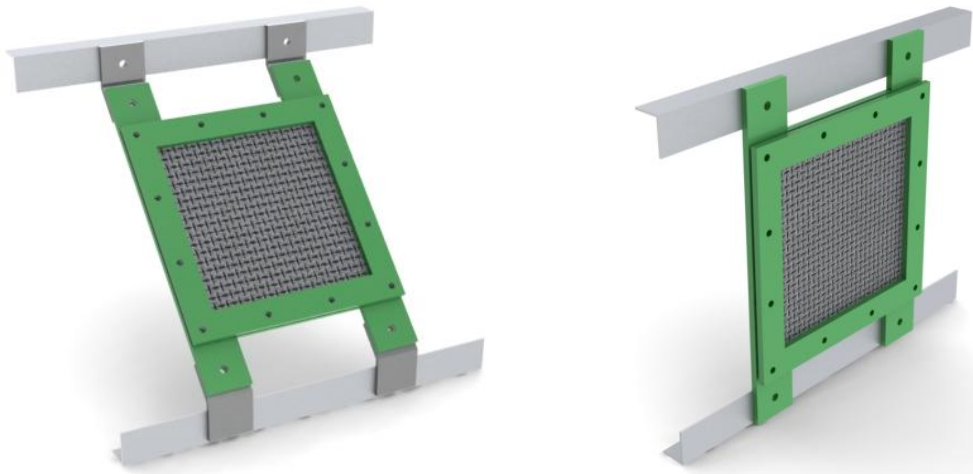
In the second sectional area, there is an A36 steel frame with 349.25 x 349.25 mm dimensions which was manufactured to allow two mounting systems in two angles of incidence, 45° and 90°, as shown in Figure 32. The force transducer mounting system is aluminum square tubing, which mounts to the base frame; this holds the sensor base for attaching the force transducer. The base frame is attached to the chassis of the test cabinet in a 90° angle with a stainless steel angle bracket. However in the 45° set-up, it is attached with A36 steel clamps with a horizontal spacing of 0.38 m. In addition, there are 1250 Watt halogen lights to provide appropriate illumination for the high speed camera. The high speed camera with a scale will record the impact event, and with this data, the terminal velocity can be determined.

The test chamber was redesigned with gas shocks to provide an unattended open position of the doors for the new test set-ups. There are also inspection windows made of Plexiglass that allow quick and easy access during fine tuning equipment and test specimen replacement. There is a sliding door that prevents wind blast that may alter recorded velocities; also if there is discrepancy with the

path of the projectile in the first section, this will provide ricochet protection, and it allows access to the charging of ice projectiles diameters to the cannon.



**Figure 31** Experimental set-up frame



**Figure 32** Targets at 45° and 90°

### **Equipment Cabinet**

This cabinet is the housing for all electronic data logging components of the experimental set-up, such as the signal conditioner model 482A21, computers, and power supply. The software

installed on the computer for data acquisition is Hot Shot SC, and the information collected will be simultaneously recorded for post-analysis.

There are two kinds of experiments:


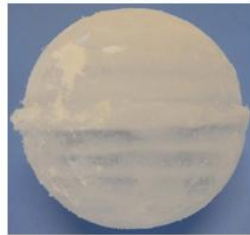
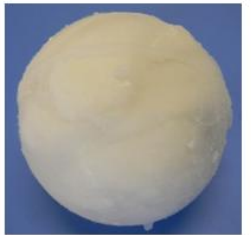
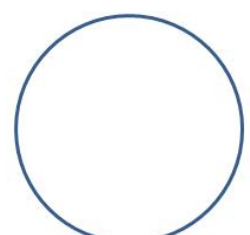


- **Ice impact force measurement** for observing and measuring the parameters of ice such as diameter, velocity and kinetic energy.
- **Ice impact on the target** for measuring the damage or failure of the value of impacting kinetic energy on polymer configuration.

The camera is placed beside the test chamber, and both test configurations are recorded using the high speed camera NAC HotShot 512 SC, that has an attached Multi Channel Wave Inserter communicating via high speed serial IO port. The collected data as a time waveform can be played in sequence with the image frame. The camera can take up to 10,000 frames per second with a shutter time (exposure time) of 10  $\mu$ s in order to record the images of the impact event. The velocity of the impact was measured using the software HotShot SC Link and its measurement tools. To calibrate the image, the “pixels per unit” are determined by selecting two points on a frame with a metric scale along the trajectory. From knowing this value and tracking two interval positions along the flight path on the recorded images, the velocity is calculated.

### **Ice impact force measurement**

Three different ice spheres diameters of 28.5, 40.5 and 57 mm (1.12, 1.59, 2.24 in) were formed to simulate hail in ice trays molds at -18°C (0°F). The densities of the ice spheres used in this experiment were roughly 0.94 gm/cm<sup>3</sup>.

Three different ice sphere structures were molded due to the absence of real hailstones, which have a similar spherical layer formation to that of an onion. These three structures are shown in Figure 33. The monolithic ice construction was cast by filling the mold with water in one session. The layered ice construction was made in multiple events, approximately 10 layers, by pouring water in the mold. The cotton filler ice construction was prepared with cotton filler previously dipped in water and placed into the mold, and then the mold was filled with water. The layered ice and the ice sphere with cotton filler constructions were produced to simulate a tougher ice projectile than a monolithic sphere. Table 7 indicates the weight proportion of cotton to ice according to diameter base on the standard test method F 320.

| <b>Construction</b>   |   |  |
|---|---|--|
| <b>Monolithic</b>   | <b>Layered</b>  | <b>Cotton fillers</b>  |
|  |  |  |
|  |  |  |

**Figure 33** Ice constructions

**Table 7** Filler weight for each diameter

| Diameter (mm) | Filler weight (g) |
|---------------|-------------------|
| 28.50         | 1.37 – 1.43       |
| 40.50         | 3.86 – 1.43       |
| 57.00         | 10.83 – 11.29     |

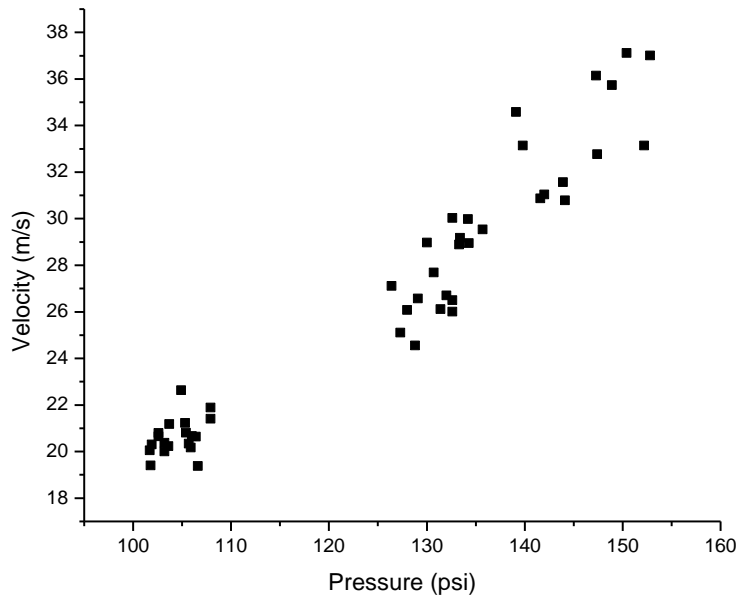
The molds were placed in a refrigerator at -15 to -21°C (5 to -6 °F). The ice spheres were removed from the mold and stored in polyethylene bags and then placed back in a freezer. The ice sphere was taken out from the freezer approximately 3 minutes before the launch. During this 3 minute period, the mass of the ice was recorded and put into a foam sabot. A foam sabot as shown in Figure 34 for each diameter was used to carry the ice projectiles. The ice spheres were launched from the compressed air cannon at different pressures in order to determine the impact velocity as is shown in Figure 35. The pressure was regulated by a valve just before the inlet of the pressure gauge, and then the ice projectiles were fired at the desired impact velocity.



**Figure 34** Foam sabot for varying diameter projectiles

A comparison of the impact results was conducted in order to visualize any effect of the simulated ice constructions.

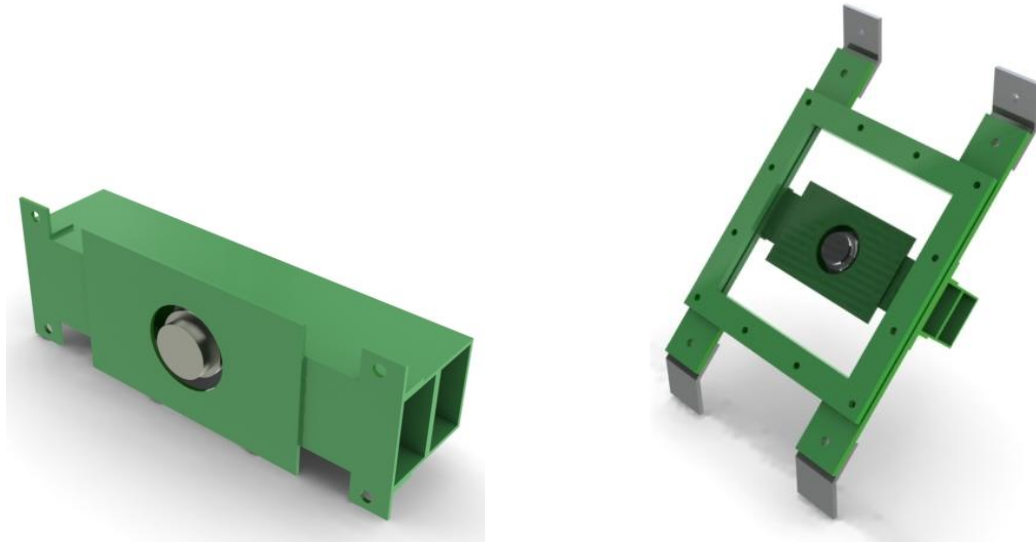




**Figure 35** Pressure vs. Velocity

The initial ice impact force measurement is conducted with a dynamic force transducer (Figure 36), a PCB model 200C50 with 50,000 lb (222.4 kN) compression rating, that has a stud where the ice impacts. The force transducer’s voltage output is transmitted to the BNC input jack on a sensor signal conditioner PCB model 482A21. The signal conditioner amplifies and filters the DC signals from noise and sends them to the Multi Channel Wave Inserter that is connected to the camera.

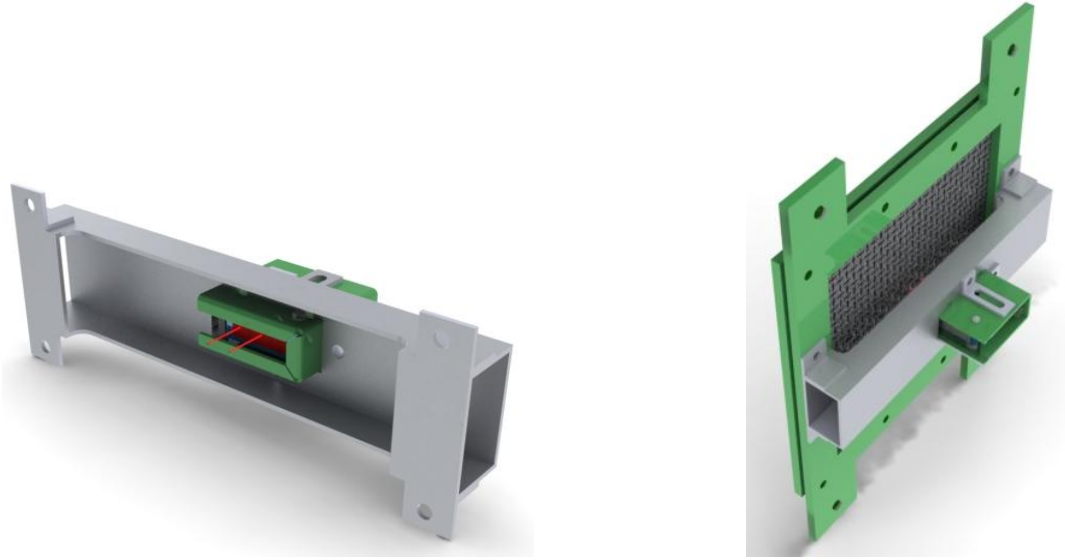
Approximately 90 individual shots impacted against the force transducer at 90° angle and 40 at 45° angle. With this initial set-up, the recorded and observed data such as the ice size, velocity, and impact force are analyzed and quantified to provide appropriate parameters for the second part of the experiment.



**Figure 36** Force transducer set-up

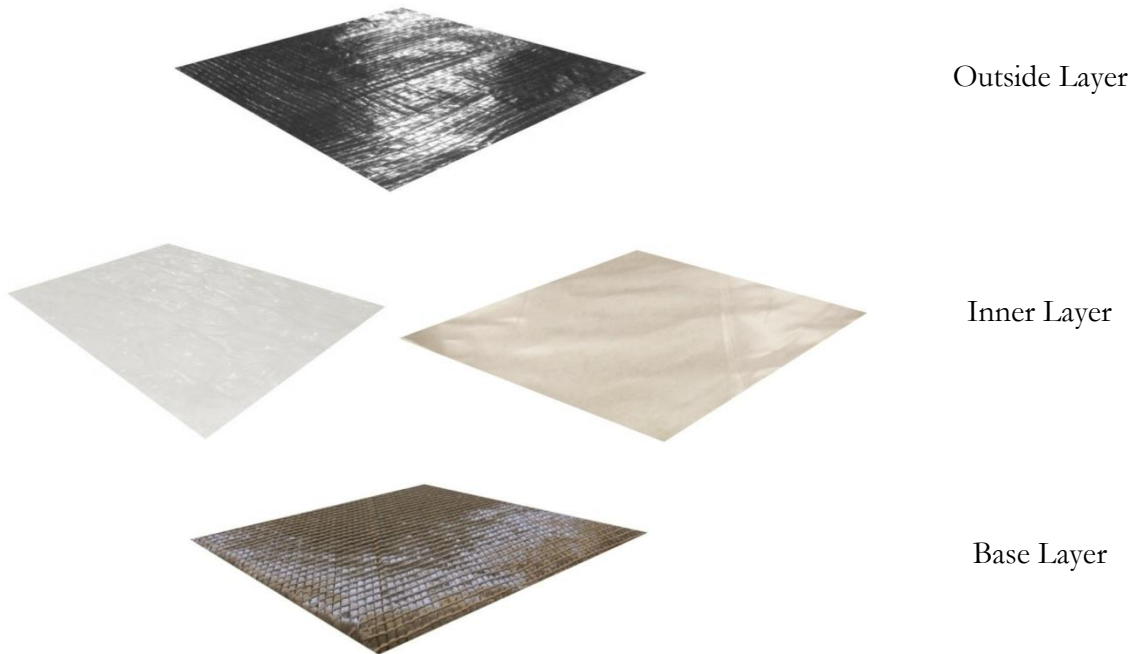
### **Ice impact on the target**

The second set-up is for composite material testing. The testing apparatus has a square frame (Figure 37) which symmetrically clamps the specimen. This provides a uniform compressive force along the perimeter of the tested material in order to prevent rotating, and allows in-plane freedom. Spherical ice projectiles of monolithic, layered and cotton filler constructions had three different diameters each (28.5, 40.5, and 57 mm). Each kind of projectile was shot toward the composite target that is fixed in the A36 base frame which presents a free surface of 266.7 x 266.7 mm. The velocity ranged from 20 to 30 meters per second. The impact point is positioned at the center of the square surface material. Behind the material, a laser displacement sensor (SICK OD2-P30W04U0) is placed to 30 mm from the center with a measuring range of 26 to 34 mm with an accuracy of  $\pm 0.02$  mm. The response time of the displacement sensor is 3.5 ms with a resolution of 0.002 mm. Once the composite specimen was impacted, the deformation was measured at a pre-located point on the material during impact conditions.



**Figure 37** Laser displacement transducer set-up

The test targets that were evaluated included two sample composite configurations according to the results of the test in Step 1. Figure 38 shows the layer arrangement of each composite material tested.



**Figure 38** Composite target model detailing its composition

The polyethylene film configuration in this experiment consisted of pumping air between the two films in order to create a cushion. Ten composite targets of each configuration were impacted. Each configuration was impacted by the launched ice projectiles of 28.5, 40.5 and 57 mm diameters.

The ice spheres impacted the selected composite targets which were at 45° and 90° angles to the test target plane. At a 45° angle, the ice projectile's kinetic energy increases considerably. This scenario simulates hail in an extreme wind. Figure 39 shows the ice's expected projectile path.



**Figure 39** Expected ice projectile path

The frames of the composite center deflection time history were recorded using the high speed camera during the impact event.

## 4. EXPERIMENTAL RESULTS

### 4.1 Areal density

Table 8 summarizes the areal densities of each material. For the outside layer, the heat reflecting fabric has the lowest areal density while the single bubble/double foil has the highest value. Bubble wrap and carbon fiber fabric have the lowest areal density for the inner and base layers, respectively.

**Table 8** Areal density results

| Layer   | Material                            | Thickness (mm) | Area (m <sup>2</sup> ) | Weight (g) | Areal density (g/m <sup>2</sup> ) |
|---------|-------------------------------------|----------------|------------------------|------------|-----------------------------------|
| Outside | Single Bubble/Double Foil           | 4.32           | 0.024                  | 4.27       | 177.95                            |
|         | Single Bubble/White Foil            | 3.24           | 0.024                  | 3.79       | 155.47                            |
|         | Heat Reflecting Fabric              | 0.39           | 0.022                  | 2.11       | 96.34                             |
|         | Two-sided Film with Polyester Scrim | 0.18           | 0.023                  | 2.96       | 127.84                            |
| Inner   | Polyethylene Film                   | 0.09           | 0.023                  | 2.17       | 96.22                             |
|         | Bubble Wrap                         | 11.54          | 0.090                  | 7.77       | 85.99                             |
| Base    | Carbon Fiber Fabric                 | 0.78           | 0.020                  | 9.14       | 446.72                            |
|         | 50% Carbon Fiber/50% Kevlar         | 1.33           | 0.034                  | 17.08      | 504.40                            |

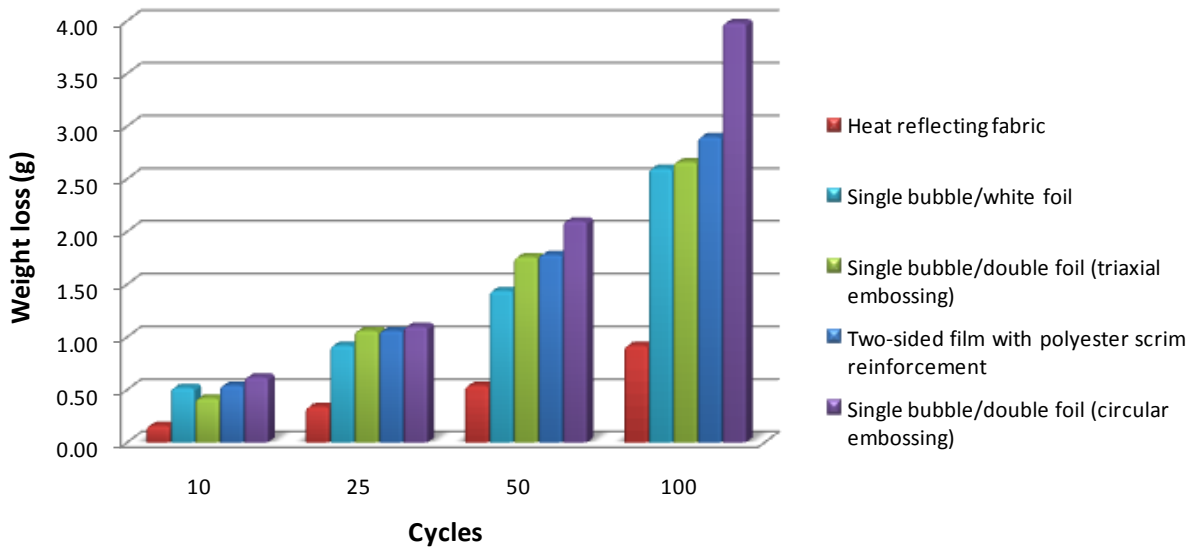
After selecting the lowest values of areal density from each layer and then combining them, the weight of a cover design can be calculated. For example, the wings of an aircraft such as Cessna 172 with a wing area of 16.2 m<sup>2</sup> (174 ft<sup>2</sup>) weighs 10.19 kilograms. The areal density results can be used when the final cover is defined with the rest of the properties.

## 4.2 Abrasion test

The weight loss for the 10, 25, 50 and 100 cycles of abrasion of the outside layers was reported in Table 9. As shown in Figure 40, it has been observed that the heat reflecting fabric has a better response to weight loss when it is exposed to an abrasive medium after 100 cycles. However, its performance after the first 10 cycles did not have good visual results. Table 10 presents a visual historic comparison of the wear abrasion.

**Table 9** Comparison of weight loss on samples after abrasion (g)

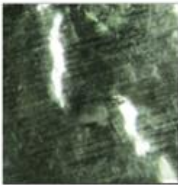
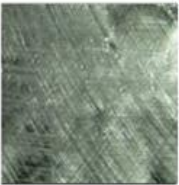

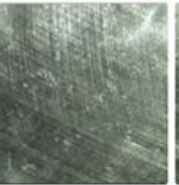

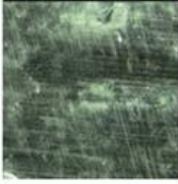
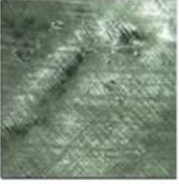
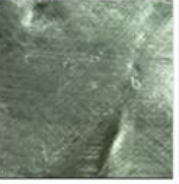
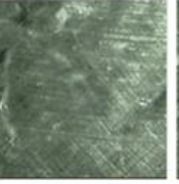
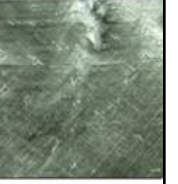

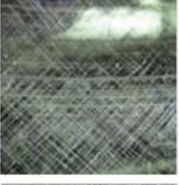
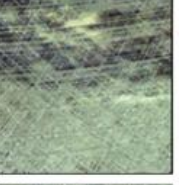
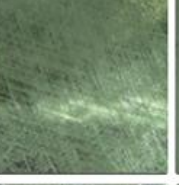


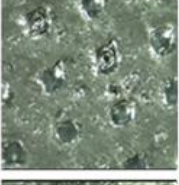
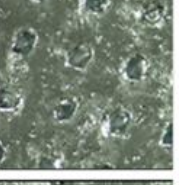
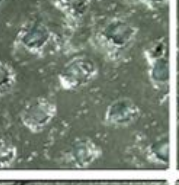
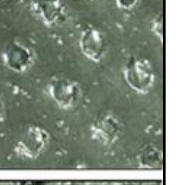
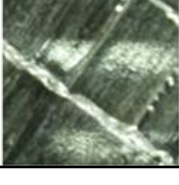
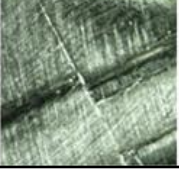
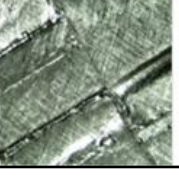
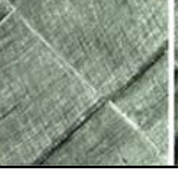
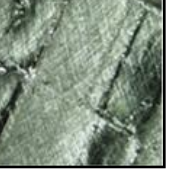
| Material  | Cycles |      |      |      |      |
|---|--------|------|------|------|------|
|   | 0      | 10   | 25   | 50   | 100  |
| Two-sided Film with Polyester Scrim Reinforcement | 0.00   | 0.54 | 1.06 | 1.78 | 2.90 |
| Heat Reflecting Fabric                            | 0.00   | 0.16 | 0.34 | 0.54 | 0.92 |
| Single Bubble/Double Foil (triaxial embossing)    | 0.00   | 0.42 | 1.06 | 1.76 | 2.66 |
| Single Bubble/Double Foil (circular embossing)    | 0.00   | 0.62 | 1.10 | 2.10 | 3.98 |
| Single Bubble/White Foil                          | 0.00   | 0.52 | 0.92 | 1.44 | 2.60 |



**Figure 40** Comparison of weight loss on samples after abrasion

Table 10 clearly illustrates the better performance of the two-sided film material and the double foil on both sides.

**Table 10** Visual comparison of wear abrasion on samples

| Sample   | Cycles  |   |  |   |   |
|--|---|---|--|---|---|
|  | Control   | 10  | 25   | 50  | 100   |
| Single Bubble/Double Foil (circular embossing) |    |    |    |    |    |
| Single Bubble/Double Foil (triaxial embossing) |    |    |    |    |    |
| Single Bubble/White Foil                       |   |   |   |   |   |
| Heat Reflecting Fabric                         |  |  |  |  |  |
| Two-sided Film Polyester Scrim Reinforcement   |  |  |  |  |  |

The heat reflecting fabric lost most of its reflecting coating after the 10<sup>th</sup> abrasion cycle. After the 50<sup>th</sup> cycle, the single bubble/white foil lost part of its metalized coating, and after the 100<sup>th</sup> cycle, it disappeared completely. The double foil material has better performance on the reflecting side with triaxial embossing.

### 4.3 Friction test

The dynamic coefficient of friction was calculated with the average friction force divided by the sled weight. The static coefficient of friction was calculated with the first maximum peak force divided by the sled weight. As shown in Table 11, the best outside layer evaluation result of the dynamic and static coefficients of friction was for the two-sided reflecting film.

**Table 11** Friction test results

| Material                             | Average friction force (Integral) (gf) | Dynamic Coefficient of Friction | Static Coefficient of Friction |
|--------------------------------------|--|---------------------------------|--------------------------------|
| Single Bubble/Double Foil (circular) | 36.40                                  | 0.17                            | 0.22                           |
| Single Bubble/Double Foil (triaxial) | 18.84                                  | 0.10                            | 0.13                           |
| Single Bubble/White Foil             | 50.75                                  | 0.24                            | 0.33                           |
| Two-sided Reflecting Metalized Film  | 10.52                                  | 0.05                            | 0.09                           |
| Heat Reflecting Fabric               | 17.51                                  | 0.09                            | 0.12                           |

### 4.4 Folding test

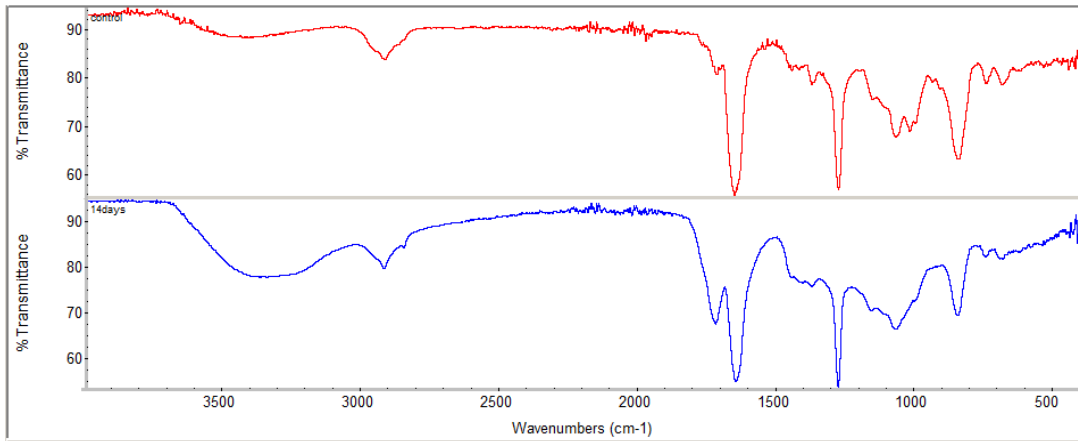
No cracks or ruptures were observed in the samples materials after 1000 cycles, which likely represents more than the occurrence of folding during the life-span of the protective cover.

### 4.5 UV resistance test

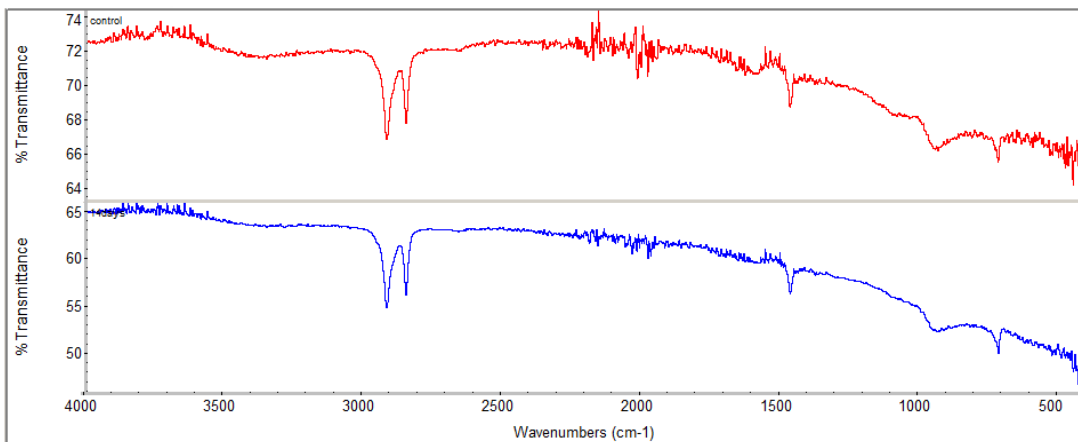
After the exposure of the outside layer materials, no loss of gloss, fading, or cracking were observed. As shown in Figure 40, there are two spectrums plotted for each exposed sample. The red color represents a control specimen and the blue color represents a test specimen. No molecular alterations or new peaks were observed in the heat reflecting fabric, Figure 41(b), when exposed to the ultraviolet light. In the two-sided film, Figure 42(a), there was an observation of a new peak at 955.9 wavenumber, and this may be due to decomposition of the coating material. Diminishing of



the peaks at 1078.5 and 1378.8 wavenumbers in the white foil material was observed, Figure 41(a), but the exact reasons for these changes were not identified. The intensity of a few peaks are observed to be high when compared to their control specimen in white foil and double foil samples.

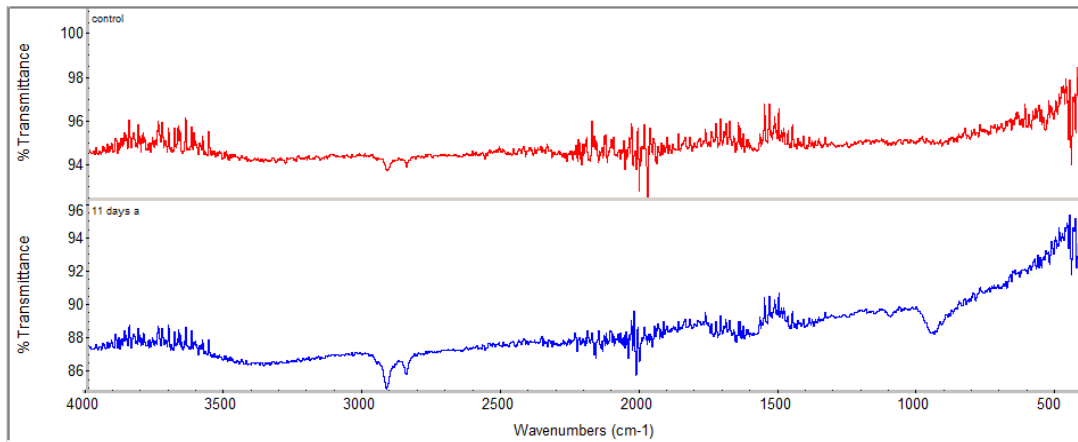


(a) Single Bubble/White Foil

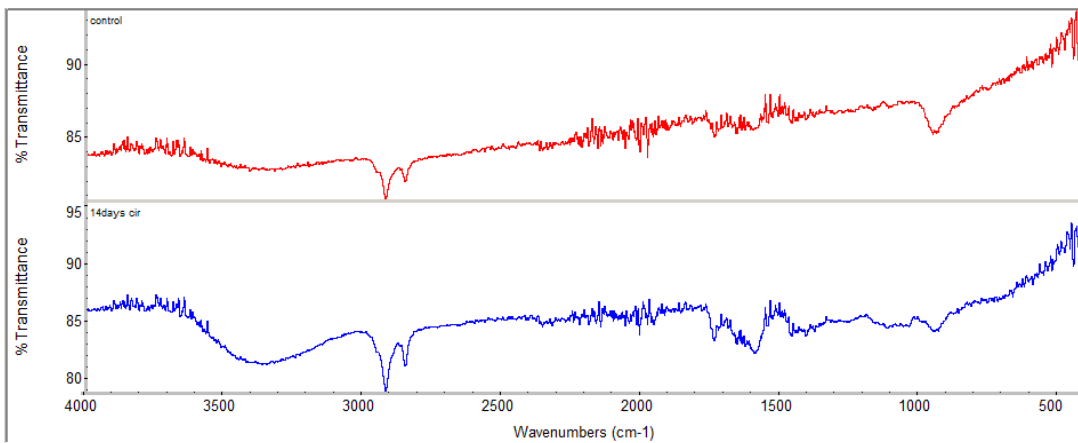


(b) Heat Reflecting Fabric

**Figure 41** FTIR spectra of the outside layers



(a) Two-sided Film with Polyester Scrim



(d) Single Bubble/Double Foil

**Figure 42** FTIR spectra of the outside layers

#### 4.6 Impact resistance (impact test)

Table 12 shows the results of the impact tests. As indicated graphically, the impact energy was similar for all the tests. The energies obtained from the impact tests were similar to hailstone impact of 1 to 1 ¼ in diameter. Their energies were measured between 1.36 to 5.4 J. The outside material that exhibited a better impact response was the two-sided film. Polyethylene film had more than double the energy of the maximum load of the bubble wrap material.

**Table 12** Impact test results

| Layer   | Material                            | Maximum Load (N) | Time to max load-1 (ms) | Impact velocity-1 (m/s) | Total energy-1 (J) | Energy to max load-1 (J) | Total time-1 (ms) | Impact energy-1 (J) |
|---------|-------------------------------------|------------------|-------------------------|-------------------------|--------------------|--------------------------|-------------------|---------------------|
| Outside | Single Bubble/Double Foil           | 33.38            | 6.25                    | 1.51                    | 0.31               | 0.18                     | 20.58             | 3.12                |
|         | Single Bubble/White Foil            | 120.88           | 9.90                    | 1.51                    | 0.89               | 0.83                     | 12.04             | 3.12                |
|         | Heat Reflecting Fabric              | 86.82            | 8.77                    | 1.52                    | 0.56               | 0.52                     | 9.37              | 3.17                |
|         | Two-sided Film with Polyester Scrim | 262.24           | 9.21                    | 1.51                    | 1.34               | 1.28                     | 9.53              | 3.12                |
| Inner   | Polyethylene Film                   | 125.83           | 8.53                    | 1.52                    | 0.78               | 0.70                     | 12.88             | 3.13                |
|         | Bubble Wrap                         | 33.60            | 9.35                    | 1.53                    | 0.30               | 0.27                     | 17.31             | 3.21                |

#### 4.7 Tear resistance

From Table 13, it has been determined that the material that has the best tear strength is the two sided film, but with low extension at maximum load. This material has polyester scrim reinforcement which leads to more tear strength compare to the other materials. It was also observed that the double foil and white foil have high extension at maximum load due to the barrier bubble film. Double foil has uniform tear propagation resistance may be due to the metalized film on both sides.

**Table 13** Tear resistance test results

| Material                            | Average Load (Integral) (N) | First Peak (Load 10 % Change) (N) | Maximum Load (N) | Extension at Maximum Load (mm) |
|-------------------------------------|-----------------------------|-----------------------------------|------------------|--------------------------------|
| Single Bubble/Double Foil           | 12.62                       | 18.13                             | 18.13            | 77.17                          |
| Single Bubble/White Foil            | 12.62                       | 16.85                             | 18.42            | 60.25                          |
| Heat Reflecting Fabric              | 12.37                       | 18.96                             | 19.09            | 39.67                          |
| Two-sided Film with Polyester Scrim | 18.39                       | 23.56                             | 27.42            | 27.25                          |

#### 4.8 Bursting strength resistance

Table 14 summarizes the results of the test for bursting strength for the outside and inner layers. It has been observed that the two-sided film has almost double the bursting strength of the other outside materials tested. For the tested inner layers, it was found that bursting strengths were very close for both materials, but the extension at maximum load was double for the bubble wrap.

**Table 14** Burst resistance test results

| Layer   | Material                            | Maximum Load (N) | Extension at Maximum Load (mm) |
|---------|-------------------------------------|------------------|--------------------------------|
| Outside | Single Bubble/Double Foil           | 134.31           | 30.58                          |
|         | Single Bubble/White Foil            | 234.86           | 21.44                          |
|         | Heat Reflecting Fabric              | 288.08           | 21.94                          |
|         | Two-sided Film with Polyester Scrim | 591.19           | 18.40                          |
| Inner   | Polyethylene Film                   | 63.18            | 18.40                          |
|         | Bubble Wrap                         | 57.24            | 34.89                          |

#### 4.9 Static charge resistance

Carbon fiber showed the results for high electrostatic discharge generation. The electrostatic discharge surface voltage generated using 50% carbon fiber/50% Kevlar produced less voltage than the pure carbon and Kevlar fabric for the two lowest rpm settings. At higher rpm levels, the carbon fabric produces the least electrostatic charge. Kevlar generated electrostatic discharge surface voltage between volts.

**Table 15** Electrostatic charge of materials tested (volts or potential)

| rpm  | Painted Aircraft Aluminum |                             |        | Unpainted Aircraft Aluminum |                             |        |
|------|---------------------------|-----------------------------|--------|-----------------------------|-----------------------------|--------|
|      | 100% Carbon Fiber         | 50% Carbon Fiber/50% Kevlar | Kevlar | 100% Carbon Fiber           | 50% Carbon Fiber/50% Kevlar | Kevlar |
| 1330 | -21                       | -8                          | -25    | -17                         | -7                          | -25    |
| 2330 | -22                       | -20                         | -28    | -22                         | -19                         | -26    |
| 2980 | -30                       | -50                         | -42    | -25                         | -29                         | -36    |

#### 4.10 Flame resistance

The following are the observations for the samples tested:

- Single bubble/white foil: burned completely
- Single bubble/double foil: partially burned for about 5 seconds
- Two-sided film with polyester scrim reinforcement: partially burned for about 4 seconds
- Heat reflecting fabric: partially burned for about 7 seconds

Figure 43 a-d shows the chronological flame test process of the material two-sided film with polyester scrim reinforcement. Figure 44 shows the result after the sample has been flame tested.



(a)



(b)

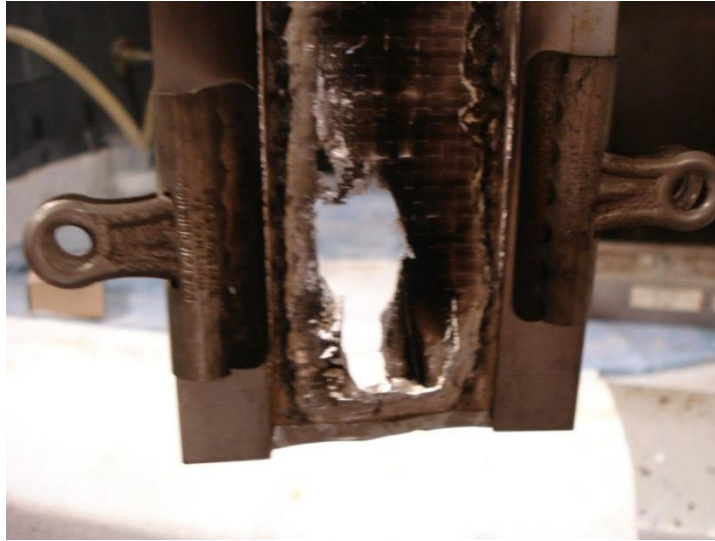


(c)



(d)

**Figure 43** Test of flame resistance



**Figure 44** Sample after test of flame resistance

#### 4.11 Air permeability

The differential air pressure was recorded, and the flow/area for each base layer sample was determined. According to a chart for a nozzle of 4 mm, both base layer fabrics as shown in Table 16 have similar flow/area values.

**Table 16** Air permeability test

| Material                    | Flow/Area<br>[(ft <sup>3</sup> /min)/ft <sup>2</sup> ] |
|-----------------------------|--|
| Carbon Fiber Fabric         | 28.59  |
| 50% Carbon Fiber/50% Kevlar | 30.66  |

After testing the individual layers' properties, the following material selection matrices were made as shown in tables 17 – 19. The rating criteria were listed between 1 and 3. The rating score of 1 means the property is optional, 2 is desirable, and 3 is a critical property. Each material is prioritized in comparison with the other material candidates; their rankings appear in the top cell of

their rating matrix. The lowest ranking of 1 is assigned to the material with the least desirable property. The number in the bottom cell of the rating matrix for a specific property is the value of the rating times the rank of the material. Therefore, the most important property which was assigned the highest rating number is more influential on the overall material selection process.

**Table 17** Material selection matrix base layer

| Expected properties     | Rating | Carbon Fiber | 50% Carbon Fiber/50% Kevlar |
|-------------------------|--------|--------------|-----------------------------|
| Lightweight             | 2      | 2            | 1                           |
|                         |        | 4            | 2                           |
| Static charge resistant | 3      | 2            | 1                           |
|                         |        | 6            | 3                           |
| Flame resistant         | 3      | 2            | 1                           |
|                         |        | 6            | 3                           |
| Air permeability        | 2      | 2            | 1                           |
|                         |        | 4            | 2                           |
| Total                   |        | 20           | 10                          |

**Table 18** Material selection matrix inner layer

| Expected properties | Rating | Polyethylene Film | Bubble Wrap |
|---------------------|--------|-------------------|-------------|
| Lightweight         | 1      | 1                 | 2           |
|                     |        | 1                 | 2           |
| Impact resistant    | 3      | 2                 | 1           |
|                     |        | 6                 | 3           |
| Burst resistant     | 2      | 2                 | 1           |
|                     |        | 4                 | 2           |
| Total               |        | 11                | 7           |

**Table 19** Material selection matrix outside layer

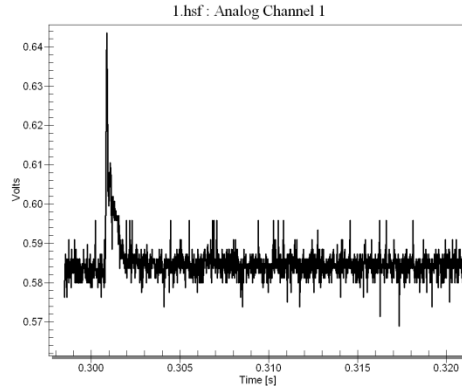
| Expected properties | Rating | Single Bubble/Double Foil | Single Bubble/White Foil | Heat Reflecting Fabric | Two-sided Film Polyester Reinforcement |
|---------------------|--------|---------------------------|--------------------------|------------------------|--|
| Lightweight         | 2      | 1                         | 2                        | 4                      | 3                                      |
|                     |        | 2                         | 4                        | 8                      | 6                                      |
| Abrasion resistant  | 2      | 4                         | 1                        | 2                      | 3                                      |
|                     |        | 8                         | 2                        | 4                      | 6                                      |
| Low Friction        | 1      | 2                         | 1                        | 3                      | 4                                      |
|                     |        | 2                         | 1                        | 3                      | 4                                      |
| Folding capability  | 2      | 0                         | 0                        | 0                      | 0                                      |
|                     |        | 0                         | 0                        | 0                      | 0                                      |
| UV resistant        | 3      | 1                         | 2                        | 4                      | 3                                      |
|                     |        | 3                         | 6                        | 12                     | 9                                      |
| Impact resistant    | 2      | 1                         | 3                        | 2                      | 4                                      |
|                     |        | 2                         | 6                        | 4                      | 8                                      |
| Tear resistant      | 2      | 1                         | 2                        | 3                      | 4                                      |
|                     |        | 2                         | 4                        | 6                      | 8                                      |
| Burst resistant     | 2      | 1                         | 2                        | 3                      | 4                                      |
|                     |        | 2                         | 4                        | 6                      | 8                                      |
| Flame resistant     | 1      | 3                         | 1                        | 2                      | 4                                      |
|                     |        | 3                         | 1                        | 2                      | 4                                      |
| <b>Total</b>        |        | <b>24</b>                 | <b>28</b>                | <b>45</b>              | <b>53</b>                              |

The specimens were constructed using a two-sided film with polyester reinforcement as an outer layer, carbon fiber as a bottom and with two options to test for the inner layer using bubble wrap or using air inside the polyethylene film pushed by an air pump.

#### 4.12 Hail impact simulations

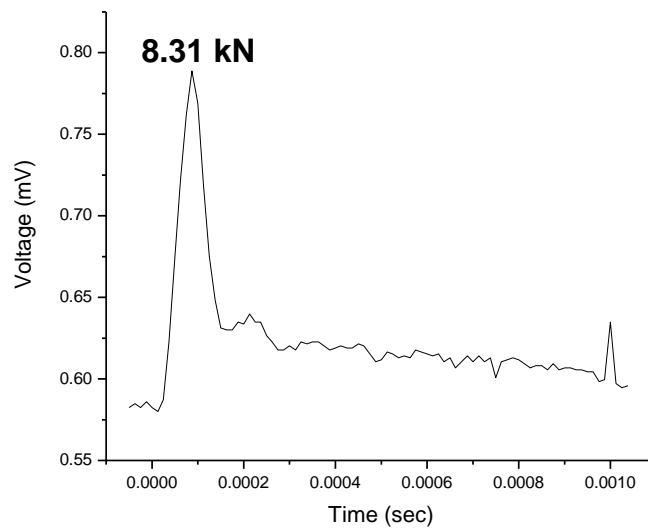
Information regarding the hail impact simulations and a full description of the test conditions is found in section 3.2.12. The output voltage signal from the force transducer and laser displacement transducer are plotted as a function of time as shown in Figure 45.



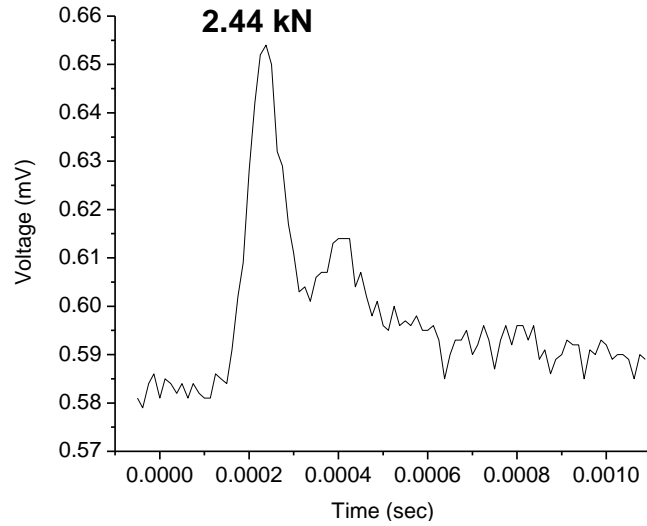


**Figure 45** Volts vs. time (output signal)

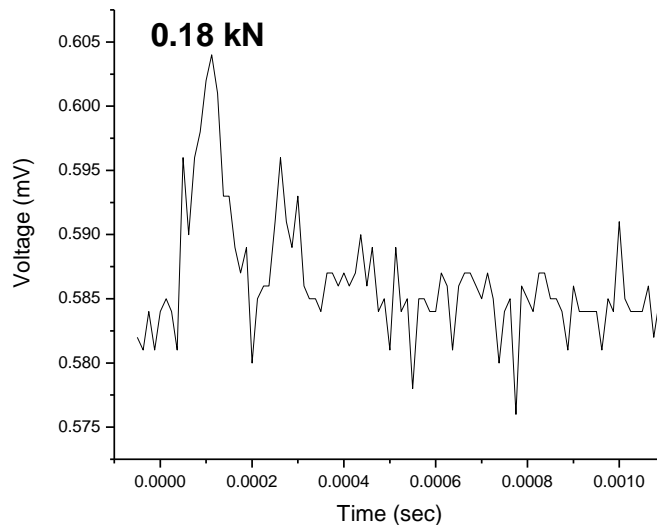
Figures 46-48 depict the dynamic force history of 57, 40.5, and 28.5 mm ice projectiles, impacting the force transducer for the following velocities 29.5 m/s, 25.5 m/s and 21.5 m/s. The peak force of the test data occurs in the first milliseconds of the impact event and varies in the magnitude of the peak force for the different projectile diameters.



**Figure 46** Peak force of layered ice (57 mm diameter) at 90° impact

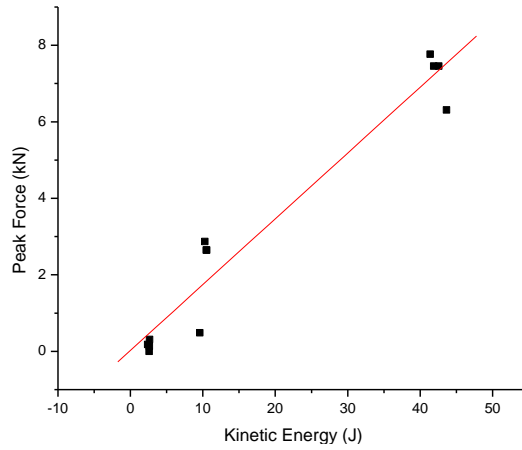


**Figure 47** Peak force of layered ice (40.5 mm diameter) at 90° impact

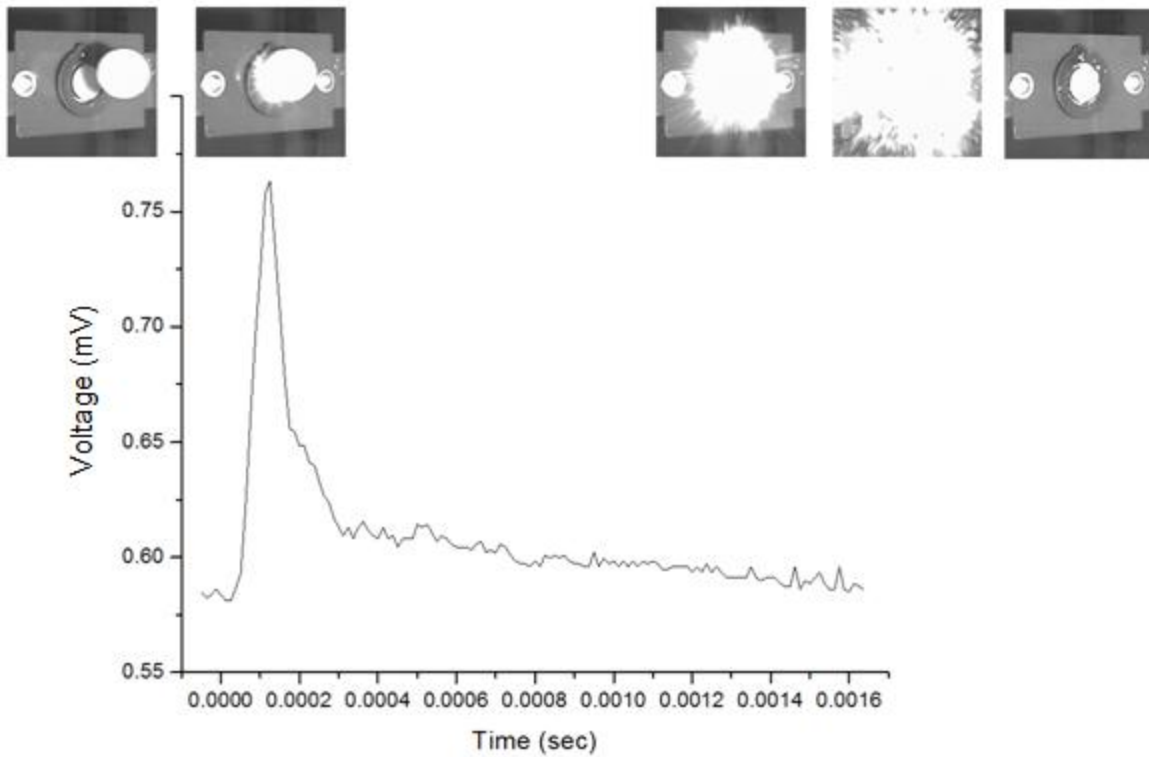


**Figure 48** Peak force of layered ice (28.5 mm diameter) at 90° impact

Figure 49 indicates that the peak force is directly proportional to the kinetic energy from all tests on the transducer. The plot in Figure 50 presents the voltage time history of an ice impact at 30 m/s.



**Figure 49** Peak force vs. Kinetic energy



**Figure 50** Summary of ice with cotton fillers (57 mm diameter) at 90° impact

The impact event of a layered ice projectile was recorded with the high speed camera, and Figure 51 shows the frames from the ice impacting the force transducer at 29.5 m/s. At 0.08 ms the ice

projectile begins to make contact with the transducer. At 0.1 ms the peak force occurs, as a very short duration impulse, and at 0.2 ms there is a complete dispersion of fragments of the ice projectile.

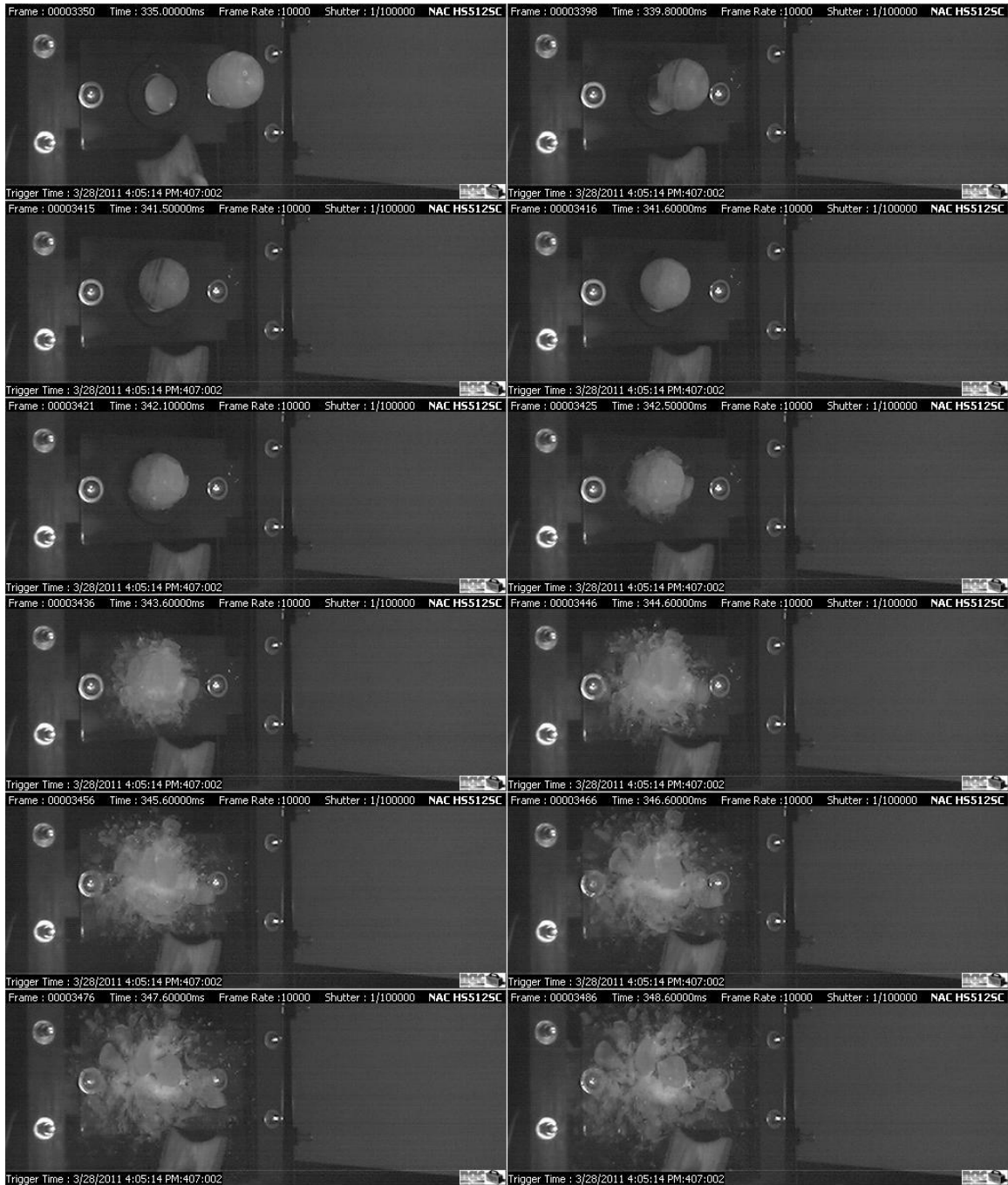
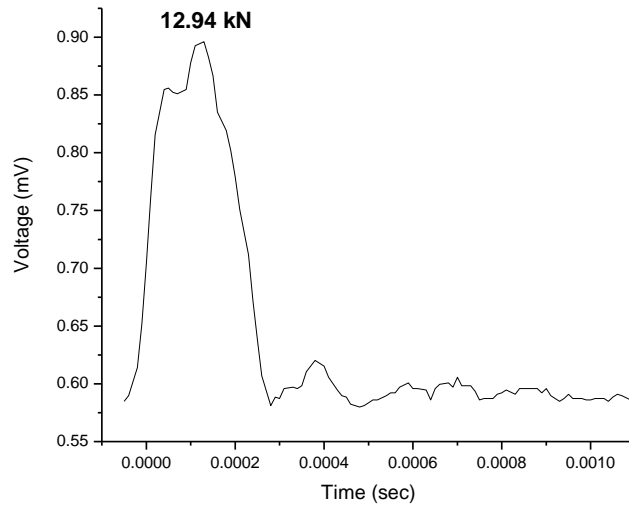
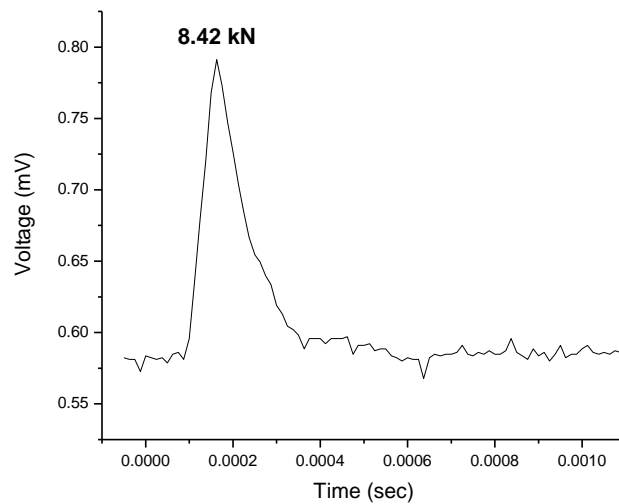


Figure 51 Summary of layered ice (57 mm diameter) at 90° impact

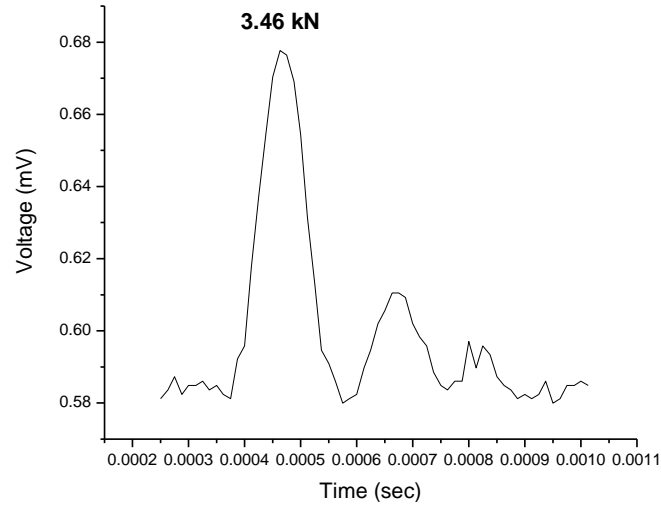
Figures 52-54 depict the dynamic force history of 57, 40.5, and 28.5 mm ice projectiles impacting the force transducer for the following velocities 29.5 m/s, 25.5 m/s and 21.5 m/s with an incidence angle of 45 degrees. The peak force of the test data has similar behavior to the 90 degree tests. Furthermore, a plausible explanation to this phenomenon lies in the effects of impact on load cell position, which are not in this research.



**Figure 52** Peak force of ice with cotton fillers (57 mm diameter) at 45° impact



**Figure 53** Peak force of ice with cotton fillers (40.5 mm diameter) at 45° impact



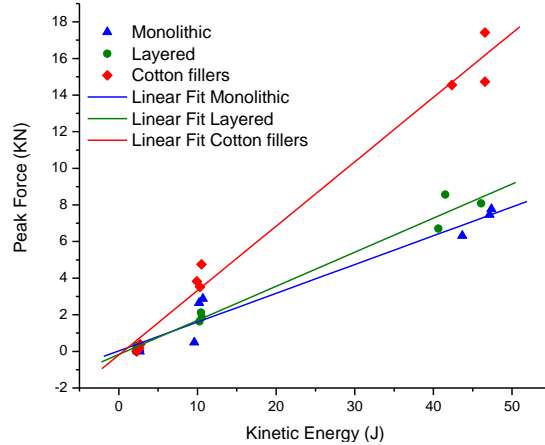
**Figure 54** Peak force of ice with cotton fillers (28.5 mm diameter) at 45° impact

Information such as mass, velocity, and kinetic energy of some selected tests are consolidated in Table 20.

**Table 20** Test summary of ice constructions

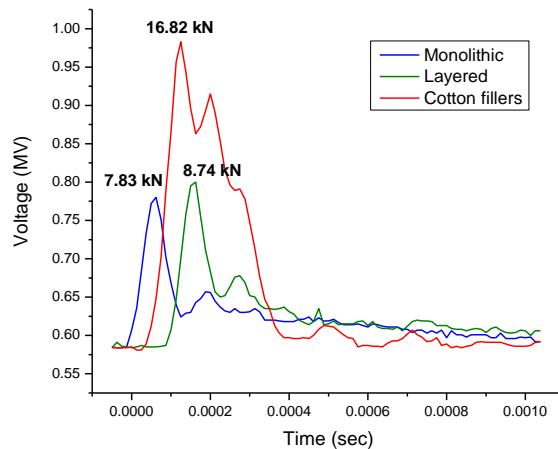
| Construction   | Diameter (mm) | Mass (g) | Velocity (m/s) | Energy (J) | Peak Force (kN) |
|----------------|---------------|----------|----------------|------------|-----------------|
| Monolithic     | 28.50         | 11.44    | 21.22          | 2.58       | 0.50            |
|                |               | 11.41    | 21.41          | 2.61       | 0.32            |
|                |               | 11.20    | 21.88          | 2.68       | 0.19            |
|                | 40.50         | 32.44    | 25.10          | 10.22      | 2.82            |
|                |               | 31.61    | 26.00          | 10.69      | 3.04            |
|                |               | 29.52    | 25.50          | 9.60       | 0.67            |
|                | 57.00         | 100.33   | 29.50          | 43.66      | 6.45            |
| 97.83          |               | 31.04    | 47.13          | 7.59       |                 |
| 95.15          |               | 31.56    | 47.39          | 7.90       |                 |
| Layered        | 28.50         | 10.53    | 20.80          | 2.28       | 0.50            |
|                |               | 10.57    | 20.34          | 2.19       | 0.28            |
|                |               | 10.58    | 20.80          | 2.29       | 0.59            |
|                | 40.50         | 31.63    | 25.50          | 10.28      | 1.90            |
|                |               | 32.15    | 25.50          | 10.45      | 2.38            |
|                |               | 32.50    | 25.50          | 10.57      | 2.12            |
|                | 57.00         | 96.98    | 28.95          | 40.63      | 6.94            |
|                |               | 96.75    | 30.86          | 46.08      | 8.29            |
|                |               | 97.50    | 29.18          | 41.51      | 8.78            |
| Cotton fillers | 28.50         | 12.17    | 21.18          | 2.73       | 2.73            |
|                |               | 11.08    | 20.30          | 2.28       | 2.34            |
|                |               | 12.20    | 20.65          | 2.60       | 2.51            |
|                | 40.50         | 32.73    | 25.11          | 10.32      | 5.84            |
|                |               | 32.40    | 24.77          | 9.94       | 6.15            |
|                |               | 32.03    | 25.60          | 10.50      | 7.07            |
|                | 57.00         | 98.21    | 30.79          | 46.54      | 16.97           |
|                |               | 103.54   | 29.98          | 46.54      | 19.64           |
|                |               | 100.85   | 28.98          | 42.34      | 16.79           |

Figure 55 presents the plotted data for the test of monolithic, layered and cotton fillers simulated hail for all three diameters. The measured peak forces vary linearly with the kinetic energy of the ice projectile, and the slope of each line changes with the ice projectile diameter.



**Figure 55** Peak force vs. Kinetic energy for all ice construction projectiles

Figure 56 compares the force history of all three constructions at 30 m/s showing almost no clear difference in the behavior during the impact event for the monolithic and layered ice projectiles. However, the ice projectile with cotton fillers shows a substantial increase in the peak force.



**Figure 56** Comparison of force history all ice construction projectiles

Table 21 presents the deformation caused by the three different diameter impacts for the combination of the three layers collected using the high speed camera.

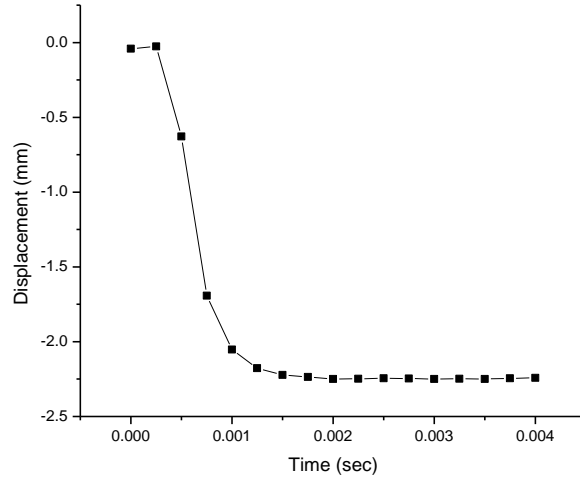
**Table 21** Displacement in material

| Construction          | Inner Material    | Mass (g) | Pressure (psi) | Deformation (mm) |
|-----------------------|-------------------|----------|----------------|------------------|
| <b>Monolithic</b>     | Polyethylene Film | 30.98    | 126.7          | 2.00             |
|                       | Polyethylene Film | 32.12    | 127.3          | 2.25             |
|                       | Bubble wrap       | 31.72    | 126.6          | 13.24            |
| <b>Layered</b>        | Polyethylene Film | 30.85    | 126.8          | 3.50             |
|                       | Polyethylene Film | 29.73    | 127.3          | 3.50             |
|                       | Bubble wrap       | 30.15    | 127.8          | 14.54            |
| <b>Cotton fillers</b> | Polyethylene Film | 32.17    | 126.5          | 1.50             |
|                       | Polyethylene Film | 33.33    | 125.9          | 2.25             |
|                       | Bubble wrap       | 33.87    | 126.4          | 17.89            |

Figures 57 and 58 show the composite center deflection history measured with the laser displacement transducer.

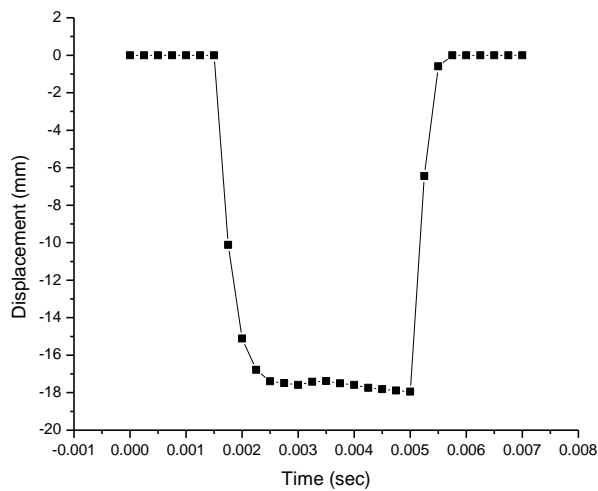
Figure 57 is a plot of the displacement (y-axis) versus time (x-axis) of the base layer. This sample includes an inflated polyethylene bladder as an inner layer. From the plot we observe upon impact the base layer deflects to approximately -2.25 mm where it remains.





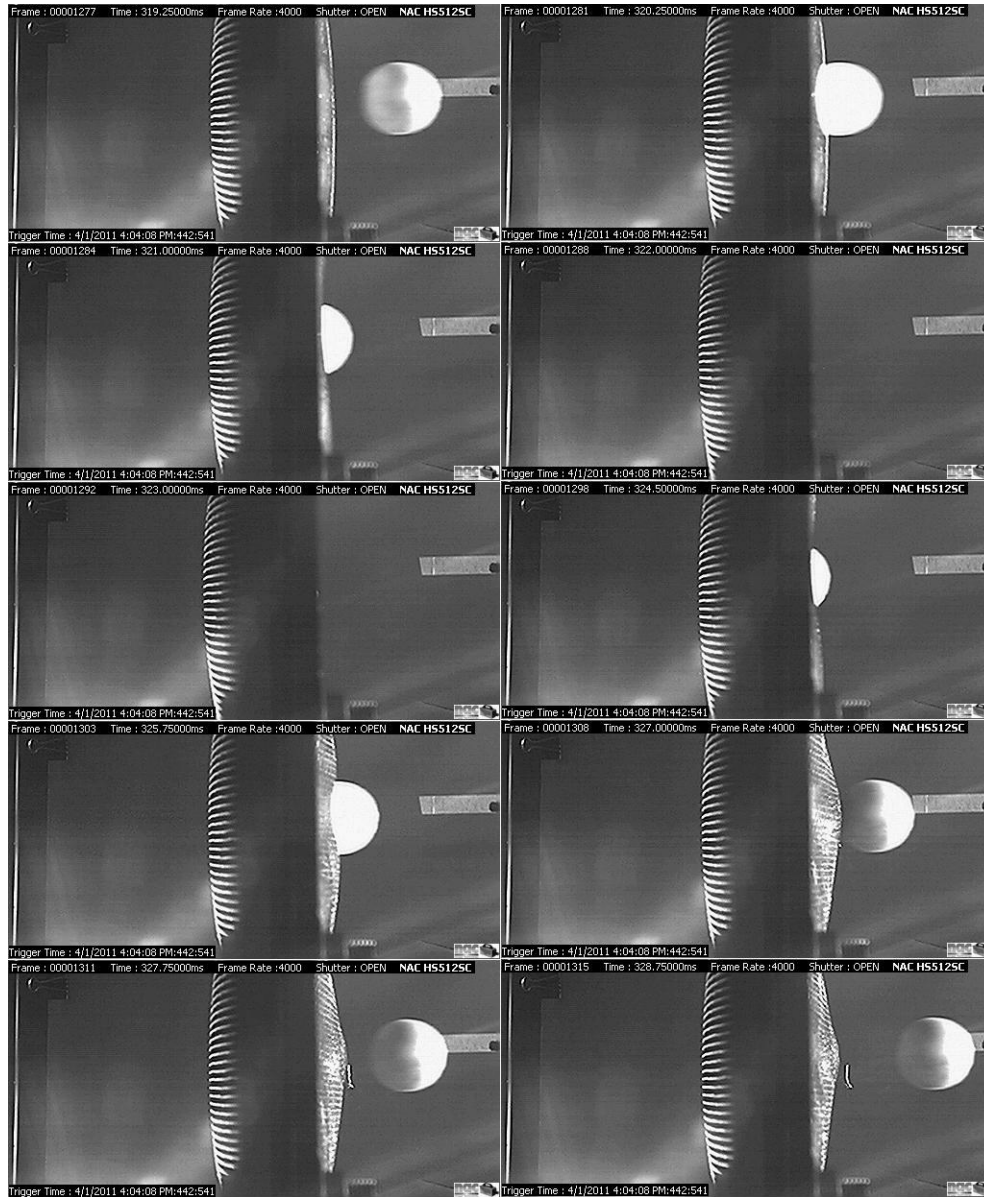
**Figure 57** Composite material with polyethylene film impacted by an ice projectile with cotton fillers (40.5 mm)

Figure 58 is a plot of the displacement (y-axis) versus time (x-axis) of the base layer. This sample includes bubble wrap as an inner layer. From the plot we observe, upon impact, the base layer deflects to approximately -18 mm and returns to the original position. Final inspections indicate that the bubbles burst during the impact.



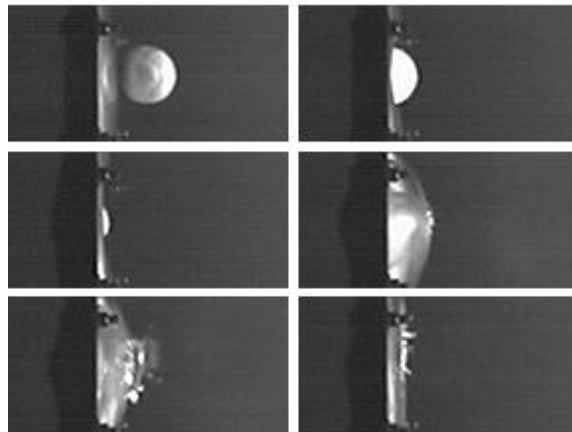
**Figure 58** Composite material with bubble wrap inner impacted by an ice projectile with cotton fillers (40.5 mm) coefficient

Figure 59 captures the specimen before, during, and after impact. The projectile impacts, deforms, and is deflected by the test specimen in Figure 59. The displacement data collected using the high speed camera and the laser displacement transducer have been verified to correlate well.



**Figure 59** Summary of deformation of composite specimen

Figure 60 presents a detailed monitoring of the deformation behavior for a composite panel impacted by an ice projectile of 57 mm at 30 m/s. Figure 60 demonstrates how the integrity of the material is compromised when impacted by the largest hailstone (57 mm), revealing that this material is unsuitable for protection against impacts of such a large size and mass. However, this material has been demonstrated to provide adequate protection against hail stones up to 46 mm in diameter.



**Figure 60** Sequence of the ice impact (57 mm diameter) on specimen

## 5. CONCLUSIONS

An experimental impact enclosure for the study and analysis of impact events of polymeric materials has been developed. The primary features of the designed, instrumented, experimental setup include data acquisition, image acquisition, high speed camera, image analysis, laser-based specimen deflection determination, force transducer, and electronically actuated compressed air cannon. The compressed air cannon is reinforced with braided high strength glass fibers and epoxy resin for safety with moderate operating pressures. Furthermore, the compressed air cannon barrel is made from PVC plastic and is easily adjustable, making it particularly suitable for ice and other large scale low speed projectiles. These unique experimental capabilities provide information which can be used to determine the requirements for protective covering of vehicles and aircraft that will be exposed to hail impact.

Based on the information obtained during the individual layer characterization experiments of chapter 4, low velocity impact tests were performed in the experimental test chamber on composite materials and polymeric films, using ice projectiles launched at velocities ranging from 20 to 30 meters per second with incidence angles of 90° and 45°.

The results presented in chapter 4 demonstrate the relationship between displacement and damage on the composite material and the influence of various ice constructions is discussed. Additionally, a high speed camera with corresponding image analysis was conducted correlating the impact with time. The behavior observed during impact of the tested composite specimen exhibits peak force followed by peak displacement. The transient occurring from peak force to peak

displacement suggests the presence of short impact response dominated by flexural and shear waves as observed in [31].

The original scope of this project involved developing a weather resistant covering for vehicles and small aircraft. Weather resistant coverings should provide resistance against natural hazards including ultraviolet degradation, wind abrasion, moisture, and impact. Resistance to impact is most critical for protection during hail storms and therefore we set out to develop an impact resistant covering against hail stones up to 2 inches in diameter. After systematic evaluation of materials based on various mechanical characterization techniques, we have determined that the available materials are unsuitable for protecting against 2 inch hail stones. However, we have concluded that the evaluated material configurations provide adequate protection against hailstones up to approximately 1.6 inches in diameter, which are more common than 2 inch diameters.

Finally, the results of this work include developing a method for evaluating polymeric materials for weather resistance, designing and constructing a custom experimental test chamber for impact studies and future material impact experiments. The significance of the work presented in this thesis supports the development of novel, weather resistant, and robust material coverings which are not currently commercially available.

## 6. RECOMMENDATIONS FOR FUTURE WORK

Additional work is required to develop a material that can provide adequate impact resistance against larger than two inch diameter hailstones. Additional layers utilizing high strength ballistic grade yarns such as Kevlar® or ballistic nylon should be investigated.

Increasing the instrumentation capabilities of the impact simulation enclosure developed in this thesis would provide detailed information about material properties. Specifically strain gages, C-scan, and thermal imaging techniques would enable more detailed evaluation of material performance. Application of appropriate micromechanics models and corresponding experiments should be investigated to determine appropriate constituent material models for developing finite element analyses. A predictive finite element model will greatly expedite the design of new material configurations used in future impact studies.

## REFERENCES

1. *Aircraft Icing*. 2002, Airplane Owners and Pilots Association's (AOPA) Air Safety Foundation.
2. Jackson, W.C. and C.C.J. Poe, *The use of impact force as a scale parameter for the impact response of composite laminates*. NASA Technical Memorandum 104189 AVSCOM Technical Report 92-B-001, 1992.
3. Manas, C. and R. Salil, *Plastics Technology Handbook*. 3rd ed, ed. M. Dekker. 1998, New York, NY.
4. Halliwell, S.M., *Weathering of Polymers*, ed. R.R. Reports. 1995, Shawbury, UK.
5. <http://quarknet.fnal.gov/quarknet-summer-research/QNET2010/Astronomy/>. [cited.
6. Brown, R., *Handbook of polymer testing, physical methods*, ed. M. Decker. 1999, New York.
7. Guillet, J.E., *Fundamental Process in the UV Degradation and Stabilization of Polymers*. Pure Appl. Chem., 1972. **30**(1-2): p. 135-144.
8. Blaga, A., *Deterioration mechanisms in weathering of plastic materials*, in *Proceedings of the 1st International Conference on Durability of Building Materials and Components, ASTM STP 691*. 1980: Ottawa, Ont. Canada. p. 827-837.
9. Li, C. and F. Yan, *Effect of Blowing Air and Floating Sand-dust Particles on the Friction and Wear Behavior of PTFE, UHMWPE and PI*. Tribology Letters, 2008. **32**(3): p. 189-198.
10. Shah, V., *Handbook of Plastics Testing and failure Analysis*. 2007, New Jersey: Wiley.
11. National Research Council, *Observing Weather and Climate from the Ground Up: A Nationwide Network of Networks*. 2009: National Academies Press.

12. Burt, C.C., *Extreme Weather: A Guide and Record Book*. 2007, New York: W. W. Norton & Company.
13. Schleusener, R.A. and P.C. Jennings, *An Energy Method for Relative Estimates of Hail Intensity*. American Meteorological Society. Vol. 41. 1960, Lancaster, Pa.
14. Matson, R.J. and A.W. Huggins, *The Direct Measurement of the Sizes, Shapes and Kinematics of Falling Hailstones*. Journal of the Atmospheric Sciences, 1980. **37**(5): p. 1107-1125.
15. Sioutas, M., T. Meaden, and J.D.C. Webb, *Hail frequency, distribution and intensity in Northern Greece*. Atmospheric Research, 2009. **93**: p. 526-533.
16. Fasanella, E.L. and R.L. Boinnott. *Test and Analysis Correlation of High Speed Impacts of Ice Cylinders*. in *9th International LS-DYNA Users Conference*. 2006. Dearborn, Michigan
17. Schulson, E.M., *The Brittle Failure of Ice under Compression*. J. Phys. Chem. B, 1997. **101**: p. 6254-6258.
18. Haynes, F.D., *Effect of Temperature on the Strength of Snow-Ice*. 1978, Department of the Army, Cold Regions Research and Engineering Laboratory, Corps of Engineers, CRREL Report 78-27: Hanover, New Hampshire.
19. Petrovic, J.J., *Mechanical properties of ice and snow*. Journal of Materials Science, 2003. **38**: p. 1-6.
20. Gold, L.W., *On the Elasticity of Ice Plates*. Canadian Journal of Civil Engineering, 1988. **15**(6): p. 1080-1984.
21. Schroeder, R.C. and W.H. McMaster, *Shock-compression freezing and melting of water and ice*. Journal of Applied Physics, 1973. **44**(6): p. 2591-2594.
22. Gokhale, N.R., *Hailstorms and hailstone growth*. 1975, Albany: State University of New York Press.
23. Ross, D.v.d.S. and A.E. Carte, *The Falling Behaviour of Oblate and Spiky Hailstones*. Journal de Recherches Atmospheriques, 1973. **7**: p. 39-52.



24. Lozowski, E.P. and G.S. Strong, *Further reflections on the calibration of hailpads*. Atmosphere Ocean, 1978. **16**: p. 69-80.
25. Beattie, A.G., *Measurements of the kinematics of natural hailstones near ground*. Quarterly Journal of the Royal Meteorological Society, 1979. **105**(453-459).
26. Nave, R., *Hyper Physics, Mechanics*. 2001, National Science Teachers Association.
27. Crenshaw, V.A. and J.D. Koontz, *Simulated hail damage and impact resistance test procedures for roof coverings and membranes*. 2001, RCI Interface. p. 4-10.
28. Laurie, J.A.P., *Hail and Its Effects on Buildings*, in *Research Report 176*, NBRI, Editor. 1960: Pretoria, South Africa.
29. Bilham, E.G. and E.F. Relf, *The dynamics of large hailstones*. Quarterly Journal of the Royal Meteorological Society, 1937. **63**: p. 149–162.
30. Abrate, S., *Impact on Composites Structures*. 2005, New York: Cambridge University Press.
31. Olsson, R., *Mass criterion for wave controlled impact response of composite plates*. Composites Part A: Applied Science and Manufacturing, 2000. **31**(8): p. 879-887.
32. Olsson, R., *Closed form prediction of peak load and delamination onset under small mass impact*. Composite Structures, 2003. **59**(3): p. 341-349.
33. Fischer-Cripps, A.C., *Introduction to Contact Mechanics*. 2007, New York: Springer Science.
34. Johnson, K.L., *Contact Mechanics*. 1985, Cambridge, United Kingdom: Cambridge University Press.
35. Fischer-Cripps, A.C., *The Hertzian contact surface*. Journal of Materials Science, 1999. **34**(1): p. 129-137.
36. Kim, H., D.A. Welch, and K.T. Kedward, *Experimental investigation of high velocity ice impacts on woven carbon/epoxy composite panels*. Composites Part A: Applied Science and Manufacturing, 2003. **34**(1): p. 25-41.

37. Asp, L.E. and R. Juntikka, *High velocity impact on NCF reinforced composites*. Composites Science and Technology, 2009. **69**(9): p. 1478-1482.
38. Olsson, R., *Analytical prediction of large mass impact damage in composite laminates*. Composites Part A: Applied Science and Manufacturing, 2001. **32**(9): p. 1207-1215.
39. Thomson, R.G. and R.J. Hayduk, *An analytical evaluation of the denting of airplane surfaces by hail*. NASA technical note D-5363, Washington, DC, 1969: p. 1-34.
40. Sun, B., D. Hu, and B. Gu, *Transverse impact damage and energy absorption of 3-D multi-structured knitted composite*. Composites Part B: Engineering, 2009. **40**(6): p. 572-583.
41. Nasr-Isfahani, M., M. Amani-Tehran, and M. Latifi, *Simulation of ballistic impact on fabric armour using finite-element method*. Journal of the Textile Institute, 2009. **100**(4): p. 314 - 318.
42. <http://www.radiantbarrier.com/index.htm>. [cited].

## APPENDICES

### Appendix A. Specifications of materials acquired to Innovative Insulation Inc. [42]

| <b>TempShield™ Single Bubble Foil/Foil</b> |                                    |
|--|------------------------------------|
| CONTACT TEMPERATURE RANGE                  | -60 °F to 180 °F (-51 °C to 82 °C) |
| THICKNESS                                  | 5/32" nominal                      |
| WATER VAPOR TRANSMISSION                   | 0.02 perms [ASTM E-96 Method A]    |
| PUNCTURE RESISTANCE                        | 60 lbs/in [ASTM Test Method D-781] |
| PLIABILITY                                 | No Cracking                        |
| LINEAR SHRINKAGE                           | None                               |
| MOLD AND MILDEW                            | No Growth                          |
| FLAME SPREAD                               | 0 [ASTM E84-08]                    |
| SMOKE DEVELOPMENT                          | 25 [ASTM E84-08]                   |
| FIRE RATING                                | Class A/Class 1                    |
| REFLECTIVITY                               | 95%                                |
| EMITTANCE                                  | 0.04 on metalized film side        |

| <b>TempShield™ Single Bubble White/Foil</b> |                                    |
|---|------------------------------------|
| CONTACT TEMPERATURE RANGE                   | -60 °F to 180 °F (-51 °C to 82 °C) |
| THICKNESS                                   | 5/32" nominal                      |
| WATER VAPOR TRANSMISSION                    | 0.02 perms [ASTM E-96 Method A]    |
| PUNCTURE RESISTANCE                         | 60 lbs/in [ASTM Test Method D-781] |
| PLIABILITY                                  | No Cracking                        |
| LINEAR SHRINKAGE                            | None                               |
| MOLD AND MILDEW                             | No Growth                          |
| FLAME SPREAD                                | 0 [ASTM E84-08]                    |
| SMOKE DEVELOPMENT                           | 20 [ASTM E84-08]                   |
| FIRE RATING                                 | Class A/Class 1                    |
| REFLECTIVITY                                | 95%                                |
| EMITTANCE                                   | 0.04 on metalized film side        |

| <b>Temptrol™ Heat Reflecting Fabric</b> |   |
|---|---|
| NOMINAL THICKNESS                       | 10.9 mils   |
| TENSILE STRENGTH                        | 47.0 lb/in width [ASTM Test Method D751]                      |
| TEAR STRENGTH                           | 6.0 lb/in width [ASTM Test Method D751]                       |
| PUNCTURE RESISTANCE                     | 17 lbs. [ASTM Test Method 4833]                               |
| MULLEN BURST STRENGTH                   | 55.0 psi [ASTM Test Method D751]                              |
| LOW TEMPERATURE BEND                    | 131° F PASS [ASTM D2136]                                      |
| WATER VAPOR PERMEABILITY                | 87.5g/m2/24hr [ASTM E96]                                      |
| FLAMMABILITY                            | Class B [ASTM E84-94]   |
| THERMAL PROPERTIES                      | Emissivity 0.05 (Reflects 95% of Infrared Energy) [ASTM E408] |

| <b>Super R Plus™</b>  |  |                      |
|-----------------------|--|----------------------|
| TENSILE/TEAR STRENGTH | Length 13.23 pounds force  | [ASTM D2261]         |
|                       | Width 13.98 pounds force   |                      |
| PLIABILITY            | 70°F±5°F & 50±5% Relative Humidity – No Cracking or Delamination | [ASTM C1313-05]      |
| ADHESIVE PERFORMANCE  | 180°F±5°F & 50% Relative Humidity – No Bleeding or Delamination  | [ASTM C1313-05]      |
| FLAME SPREAD & SMOKE  | Class A/ Class 1   | [ASTM Method E84-10] |
|                       | 0 Flame Spread, 5 Smoke Development                              |                      |
| CORROSIVITY           | 100% humidity at 71±2°C for 7 days - PASS                        | [ASTM D3310-00]      |
| RESISTANCE TO FUNGI   | PASS – No Growth   | [ASTM C1338-08]      |
| PERMEABILITY          | 6.3 Perms  | [ASTM E96-05]        |
| THERMAL PROPERTIES    | EMISSIVITY 0.05  | [ASTM C1371-04a]     |
|                       | REFLECTIVITY 95%   |                      |

Appendix B. Complete results of abrasion test

Table 22 Results after abrasion of the heat reflecting fabric (grams)

| Cycles              | 0              |                          | 10              |                           | 25              |                           | 50              |                           | 100              |                            |
|---------------------|----------------|--------------------------|-----------------|---------------------------|-----------------|---------------------------|-----------------|---------------------------|------------------|----------------------------|
| Specimen            | W <sub>0</sub> | Weight loss <sub>0</sub> | W <sub>10</sub> | Weight loss <sub>10</sub> | W <sub>25</sub> | Weight loss <sub>25</sub> | W <sub>50</sub> | Weight loss <sub>50</sub> | W <sub>100</sub> | Weight loss <sub>100</sub> |
| 1                   | 783.10         | 0.00                     | 782.90          | 0.20                      | 782.70          | 0.40                      | 782.50          | 0.60                      | 782.00           | 1.10                       |
| 2                   | 744.80         | 0.00                     | 744.70          | 0.10                      | 744.50          | 0.30                      | 744.30          | 0.50                      | 744.00           | 0.80                       |
| 3                   | 721.00         | 0.00                     | 720.80          | 0.20                      | 720.70          | 0.30                      | 720.50          | 0.50                      | 720.10           | 0.90                       |
| 4                   | 708.20         | 0.00                     | 708.10          | 0.10                      | 707.80          | 0.40                      | 707.60          | 0.60                      | 707.30           | 0.90                       |
| 5                   | 817.00         | 0.00                     | 816.80          | 0.20                      | 816.70          | 0.30                      | 816.50          | 0.50                      | 816.10           | 0.90                       |
| Average             | 754.82         | 0.00                     | 754.66          | 0.16                      | 754.48          | 0.34                      | 754.28          | 0.54                      | 753.90           | 0.92                       |
| Standard deviation  |                |                          |                 | 0.05                      |                 | 0.05                      |                 | 0.05                      |                  | 0.11                       |
| Confidence interval |                |                          |                 | 0.04                      |                 | 0.04                      |                 | 0.04                      |                  | 0.08                       |

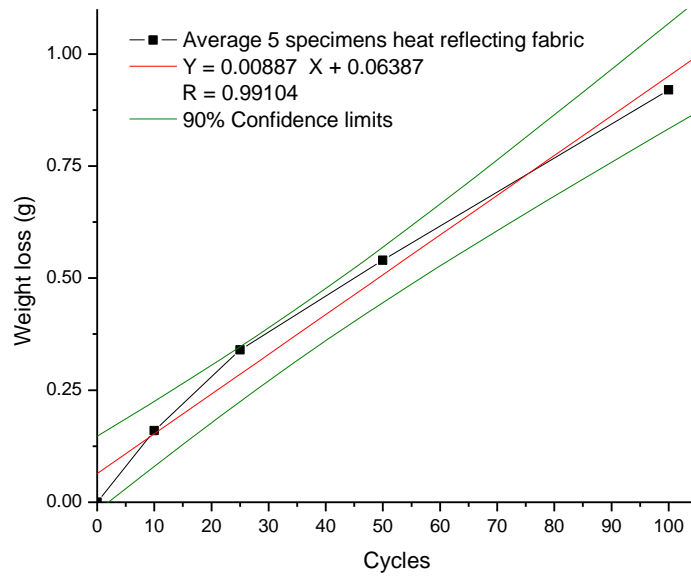
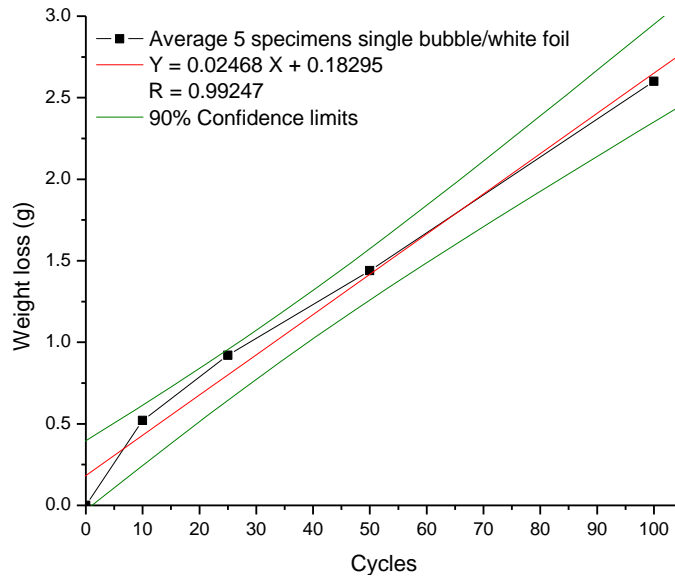


Figure 61 Average of weight loss vs. number cycles of the heat reflecting fabric

**Table 23** Results after abrasion of the single bubble/white foil (grams)

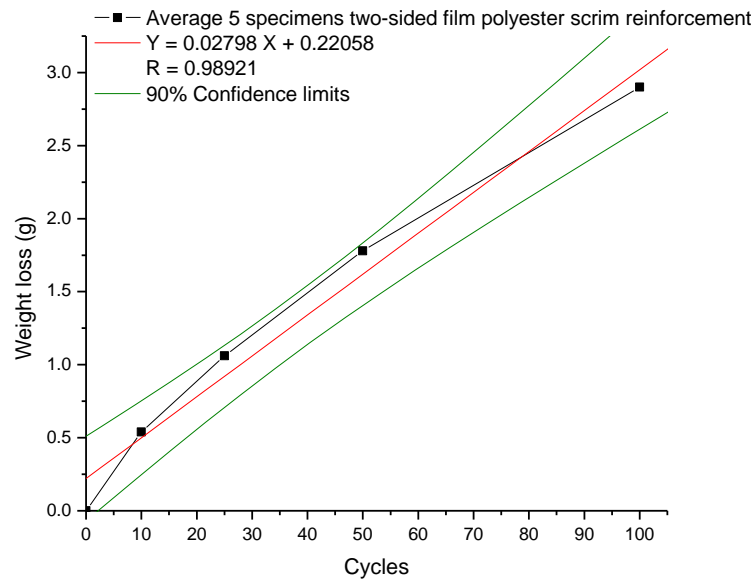
| Cycles              | 0              |                          | 10              |                           | 25              |                           | 50              |                           | 100              |                            |
|---------------------|----------------|--------------------------|-----------------|---------------------------|-----------------|---------------------------|-----------------|---------------------------|------------------|----------------------------|
| Specimen            | W <sub>0</sub> | Weight loss <sub>0</sub> | W <sub>10</sub> | Weight loss <sub>10</sub> | W <sub>25</sub> | Weight loss <sub>25</sub> | W <sub>50</sub> | Weight loss <sub>50</sub> | W <sub>100</sub> | Weight loss <sub>100</sub> |
| 1                   | 1256.80        | 0.00                     | 1256.20         | 0.60                      | 1255.80         | 1.00                      | 1255.50         | 1.30                      | 1254.30          | 2.50                       |
| 2                   | 1259.60        | 0.00                     | 1258.90         | 0.70                      | 1258.50         | 1.10                      | 1257.90         | 1.70                      | 1256.50          | 3.10                       |
| 3                   | 1273.10        | 0.00                     | 1272.80         | 0.30                      | 1272.50         | 0.60                      | 1271.80         | 1.30                      | 1270.70          | 2.40                       |
| 4                   | 1232.50        | 0.00                     | 1232.00         | 0.50                      | 1231.60         | 0.90                      | 1231.10         | 1.40                      | 1229.90          | 2.60                       |
| 5                   | 1310.70        | 0.00                     | 1310.20         | 0.50                      | 1309.70         | 1.00                      | 1309.20         | 1.50                      | 1308.30          | 2.40                       |
| Average             | 1266.54        | 0.00                     | 1266.02         | 0.52                      | 1265.62         | 0.92                      | 1265.10         | 1.44                      | 1263.94          | 2.60                       |
| Standard deviation  |                |                          |                 | 0.15                      |                 | 0.19                      |                 | 0.17                      |                  | 0.29                       |
| Confidence interval |                |                          |                 | 0.11                      |                 | 0.14                      |                 | 0.12                      |                  | 0.21                       |



**Figure 62** Average of weight loss vs. number cycles of the single bubble/white foil

**Table 24** Results after abrasion of the two-sided film with polyester scrim reinforcement  
(grams)

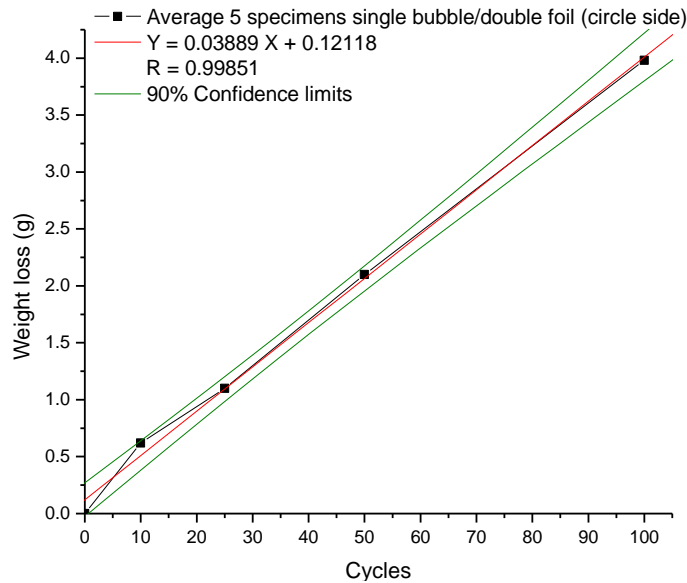
| Cycles                     | 0              |                          | 10              |                           | 25              |                           | 50              |                           | 100              |                            |
|----------------------------|----------------|--------------------------|-----------------|---------------------------|-----------------|---------------------------|-----------------|---------------------------|------------------|----------------------------|
| Specimen                   | W <sub>0</sub> | Weight loss <sub>0</sub> | W <sub>10</sub> | Weight loss <sub>10</sub> | W <sub>25</sub> | Weight loss <sub>25</sub> | W <sub>50</sub> | Weight loss <sub>50</sub> | W <sub>100</sub> | Weight loss <sub>100</sub> |
| 1                          | 1070.20        | 0.00                     | 1069.60         | 0.60                      | 1068.90         | 1.30                      | 1068.20         | 2.00                      | 1067.10          | 3.10                       |
| 2                          | 1064.30        | 0.00                     | 1063.70         | 0.60                      | 1063.10         | 1.20                      | 1062.30         | 2.00                      | 1060.90          | 3.40                       |
| 3                          | 1066.20        | 0.00                     | 1065.60         | 0.60                      | 1065.10         | 1.10                      | 1064.50         | 1.70                      | 1063.50          | 2.70                       |
| 4                          | 1060.40        | 0.00                     | 1059.90         | 0.50                      | 1059.60         | 0.80                      | 1058.90         | 1.50                      | 1058.00          | 2.40                       |
| 5                          | 1077.40        | 0.00                     | 1077.00         | 0.40                      | 1076.50         | 0.90                      | 1075.70         | 1.70                      | 1074.50          | 2.90                       |
| <b>Average</b>             | 1067.70        | 0.00                     | 1067.16         | 0.54                      | 1066.64         | 1.06                      | 1065.92         | 1.78                      | 1064.80          | 2.90                       |
| <b>Standard deviation</b>  |                |                          |                 | 0.09                      |                 | 0.21                      |                 | 0.22                      |                  | 0.38                       |
| <b>Confidence interval</b> |                |                          |                 | 0.07                      |                 | 0.15                      |                 | 0.16                      |                  | 0.28                       |



**Figure 63** Average of weight loss vs. number cycles of the two-sided film with polyester scrim reinforcement

**Table 25** Results after abrasion of the single bubble/double foil (circular embossing) (grams)

| Cycles              | 0              |                          | 10              |                           | 25              |                           | 50              |                           | 100              |                            |
|---------------------|----------------|--------------------------|-----------------|---------------------------|-----------------|---------------------------|-----------------|---------------------------|------------------|----------------------------|
| Specimen            | W <sub>0</sub> | Weight loss <sub>0</sub> | W <sub>10</sub> | Weight loss <sub>10</sub> | W <sub>25</sub> | Weight loss <sub>25</sub> | W <sub>50</sub> | Weight loss <sub>50</sub> | W <sub>100</sub> | Weight loss <sub>100</sub> |
| 1                   | 1440.30        | 0.00                     | 1439.60         | 0.70                      | 1439.00         | 1.30                      | 1437.80         | 2.50                      | 1435.60          | 4.70                       |
| 2                   | 1452.90        | 0.00                     | 1452.20         | 0.70                      | 1451.70         | 1.20                      | 1450.80         | 2.10                      | 1449.00          | 3.90                       |
| 3                   | 1454.90        | 0.00                     | 1454.20         | 0.70                      | 1453.80         | 1.10                      | 1452.80         | 2.10                      | 1451.00          | 3.90                       |
| 4                   | 1447.30        | 0.00                     | 1446.70         | 0.60                      | 1446.20         | 1.10                      | 1445.30         | 2.00                      | 1443.50          | 3.80                       |
| 5                   | 1435.90        | 0.00                     | 1435.50         | 0.40                      | 1435.10         | 0.80                      | 1434.10         | 1.80                      | 1432.30          | 3.60                       |
| Average             | 1446.26        | 0.00                     | 1445.64         | 0.62                      | 1445.16         | 1.10                      | 1444.16         | 2.10                      | 1442.28          | 3.98                       |
| Standard deviation  |                |                          |                 | 0.13                      |                 | 0.19                      |                 | 0.25                      |                  | 0.42                       |
| Confidence interval |                |                          |                 | 0.10                      |                 | 0.14                      |                 | 0.19                      |                  | 0.31                       |

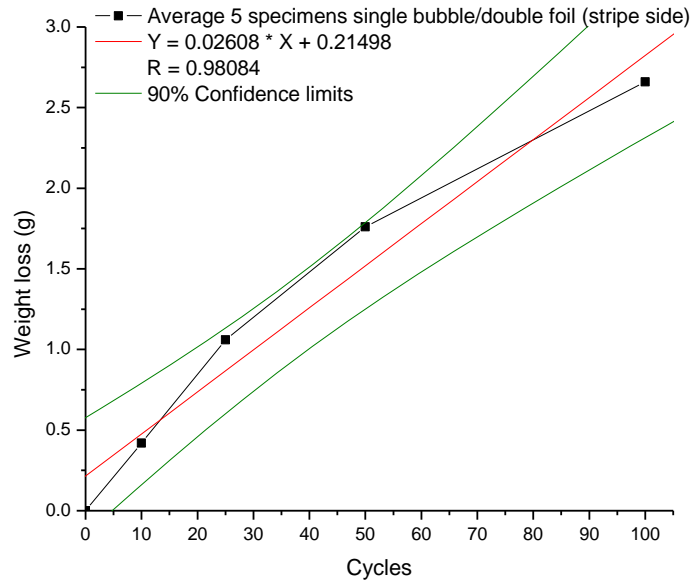


**Figure 64** Average of weight loss vs. number cycles of the single bubble/double foil (circular embossing)



**Table 26** Results after abrasion of the single bubble/double foil (triaxial embossing) (grams)

| Cycles                     | 0              |                          | 10              |                           | 25              |                           | 50              |                           | 100              |                            |
|----------------------------|----------------|--------------------------|-----------------|---------------------------|-----------------|---------------------------|-----------------|---------------------------|------------------|----------------------------|
| Specimen                   | W <sub>0</sub> | Weight loss <sub>0</sub> | W <sub>10</sub> | Weight loss <sub>10</sub> | W <sub>25</sub> | Weight loss <sub>25</sub> | W <sub>50</sub> | Weight loss <sub>50</sub> | W <sub>100</sub> | Weight loss <sub>100</sub> |
| 1                          | 1428.20        | 0.00                     | 1427.70         | 0.50                      | 1427.20         | 1.00                      | 1426.40         | 1.80                      | 1425.40          | 2.80                       |
| 2                          | 1469.60        | 0.00                     | 1469.20         | 0.40                      | 1468.60         | 1.00                      | 1467.80         | 1.80                      | 1467.10          | 2.50                       |
| 3                          | 1435.70        | 0.00                     | 1435.30         | 0.40                      | 1434.40         | 1.30                      | 1434.00         | 1.70                      | 1433.20          | 2.50                       |
| 4                          | 1460.70        | 0.00                     | 1460.30         | 0.40                      | 1459.70         | 1.00                      | 1459.00         | 1.70                      | 1458.00          | 2.70                       |
| 5                          | 1463.40        | 0.00                     | 1463.00         | 0.40                      | 1462.40         | 1.00                      | 1461.60         | 1.80                      | 1460.60          | 2.80                       |
| <b>Average</b>             | 1451.52        | 0.00                     | 1451.10         | 0.42                      | 1450.46         | 1.06                      | 1449.76         | 1.76                      | 1448.86          | 2.66                       |
| <b>Standard deviation</b>  |                |                          |                 | 0.04                      |                 | 0.13                      |                 | 0.05                      |                  | 0.15                       |
| <b>Confidence interval</b> |                |                          |                 | 0.03                      |                 | 0.10                      |                 | 0.04                      |                  | 0.11                       |



**Figure 65** Average of weight loss vs. number cycles of the single bubble/double foil (triaxial embossing)

Appendix C. Complete results of impact resistance test

Table 27 Results after impact resistance test of the two-sided film with polyester scrim reinforcement

| Specimen            | Maximum Load (N) | Time to max load-1 (ms) | Impact velocity-1 (m/s) | Total energy-1 (J) | Energy to max load-1 (J) | Total time-1 (ms) | Impact energy-1 (J) |
|---------------------|------------------|-------------------------|-------------------------|--------------------|--------------------------|-------------------|---------------------|
| 1                   | 240.90           | 8.67                    | 1.51                    | 1.16               | 1.12                     | 8.95              | 3.12                |
| 2                   | 272.70           | 9.40                    | 1.52                    | 1.36               | 1.34                     | 9.51              | 3.14                |
| 3                   | 304.30           | 10.13                   | 1.52                    | 1.62               | 1.59                     | 10.29             | 3.13                |
| 4                   | 256.90           | 9.21                    | 1.51                    | 1.28               | 1.24                     | 9.39              | 3.11                |
| 5                   | 236.40           | 8.63                    | 1.51                    | 1.31               | 1.10                     | 9.50              | 3.11                |
| Average             | 262.24           | 9.21                    | 1.51                    | 1.34               | 1.28                     | 9.53              | 3.12                |
| Standard deviation  | 27.52            | 0.62                    | 0.00                    | 0.17               | 0.20                     | 0.48              | 0.01                |
| Confidence interval | 20.25            | 0.45                    | 0.00                    | 0.13               | 0.15                     | 0.35              | 0.01                |

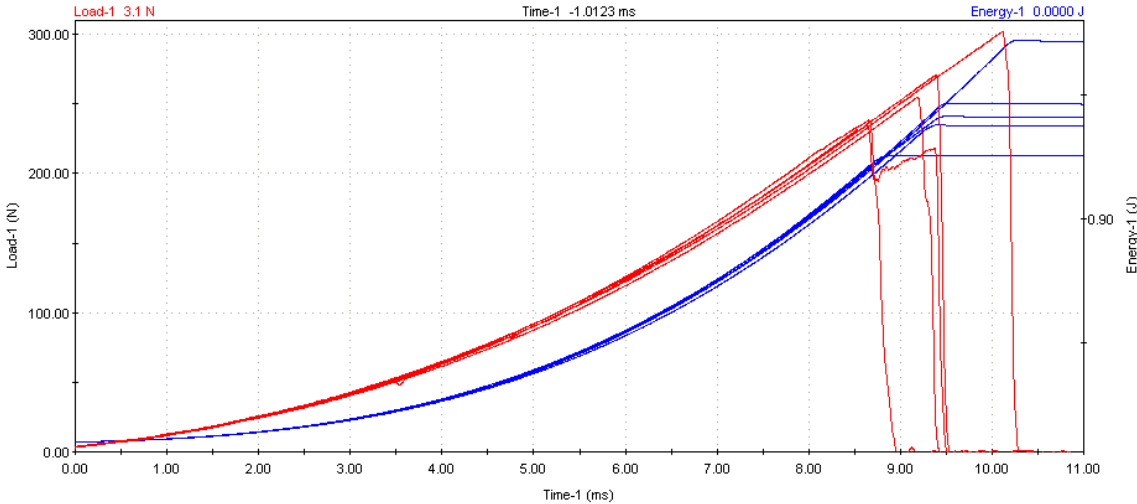
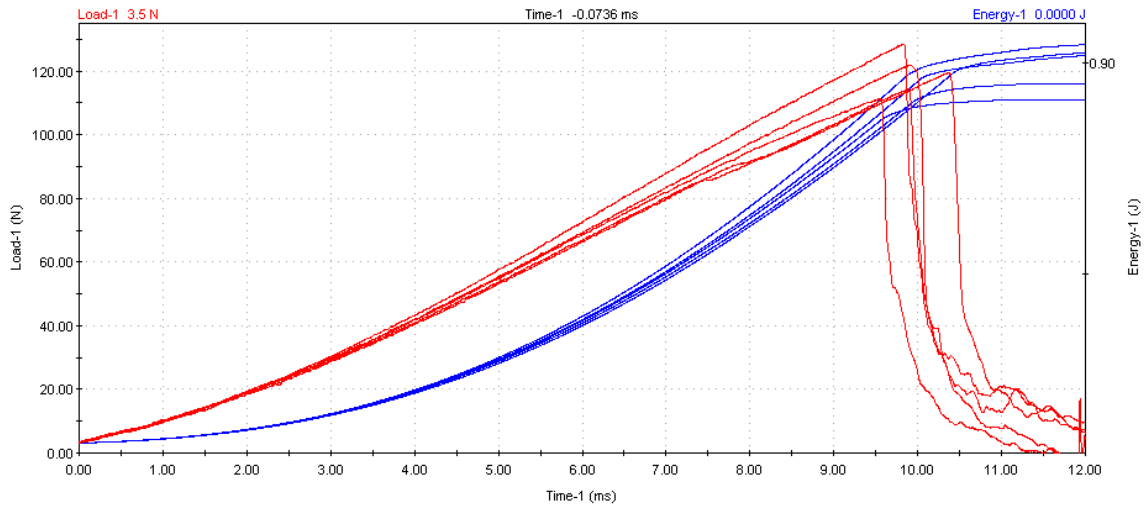


Figure 66 Load vs. Time of two-sided film with polyester scrim reinforcement

**Table 28** Results after impact resistance test of the single bubble/double foil

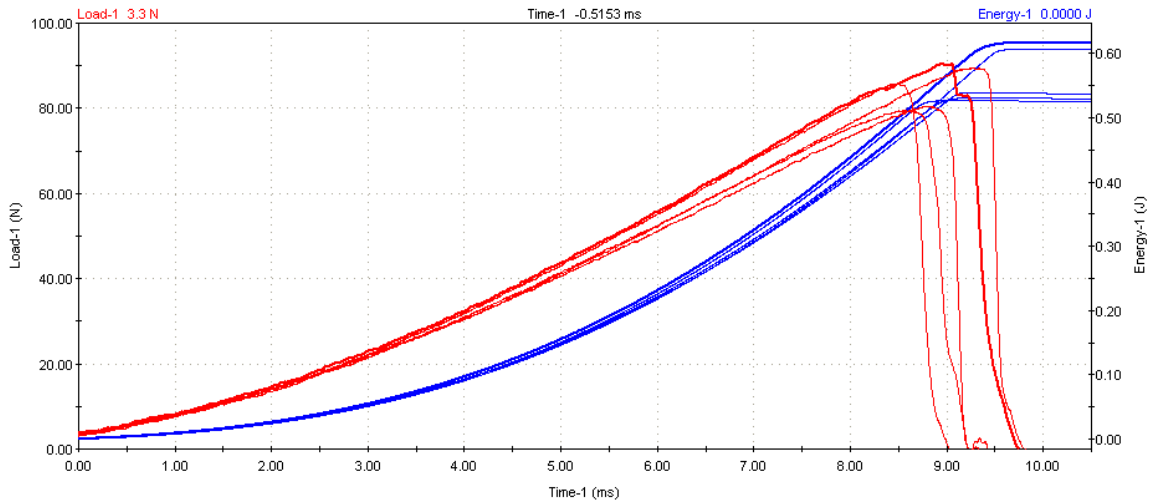
| Specimen                   | Maximum Load (N) | Time to max load-1 (ms) | Impact velocity-1 (m/s) | Total energy-1 (J) | Energy to max load-1 (J) | Total time-1 (ms) | Impact energy-1 (J) |
|----------------------------|------------------|-------------------------|-------------------------|--------------------|--------------------------|-------------------|---------------------|
| 1                          | 112.90           | 9.55                    | 1.51                    | 0.81               | 0.76                     | 11.10             | 3.12                |
| 2                          | 121.00           | 10.38                   | 1.50                    | 0.93               | 0.87                     | 12.50             | 3.08                |
| 3                          | 116.70           | 9.91                    | 1.51                    | 0.85               | 0.80                     | 11.43             | 3.12                |
| 4                          | 123.60           | 9.88                    | 1.52                    | 0.93               | 0.84                     | 12.75             | 3.14                |
| 5                          | 130.20           | 9.80                    | 1.52                    | 0.95               | 0.86                     | 12.40             | 3.13                |
| <b>Average</b>             | 120.88           | 9.90                    | 1.51                    | 0.89               | 0.83                     | 12.04             | 3.12                |
| <b>Standard deviation</b>  | 6.62             | 0.30                    | 0.01                    | 0.06               | 0.04                     | 0.72              | 0.02                |
| <b>Confidence interval</b> | 4.87             | 0.22                    | 0.00                    | 0.04               | 0.03                     | 0.53              | 0.02                |



**Figure 67** Load vs. Time of single bubble/white foil

**Table 29** Results after impact resistance test of heat reflecting fabric

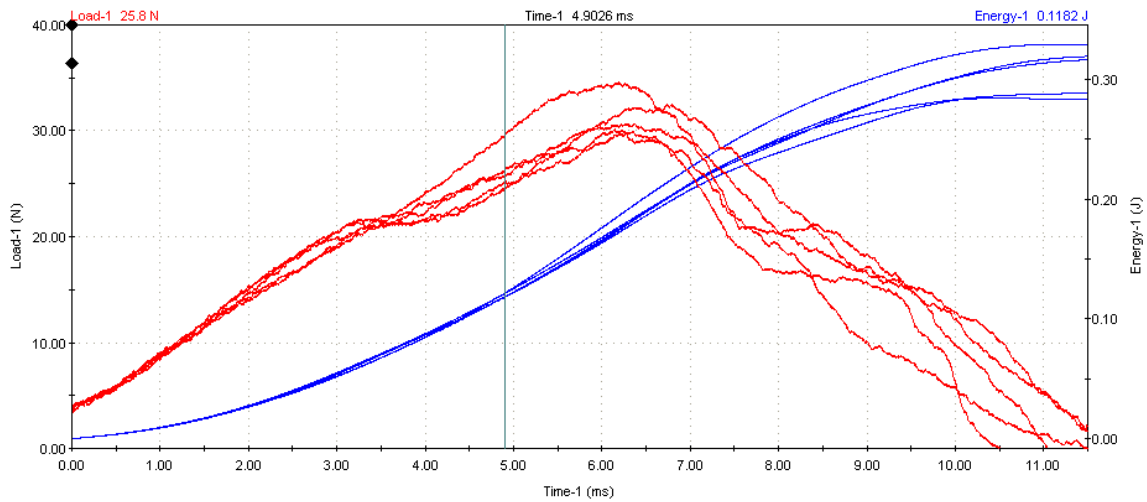
| Specimen                   | Maximum Load (N) | Time to max load-1 (ms) | Impact velocity-1 (m/s) | Total energy-1 (J) | Energy to max load-1 (J) | Total time-1 (ms) | Impact energy-1 (J) |
|----------------------------|------------------|-------------------------|-------------------------|--------------------|--------------------------|-------------------|---------------------|
| 1                          | 91.10            | 9.24                    | 1.53                    | 0.61               | 0.57                     | 9.76              | 3.17                |
| 2                          | 82.30            | 8.78                    | 1.53                    | 0.54               | 0.50                     | 9.19              | 3.18                |
| 3                          | 81.10            | 8.51                    | 1.53                    | 0.53               | 0.48                     | 9.21              | 3.18                |
| 4                          | 92.00            | 8.91                    | 1.52                    | 0.62               | 0.55                     | 9.70              | 3.15                |
| 5                          | 87.60            | 8.41                    | 1.52                    | 0.53               | 0.48                     | 8.98              | 3.15                |
| <b>Average</b>             | 86.82            | 8.77                    | 1.52                    | 0.56               | 0.52                     | 9.37              | 3.17                |
| <b>Standard deviation</b>  | 4.97             | 0.33                    | 0.00                    | 0.04               | 0.04                     | 0.34              | 0.02                |
| <b>Confidence interval</b> | 3.66             | 0.24                    | 0.00                    | 0.03               | 0.03                     | 0.25              | 0.01                |



**Figure 68** Load vs. Time of heat reflecting fabric

**Table 30** Results after impact resistance test of single bubble/double foil

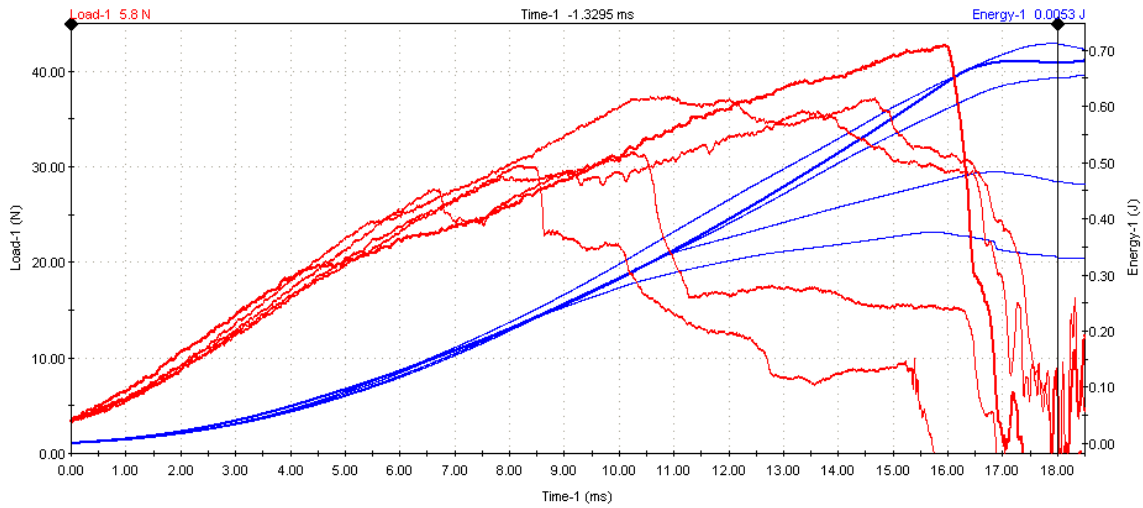
| Specimen            | Maximum Load (N) | Time to max load-1 (ms) | Impact velocity-1 (m/s) | Total energy-1 (J) | Energy to max load-1 (J) | Total time-1 (ms) | Impact energy-1 (J) |
|---------------------|------------------|-------------------------|-------------------------|--------------------|--------------------------|-------------------|---------------------|
| 1                   | 32.70            | 6.39                    | 1.51                    | 0.32               | 0.18                     | 20.67             | 3.12                |
| 2                   | 36.60            | 6.20                    | 1.51                    | 0.33               | 0.19                     | 20.42             | 3.09                |
| 3                   | 34.00            | 6.27                    | 1.52                    | 0.29               | 0.18                     | 20.61             | 3.14                |
| 4                   | 31.80            | 6.09                    | 1.51                    | 0.31               | 0.17                     | 20.64             | 3.12                |
| 5                   | 31.80            | 6.28                    | 1.52                    | 0.28               | 0.18                     | 20.54             | 3.13                |
| Average             | 33.38            | 6.25                    | 1.51                    | 0.31               | 0.18                     | 20.58             | 3.12                |
| Standard deviation  | 2.01             | 0.11                    | 0.00                    | 0.02               | 0.01                     | 0.10              | 0.02                |
| Confidence interval | 1.48             | 0.08                    | 0.00                    | 0.01               | 0.00                     | 0.07              | 0.01                |



**Figure 69** Load vs. Time of single bubble/double foil

**Table 31** Results after impact resistance test of bubble wrap

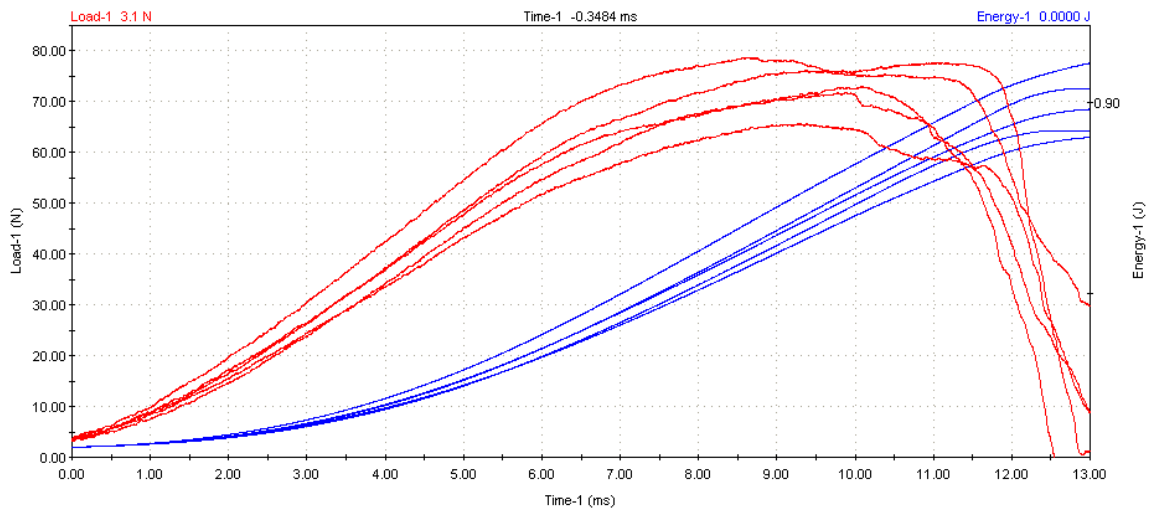
| Specimen                   | Maximum Load (N) | Time to max load-1 (ms) | Impact velocity-1 (m/s) | Total energy-1 (J) | Energy to max load-1 (J) | Total time-1 (ms) | Impact energy-1 (J) |
|----------------------------|------------------|-------------------------|-------------------------|--------------------|--------------------------|-------------------|---------------------|
| 1                          | 32.20            | 8.16                    | 1.53                    | 0.28               | 0.21                     | 16.93             | 3.20                |
| 2                          | 38.30            | 9.95                    | 1.53                    | 0.32               | 0.32                     | 17.90             | 3.21                |
| 3                          | 33.10            | 9.84                    | 1.54                    | 0.30               | 0.29                     | 16.86             | 3.22                |
| 4                          | 33.10            | 9.88                    | 1.53                    | 0.29               | 0.29                     | 16.98             | 3.20                |
| 5                          | 31.30            | 8.92                    | 1.53                    | 0.30               | 0.25                     | 17.87             | 3.21                |
| <b>Average</b>             | 33.60            | 9.35                    | 1.53                    | 0.30               | 0.27                     | 17.31             | 3.21                |
| <b>Standard deviation</b>  | 2.73             | 0.79                    | 0.00                    | 0.02               | 0.04                     | 0.53              | 0.01                |
| <b>Confidence interval</b> | 2.01             | 0.58                    | 0.00                    | 0.01               | 0.03                     | 0.39              | 0.01                |



**Figure 70** Load vs. Time of bubble wrap

**Table 32** Results after impact resistance test of polyethylene film

| Specimen                   | Maximum Load (N) | Time to max load-1 (ms) | Impact velocity-1 (m/s) | Total energy-1 (J) | Energy to max load-1 (J) | Total time-1 (ms) | Impact energy-1 (J) |
|----------------------------|------------------|-------------------------|-------------------------|--------------------|--------------------------|-------------------|---------------------|
| 1                          | 75.00            | 10.10                   | 1.52                    | 0.83               | 0.64                     | 12.52             | 3.16                |
| 2                          | 67.60            | 9.11                    | 1.53                    | 0.81               | 0.52                     | 13.28             | 3.19                |
| 3                          | 79.30            | 10.73                   | 1.52                    | 0.94               | 0.76                     | 12.84             | 3.14                |
| 4                          | 80.60            | 8.63                    | 1.53                    | 1.05               | 0.58                     | 16.13             | 3.18                |
| 5                          | 73.60            | 9.77                    | 1.53                    | 0.88               | 0.63                     | 13.45             | 3.18                |
| <b>Average</b>             | 75.22            | 9.67                    | 1.53                    | 0.90               | 0.63                     | 13.64             | 3.17                |
| <b>Standard deviation</b>  | 5.16             | 0.82                    | 0.01                    | 0.10               | 0.09                     | 1.44              | 0.02                |
| <b>Confidence interval</b> | 3.79             | 0.61                    | 0.00                    | 0.07               | 0.06                     | 1.06              | 0.02                |



**Figure 71** Load vs. Time of polyethylene film

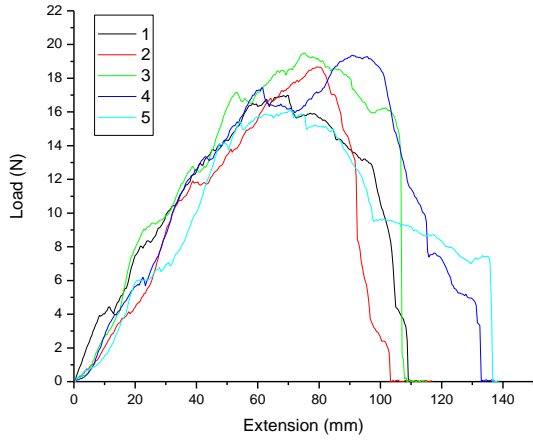
Appendix D. Complete results of tear resistance test

**Table 33** Results after tear resistance test

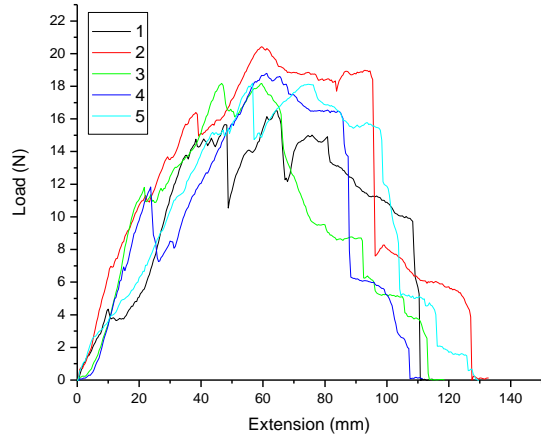
| Specimen                   | Single Bubble/Double Foil   |                                   |                  |                                | Single Bubble/White Foil    |                                   |                  |                                |
|----------------------------|-----------------------------|-----------------------------------|------------------|--------------------------------|-----------------------------|-----------------------------------|------------------|--------------------------------|
|                            | Average Load (Integral) (N) | First Peak (Load 10 % Change) (N) | Maximum Load (N) | Extension at Maximum Load (mm) | Average Load (Integral) (N) | First Peak (Load 10 % Change) (N) | Maximum Load (N) | Extension at Maximum Load (mm) |
| 1                          | 12.68                       | 16.99                             | 16.99            | 69.58                          | 11.99                       | 15.65                             | 16.51            | 64.17                          |
| 2                          | 11.31                       | 18.67                             | 18.67            | 79.17                          | 14.32                       | 20.42                             | 20.42            | 59.58                          |
| 3                          | 14.53                       | 19.50                             | 19.50            | 75.42                          | 11.66                       | 18.18                             | 18.18            | 59.58                          |
| 4                          | 13.40                       | 19.37                             | 19.37            | 90.83                          | 12.50                       | 11.83                             | 18.79            | 61.25                          |
| 5                          | 11.16                       | 16.14                             | 16.14            | 70.83                          | 12.62                       | 18.19                             | 18.19            | 56.67                          |
| <b>Average</b>             | 12.62                       | 18.13                             | 18.13            | 77.17                          | 12.62                       | 16.85                             | 18.42            | 60.25                          |
| <b>Standard deviation</b>  | 1.42                        | 1.50                              | 1.50             | 8.54                           | 1.03                        | 3.28                              | 1.41             | 2.74                           |
| <b>Confidence interval</b> | 1.05                        | 1.10                              | 1.10             | 6.28                           | 0.76                        | 2.41                              | 1.03             | 2.02                           |

| Specimen                   | Heat Reflecting Fabric      |                                   |                  |                                | Two-sided Film Polyester with Scrim Reinforcement |                                   |                  |                                |
|----------------------------|-----------------------------|-----------------------------------|------------------|--------------------------------|---|-----------------------------------|------------------|--------------------------------|
|                            | Average Load (Integral) (N) | First Peak (Load 10 % Change) (N) | Maximum Load (N) | Extension at Maximum Load (mm) | Average Load (Integral) (N)                       | First Peak (Load 10 % Change) (N) | Maximum Load (N) | Extension at Maximum Load (mm) |
| 1                          | 7.04                        | 13.07                             | 13.07            | 35.00                          | 16.72   | 24.62                             | 24.62            | 29.58                          |
| 2                          | 12.84                       | 21.86                             | 21.86            | 40.83                          | 15.44   | 24.29                             | 24.29            | 22.92                          |
| 3                          | 12.52                       | 16.73                             | 17.39            | 34.17                          | 18.13   | 26.40                             | 26.40            | 26.25                          |
| 4                          | 18.43                       | 24.72                             | 24.72            | 49.17                          | 21.41   | 18.79                             | 33.50            | 29.58                          |
| 5                          | 11.02                       | 18.41                             | 18.41            | 39.17                          | 20.25   | 23.70                             | 28.32            | 27.92                          |
| <b>Average</b>             | 12.37                       | 18.96                             | 19.09            | 39.67                          | 18.39   | 23.56                             | 27.42            | 27.25                          |
| <b>Standard deviation</b>  | 4.10                        | 4.52                              | 4.44             | 6.00                           | 2.46  | 2.85                              | 3.76             | 2.79                           |
| <b>Confidence interval</b> | 3.02                        | 3.32                              | 3.27             | 4.41                           | 1.81  | 2.10                              | 2.76             | 2.05                           |

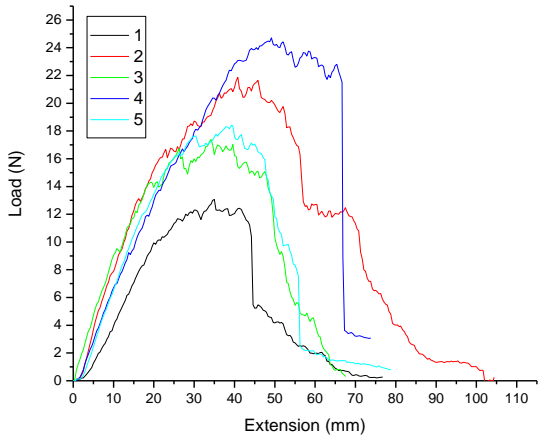




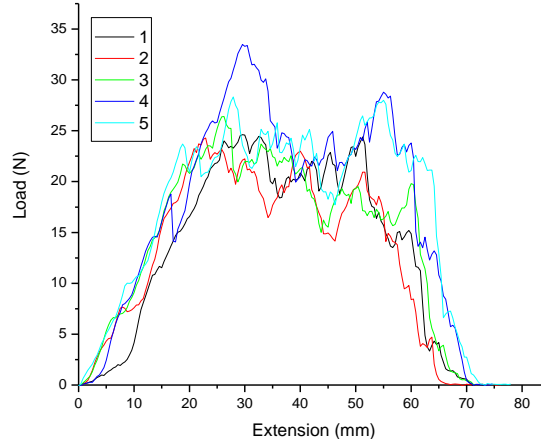
a) Single Bubble/Double Foil



(b) Single Bubble/White Foil



(c) Heat Reflecting Fabric



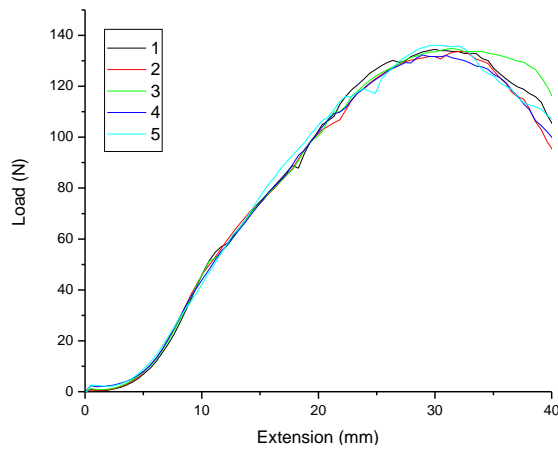
(d) Two-sided Film with Polyester Scrim

**Figure 72** Load vs. Extension of outside layers

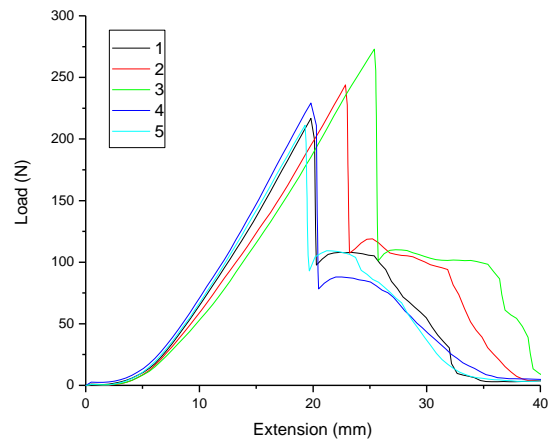
Appendix E. Complete results of bursting strength test

**Table 34** Results after bursting strength test of outside layers

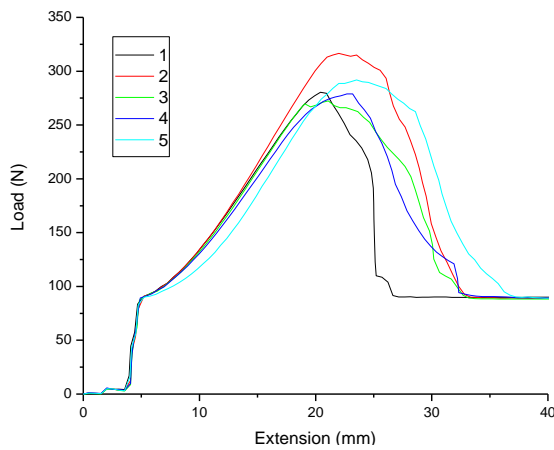
| Specimen            | Single Bubble/Double Foil |                                | Single Bubble/White Foil |                                | Heat Reflecting Fabric |                                | Two-sided Film with Polyester Scrim Reinforcement |                                |
|---------------------|---------------------------|--------------------------------|--------------------------|--------------------------------|------------------------|--------------------------------|---|--------------------------------|
|                     | Maximum Load (N)          | Extension at Maximum Load (mm) | Maximum Load (N)         | Extension at Maximum Load (mm) | Maximum Load (N)       | Extension at Maximum Load (mm) | Maximum Load (N)                                  | Extension at Maximum Load (mm) |
| 1                   | 134.50                    | 29.97                          | 216.83                   | 19.81                          | 280.51                 | 20.42                          | 597.99  | 18.21                          |
| 2                   | 133.72                    | 32.51                          | 243.99                   | 22.86                          | 316.58                 | 22.00                          | 596.11  | 15.99                          |
| 3                   | 134.81                    | 31.50                          | 273.02                   | 25.40                          | 272.39                 | 21.09                          | 584.71  | 18.35                          |
| 4                   | 132.33                    | 28.96                          | 229.23                   | 19.81                          | 278.97                 | 22.69                          | 577.81  | 19.31                          |
| 5                   | 136.17                    | 29.97                          | 211.22                   | 19.30                          | 291.93                 | 23.52                          | 599.34  | 20.15                          |
| Average             | 134.31                    | 30.58                          | 234.86                   | 21.44                          | 288.08                 | 21.94                          | 591.19  | 18.40                          |
| Standard deviation  | 1.42                      | 1.41                           | 24.77                    | 2.63                           | 17.42                  | 1.23                           | 9.46  | 1.56                           |
| Confidence interval | 1.04                      | 1.04                           | 18.22                    | 1.93                           | 12.81                  | 0.91                           | 6.96  | 1.15                           |



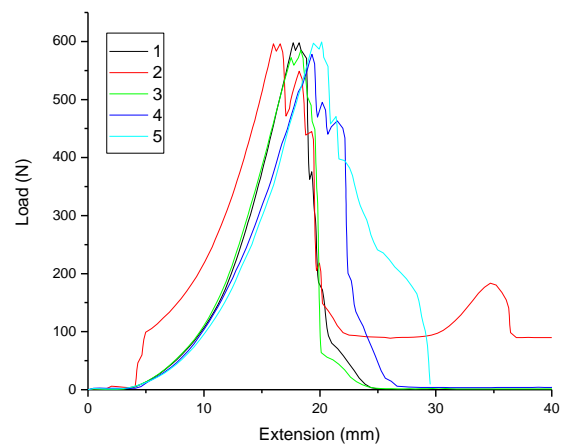
(a) Single Bubble/Double Foil



(b) Single Bubble/White Foil



(c) Heat Reflecting Fabric

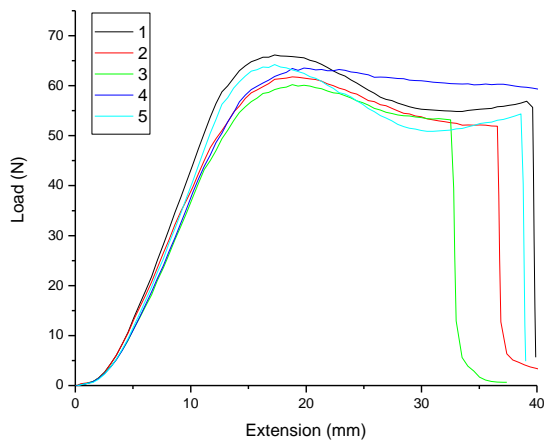


(d) Two-sided Film with Polyester Scrim

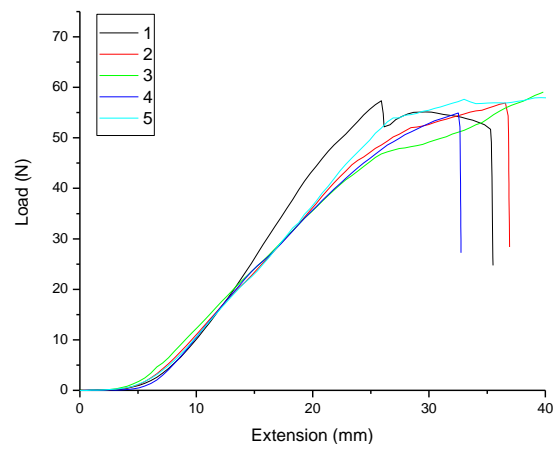
**Figure 73** Load vs. Extension of outside layers

**Table 35** Results after bursting strength test of inner layers

| Specimen                   | Film             |                                | Bubble Wrap      |                                |
|----------------------------|------------------|--------------------------------|------------------|--------------------------------|
|                            | Maximum Load (N) | Extension at Maximum Load (mm) | Maximum Load (N) | Extension at Maximum Load (mm) |
| 1                          | 66.16            | 17.30                          | 57.38            | 25.91                          |
| 2                          | 61.79            | 18.80                          | 56.89            | 36.58                          |
| 3                          | 60.20            | 18.80                          | 59.03            | 39.82                          |
| 4                          | 63.54            | 19.80                          | 54.94            | 32.51                          |
| 5                          | 64.23            | 17.30                          | 57.96            | 39.62                          |
| <b>Average</b>             | 63.18            | 18.40                          | 57.24            | 34.89                          |
| <b>Standard deviation</b>  | 2.29             | 1.08                           | 1.51             | 5.83                           |
| <b>Confidence interval</b> | 1.68             | 0.80                           | 1.11             | 4.29                           |



(a) Film



(b) Bubble Wrap

**Figure 74** Load vs. Extension of inner layers